TABLE OF CONTENTS

LIST OF FIGURES

LIST OF TABLES

LIST OF SYMBOLS

F_s	Shear force on the shear plane
F_t	Cutting force
N_s	Normal force on the shear plane
F_f	Shear force on rake face
N_f	Normal force on the rake face,
$\emptyset$	Shear angle
α	Rake angle of the cutting tool
μ	Coefficient of friction
β	Friction angle
R	Cutting ratio
F	Feed rate
t_c	Chip thickness
AB	Length of the shear plan

CHAPTER 1: INTRODUCTION

1.1 Research Background

Aluminum–silicon alloy is used extensively in the automotive and aerospace industries due to its excellent castability, good thermal conductivity, low expansion coefficient, and good corrosion resistance. Al–Si castings constitute 90% of the total aluminum cast components produced (Farahany, Ourdjini, & Idris, 2011).The complex Al-11Si-Cu-Mg alloy possesses exceptional fluidity and resistant to hot tearing due to more silicon content so that it is capable of producing intricate castings of thin sections. This alloying system is used widely in automotive applications to produce critical components such as engine blocks and cylinder heads and pumps (Uthayakumar, Prabhakaran, Aravindan, & Sivaprasad, 2012).

Most Al-Si components require machining before they can be used in assembly. Current government and consumer attention on the environmental sustainability of products and processes has motivated manufacturers to reduce the volume of their waste streams, particularly the metal cutting fluids used as coolants and lubricants. The dry machining of Al-Si alloys may become an environmentally sustainable alternative to the conventional flooded cutting of castings. The primary reasons for the shift to dry or near dry machining are: (i) concerns over the contamination of the environment that results from the use and disposal of large quantities of coolants and lubricants, (ii) expense generated by the use of these cutting fluids, and (iii) the health hazards experienced by machining operators. The dry machining of Al alloys, however desirable, remains challenging because the absence of cutting fluids allows Al chips to adhere to the tool surfaces (Bhowmick & Alpas, 2008), which causes premature tool failure.

The need for bridging the divide between the casting process and the machining process provides a strong motivation for examining the various aspects affecting the machinability of Al-Si casting alloys, given that these alloys constitute more than 80% of all aluminum alloy castings. Machinability plays an important role in the selection of material for commercial exploitation. In general, more than 90% of manufactured parts need to be machined before they are ready for use. It is an interaction phenomenon between work piece (material type and form), cutting tool (material type and geometry), and cutting medium such as air and liquid in a number of different removal sequences which include turning, drilling, tapping, milling, sawing, and cutting conditions (speed, feed, and depth of cut). The condition and physical properties of the work material have a direct influence on the machinability of the workpiece (Taylor, Schaffer, & StJohn, 1999). Operating conditions, tool material and geometry, and workpiece requirements all exert an indirect influence on machinability and can often be used to overcome difficult conditions presented by the work material. On the other hand, they can also create situations which compound difficulty of machining if they are ignored (Zedan, Samuel, Samuel, & Doty, 2010).

Modification melt treatment changes the flake morphology to a fibrous form, resulting in increased elongation and casting ductility (X. H. Zhang, Su, Ju, Wang, & Yan, 2010). Treatment applied with the intention of refining primary silicon or modifying the morphology of eutectic silicon will improve tool life substantially. By the addition of certain elements to the melt prior to solidification, chemical modification can be achieved. Certain elements are known to enhance the wet machinability of aluminum and steel; these elements are referred to as free-machining elements and include bismuth (Bi), tin (Sn), lead (Pb), and cadmium (Cd) (Swamy, Joseph, Nagarajan, & Sudarsan, 2011). They also have a marked effect on the eutectic silicon when added to molten Al-Si alloys by changing its morphology to fibrous appearance Strontium (Sr) is another modifier which

has long-term modifying effect (Bian, Zhang, & Liu, 2000). Among the various modifiers, Sr has been used extensively as it is easier to handle and its recovery rate in the melt is usually of the order of 90%. In addition, antimony (Sb) was introduced as alternative element for modifying the silicon eutectic (Hegde & Prabhu, 2008). The most important advantage of antimony is that it is stable in the melt and is not affected by holding time, remelting and degassing. Numerous investigations confirm that the quality and especially the lifetime of the dynamically loaded parts are very much dependent on the properties of the material in the surface. Therefore, in machining any component it is first necessary to satisfy the surface integrity requirements.

Silicon has an important role in the soft phase and it can change amount of ductility in the workpiece. Shape of silicon will be changed in microstructure of workpieces under different modifiers (Farahany et al., 2011). Over the past three years, some research has been attempted to improve surface roughness after the machining process. In this way, some elements with low melting points such as lead (pb), bismuth (Bi), tin (Sn), indium (In) have been used to minimize the chip size and hence, increase the machinability (J Grum & Kisin, 2003). However, there is not much literature on the effect of different silicon morphologies on machinability parameters such as surface roughness, cutting force, tool life and chip morphology during dry machining of Al-11Si-2Cu alloy. Therefore, there is a need for an in-depth understanding of the role of elements with low melting point and its effect on microstructure and machinability of Al-Si-Cu alloys containing bismuth, antimony or strontium throughout.

1.2 Problem Statement

Machinability testing is aimed at evaluating the comparative machining performance of workpiece materials, cutting tools and cutting fluids. This type of testing also aims at establishing conditions which will ultimately produce satisfactory finished

parts with the desired dimensional surface finish and functional integrity in an economical fashion. A thorough understanding of all the metallurgical factors affecting the machinability of aluminum alloys will contribute to selecting metallurgical designs which attempt to promote the optimum machining combinations essential to sustained productivity.

Among the various Al alloys, aluminum-silicon alloys are said to be the most difficult to machine, as is evidenced by the fact that the silicon phase present is almost ten times harder than the base alloy, thus causing the cutting tools to wear out rapidly. For this reason, attempts have been made to optimize the selection of cemented carbide tools, cutting conditions, and tool geometry; the further investigation of the following points also promoted the effects of flank build-up on tool wear, improve chip breakability and the improvement of machinability through the addition of certain elements.

Therefore, having an understanding of these alloys' machinability is imperative when it is necessary to fabricate some industrial products which are produced by casting process. The aim of this study is to investigate the machinability of Al-Si-Cu alloys containing 0.1%wt bismuth (Bi), 0.5%wt antimony (Sb) and 0.04%wt strontium (Sr) subjected to dry turning using coated carbide inserts.

1.3 Objectives

The research objectives are listed below:

- To investigate the effect of additive elements on microstructure and mechanical properties of Al-Si-Cu cast alloy.
- To evaluate the machinability of Al-Si-Cu cast alloy with different modifiers in terms of surface roughness and cutting force.
- To determine the wear rate of the coated carbide tools and chip morphology by addition of Bi, Sb and Sr when turning Al-Si-Cu cast alloy.

1.4 Scope of Study

The complex Al-11Si-2Cu alloy will be used as the base alloy. Different concentrations of Sr (0.01-0.06), Bi (0.1-1.5wt%) and Sb (0.2-0.5wt%) additions will be used to investigate the optimal concentration for refinement and modification. The effect of additives on microstructure, mechanical properties and machinability of Al-11Si-2Cu alloy will be investigated. Tow furnaces will be used together, one for preheating the permanent molds, and the other for melting the aluminum alloy. Gravity permanent metal mold casting technique both cylindrical tensile bars corresponding to ASTM B-108 type of impact Charpy test and tensile bars will be used for mechanical property testing. The experimental will be conducted on an OKUMA LB15-II 2-Axis CNC Lathe turning machine with 8.3 KW power drive and 6000 rpm maximum spindle speed. Physical vapor deposition (PVD) coated tool from Kennametal will be selected to conduct the machining test. The surface roughness and cutting force (Fc) during turning process will be evaluated by surface roughness tester (CS 5000 with accuracy of ±0.01μm), and Kistler 3 axis dynamometer (Model 9121, Kistler Instrument AG), respectively. Moreover, Surface

roughness will be examined via surface roughness tester Field Emission, Scanning Electron Microscopy (FESEM, Supra-35VP, Carl Zeiss) and Atomic Force Microscope (AFM) (Model SPM- 9500J2). Tool maker microscope with magnification: 6.5X-50X will be used for measuring flank wear. The cross-section of chips were observed using a scanning electron microscope (JEOL JSM- 5800LV SEM) equipped with an energy dispersive spectrometer (EDS).

CHAPTER 2: LITERTURE REVIEW

2.1 Introduction to Al-Si Alloys

Aluminum is the third most abundant element in the earth's crust and constitutes 7.3% by mass. In nature, however it only exists in very stable combinations with other materials (particularly as silicates and oxides) and it was not until 1808 that its existence was first established. Al-Si castings constitute 85 % to 90 % of the total aluminum cast parts produced. They are widely used for engineering applications, especially in the transportation industries (Gallab & Sklad, 2004). For example, aluminum castings have been applied to various automobile parts and constitute about 40 % of wheels, brackets, brake components, suspensions (control arms, supports), steering components (air bag supports, steering shafts, knuckles, housings, wheels), instrument panels, and engine blocks (Grum & Kisin, 2003). Their high strength-to-weight ratio, good formability, good corrosion resistance and recycling potential make these alloys an ideal choice for light-weight components (Grum & Kisin, 2003). Table 2.1 shows the general characteristics of aluminum.

Table 2.1: The general characteristics of aluminum (Grum & Kisin, 2003).

symbol	Al
Atomic number	13
Atomic weight	26.98
Density	2698 kg
Melting point (°C)	660.37
Boiling point	2467°C
Thermal conductivity	237 W/m

Al-Si-Cu-Mg system is a sub-family of aluminum-silicon alloys and is of great industrial importance. This aluminum alloy system consists mainly of Si, Cu and small

amount of Mg added in order to produce more age hardening effect during precipitation of phases that form during solidification, such as Al_2Cu and Mg_2Si intermetallic (Taylor et al., 1999). Al-Si-Cu-Mg alloys constitute an important class of aluminum foundry alloys including more than 90% of aluminum casting owing to their superior castability, excellent fluidity, excellent corrosion resistance, low density and good mechanical properties (Barzani, Sarhan, Farahany, Ramesh, & Maher, 2015).

Al-Si alloys are classified into three categories based on their silicon percentage: (i) eutectic, (ii) hypoeutectic, and (iii) hypereutectic. Figures 2.1 and 2.2 illustrate the binary phase diagram and the typical microstructures for these three cast Al-Si alloys. Si particles appear as platelets or needle-like particles in hypoeutectic Al-Si alloys while hypereutectic contains both the block-like primary Si phase particles and platelet or needle-like eutectic Si particles (Backerud, Chai, & Tamminen, 1990).

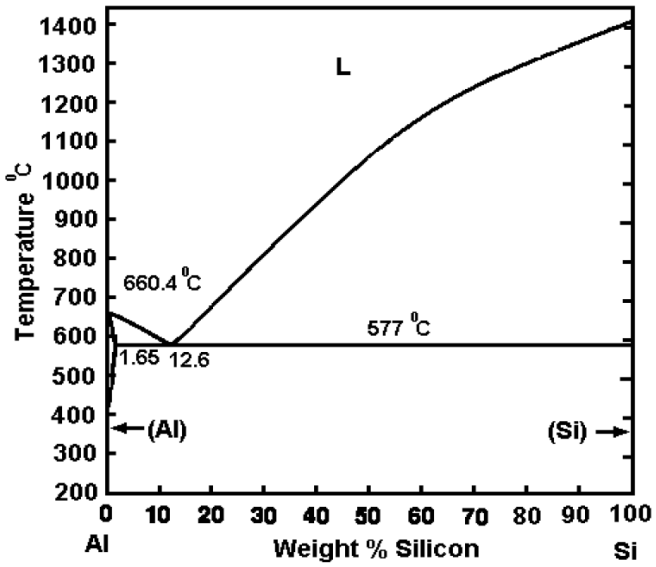

Figure 2.1: Al-Si binary phase diagram (Backerud et al., 1990).

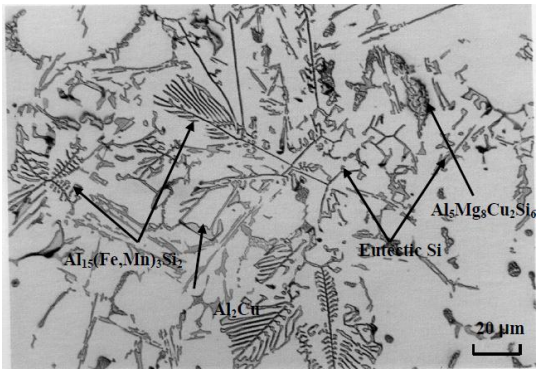

(a)

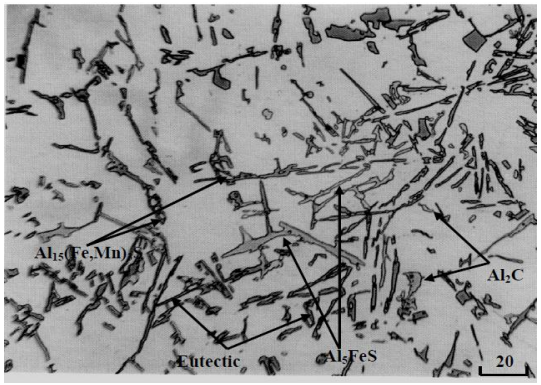

(b)

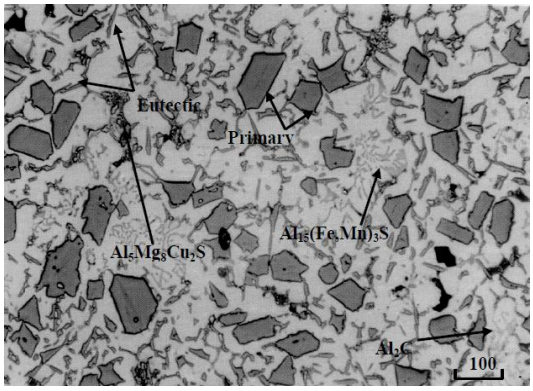

(c)

Figure 2.2 : Typical microstructure of (a) hypoeutectic , (b) near eutectic alloy, and (c) hypereutectic alloy (Backerud et al., 1990).

Aluminum-silicon system can also be classified into the category of metal matrix composite (MMCs) in which the soft and ductile aluminum matrix is reinforced with hard and brittle eutectic silicon particles which form during solidification. Thus, the size,

distribution and shape of silicon particles play a major role in the mechanical properties of these alloys (Farahany et al., 2011). Figure 2.3 shows the aluminum matrix and silicon particles that have cracked under external loading due to their brittle nature. Large plates of silicon raises the internal stress in the microstructure and provides easy path for fracture resulting in a detrimental effect on the toughness, ductility and elongation properties (Sjölander & Seifeddine, 2010).

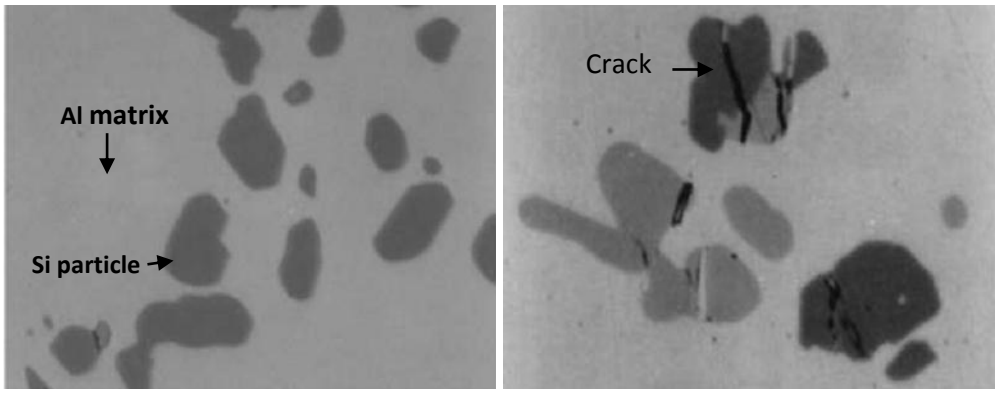

Figure 2.3: (a) Optical micrograph of brittle and (b) hard silicon particles in a soft and ductile aluminium matrix (Moustafa, Samuel, & Doty, 2003).

The very low solubility of silicon in aluminum means that Al-Si alloys contain virtually pure α-aluminum with silicon as either a primary (in hypereutectic alloy) or eutectic (in hypoeutectic or eutectic alloys) phase, depending on whether the silicon percentage is greater or less than the eutectic point (12.6 % Si), on the cooling rate, and on the concentration of modifiers added (Mohamed, Samuel, Samuel, & Doty, 2008). It has been published that alloys with silicon less than 3wt.% are utilized in heat-treatable condition for marine fittings. Moreover, silicon in the range of 3-5wt.% are generally used in fabricating rotors, vessels and valve bodies (Basavakumar, Mukunda, & Chakraborty, 2007). Eutectic alloys are used in automobile and aeronautical industries to produce critical components like pistons, cylinders, blocks and heads of engines in which silicon

is in the range of 11- 13wt.%. Alloys with silicon content more than 13% are mainly used for tribological applications (Mohamed et al., 2008).

Al-Si-Cu-Mg alloys are used where high strength is needed. However, Cu increases age hardening, strength, and machinability, but reduces the corrosion resistance (Sjölander & Seifeddine, 2010). The lower silicon and higher copper alloys of Al-3Si-4Cu are used for sand and permanent mold, whereas the higher silicon alloys, for example, Al-10Si-2Cu are used for pressure die casting (Palanikumar & Karthikeyan, 2007). Table 2.2 illustrates influence of some alloying elements in Al-Si alloy.

Table 2.2 Influence of alloying elements in Al-Si system (Backerud et al., 1990).

Elements	Effect
Copper	Enhance strength and hardness In heat treated condition through Al_2Cu precipitation. Reduce corrosion resistance, decrease castability
Magnesium	Improve strength through Mg_2Si precipitation hardening
Iron	Improve hot tear resistance, decrease tendency to die sticking, decrease ductility
Manganese	Improve strength and hardness in treated alloy

2.2 Casting Process

In general, aluminum castings can be produced by more than one process. Quality requirements, technical limitations and economic considerations dictate the choice of a casting process. The common casting processes used for aluminum alloys include the following: (i) Sand casting: large castings (up to several tons), produced in quantities of one to several thousand castings, (ii) Permanent mold casting (gravity and low pressure): medium size casting (up to 100kg) in quantities of from 1000 to 100000, (iii) High

pressure dies casting: small castings (up to 50 kg): in large quantities (10,000 to 100,000) (Govender & Ivanchev, 2005).

There are several reasons why castings should be made from aluminum alloys. These include properties like: ductility, high deformation, weight reduction, shape stability, wear resistance, and stress distribution (DeGarmo, Black, & Kohser, 2011). Permanent mold casting is metal casting process that employs reusable molds ("permanent molds"), usually made from metal. The most common process uses gravity to fill the mold, however gas pressure or a vacuum are also used. Permanent mold castings can be produced from all of the metals including iron and copper alloys, but are usually light metals such as zinc-base, magnesium and aluminum (DeGarmo et al., 2011).

Because the molten metal is poured into the die and not forcibly injected, permanent mold casting is often referred to as gravity die casting. Permanent mold casting is typically used for high-volume production of small, simple metal parts with uniform wall thickness (Sjölander & Seifeddine, 2010). Non-ferrous metals are typically used in this process, such as aluminum alloys, magnesium alloys, and copper alloys (Godowsky, 2007). However, irons and steels can also be cast using graphite molds. Common permanent mold parts include gears and gear housings, pipe fittings, and other automotive and aircraft components such as pistons, impellers, and wheels (DeGarmo et al., 2011). The flow of metal into a permanent mold using gravity only is referred to as a gravity permanent mold. Normally, gravity molding is used because it is more accurate than shell molding. It is preferred almost exclusively to shell molding for light alloy components (DeGarmo et al., 2011).

2.3 Solidification of Al-Si Alloys

Al-Si alloys differ from the "standard" phase diagram in that aluminum has zero solid solubility in silicon at any temperature. This means that there is no β phase and so

this phase is "replaced" by pure silicon. Thus, for Al-Si alloys, the eutectic composition is a structure of α + Si rather than α +β. Figure 2.4 shows the Al-Si phase diagram (Govender & Ivanchev, 2005).

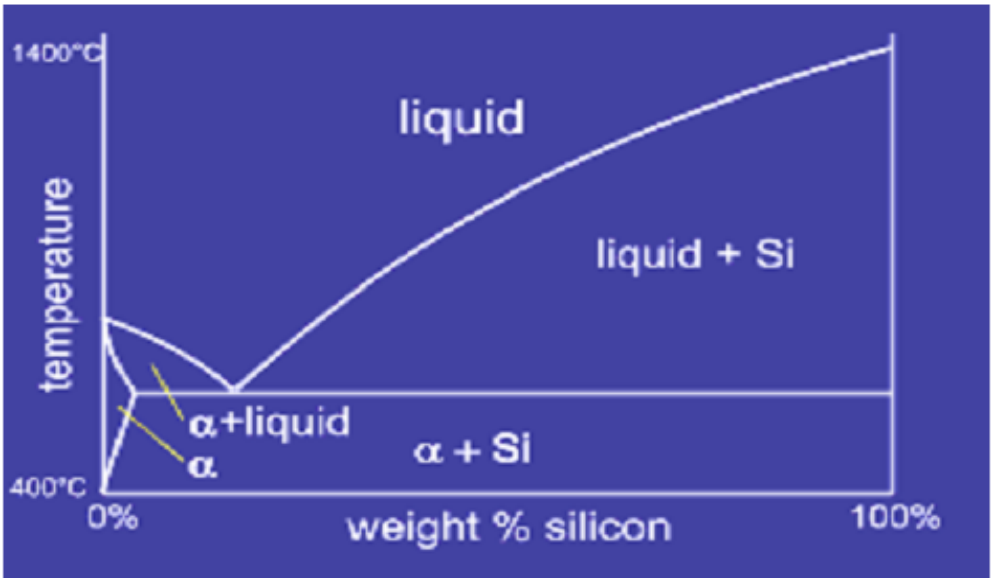

Figure 2.4: Phase diagram of Al-Si alloy (Govender & Ivanchev, 2005).

The solidification of Al-Si alloys is an important aspect because it controls final microstructure which in turn controls the mechanical properties. Therefore, it is necessary to understand the basic principle of solidification and how the microstructures form. In general, solidification of an alloy occurs in two stages: the first is nucleation and growth. In the nucleation stage, stable nuclei are formed into the liquid metal and these nuclei subsequently grow into crystals and the formation of the final grain structure (Godowsky, 2007). There are two types of grain structures that may be formed upon solidification of a metal alloy: columnar and equiaxed grains. Equiaxed grains form as a result of equal growth in all directions of the crystal (prevalent in grain refined alloy due to the presence of large number of nucleation sites) while columnar grains are present as thin, long structures normal grow under a temperature gradient during slow solidification. These

columnar grains normally grow in the direction of the mold wall and in a direction opposite the heat flow.

The preferred structure of a casting is one that has small equiaxed grains (Figure 2.5), since this type of structure improves feeding, resistance to hot tearing and enhances the mechanical properties. Improvements in the mechanical properties are the result of sound casting that can be produced during casting. Producing a structure with equiaxed grains can be achieved through control of the solidification conditions or by the use of inoculants or grain refiners (Godowsky, 2007).

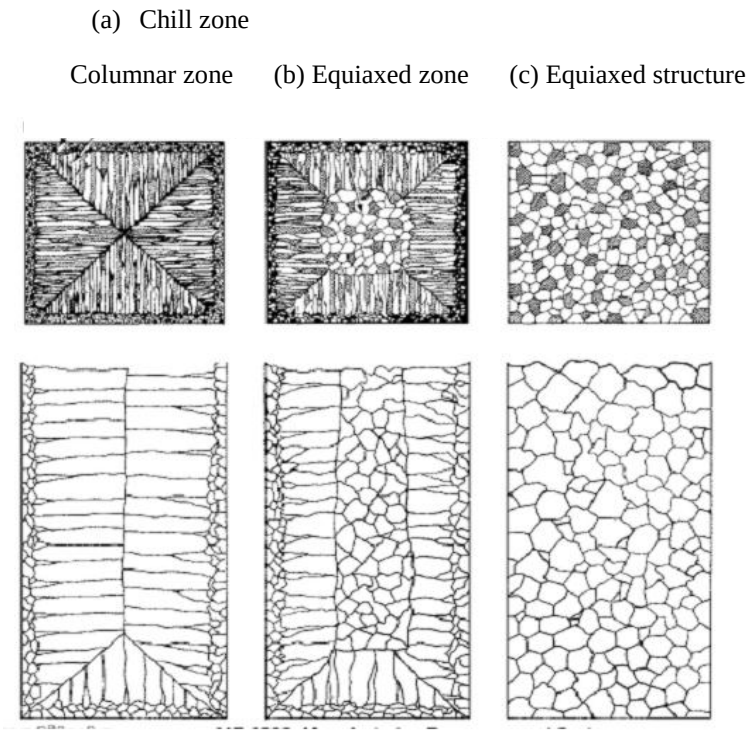

Figure 2.5: Kinds of microstructures that may form during solidification casting (Godowsky, 2007).

2.4 Modification of Eutectic Al-Si Alloys

In order to produce alloys with increased strength and improved foundry or working properties, a number of elements are added to aluminum. The mechanical properties can also be enhanced by heat treatment when other elements are added to alloying aluminum. For purposes of understanding the effects of alloying elements the majority of alloys are probably best classified as major, minor understanding, however, that impurity elements in some alloys might be major elements in others: Major elements typically include silicon (Si), copper (Cu) and magnesium (Mg). Minor elements include nickel (Ni) and tin (Sn) found largely in alloys that likely would not be used in high integrity die castings(Govender & Ivanchev, 2005).

The morphology of silicon plays an important role on the mechanical properties of finished products. The coarse silicon plates, which are of the unmodified acicularsilic structure, act as internal stress raisers in the microstructure and provide easy paths for fracture. Therefore, the eutectic silicon structure is modified to a fine fibrous structure by rapid cooling, by the addition of a chemical modifier, or by superheating the melt to 850°C (Flood & Hunt, 1981). With modification, the structure becomes finer and the silicon more rounded, both of which contribute to somewhat higher values of ultimate strength and greatly increased ductility. Any process which reduces the size of the brittle phase particles or increases their separation will improve the properties of the alloy (Farahany, Ourdjini, Idris, & Thai, 2011). Therefore, the common practice is to modify the as-cast flake or acicular silicon morphology by the addition of certain modifiers or by special heat treatment.

Typically, modified structures display somewhat higher tensile properties and appreciably improved ductility when compared to similar but unmodified structures. Improved performance in casting is characterized by improved flow and feeding as well

as by superior resistance to elevated-temperature cracking. Strontium is currently available in many forms, including aluminum-strontium master alloys ranging from approximately 10 to 90% Sr and Al-Si-Sr master alloys of varying strontium content (Farahany et al., 2011) Hypoeutectic aluminum-silicon alloys can be improved by inducing structural modification of the normally occurring eutectic. In general, the greatest benefits are achieved in alloys containing from 5% Si to the eutectic concentration; this range includes most common gravity cast compositions. The addition of certain elements, such as calcium, sodium, strontium, and antimony, to hypoeutectic aluminum-silicon alloys results in a finer lamellar or fibrous eutectic network. It is also understood that increased solidification rates are useful in providing similar structures (Abdollahi, 1998).

There are three methods available to modify the silicon in eutectic structure which induce addition of certain elements (chemical modification), using ultrasonic or electromagnetic stirring or mechanical vibration (mechanical modification) and rapid cooling rate as in chilling (Wang, Lu, & Hogan, 2003). In the first method an alkali metal (Group IA) such as sodium or an alkaline earth metal (Group IIA) such as strontium are usually added to the melt to modify the structure of silicon There is, however, no agreement on the mechanisms involved. The most popular explanations suggest that modifying additions suppress the growth of silicon crystals within the eutectic, providing a finer distribution of lamellae relative to the growth of the eutectic (Abdollahi, 1998).

The results of modification by strontium, sodium, and calcium are similar (Barzani, Farahany, Yusof, & Ourdjini, 2013). Sodium has been shown to be the superior modifier, followed by strontium and calcium, respectively. Each of these elements is mutually compatible so that combinations of modification additions can be made without adverse effects. Sodium, strontium and antimony are used most commonly in industry today to alter the form of the silicon from an acicular shape to a fine fibrous one

(Abdollahi, 1998). Eutectic modification is, however, transient when artificially promoted by additions of these elements.

The use of sodium as the modifying agent does present founding problems because the fluidity of the melt is reduced, but the major difficulty is its rapid and uncertain loss through evaporation or oxidation (Moustafa et al., 2003). It is therefore necessary to add an excess amount and difficulties in controlling the content in the melt can lead to the under or over-modification of the final castings. For the same reason, the effects of modification are lost if Al–Si castings are remelted which prevents foundries being supplied with pre-modified ingots. Attention has therefore been directed at alternative methods and modification today is carried out mostly by using additions of strontium. The amounts needed vary with the silicon content of the alloy and range from 0.015 to 0.02% for hypoeutectic permanent mold castings and slightly more for sand castings that solidify more slowly, or for alloys with higher silicon contents (Moustafa et al., 2003).

2.4.1 Modification Rating System

Modifiers are added to the melt either in element forms in master alloys or through fluxes. Alkali metals such as Sodium (Na), potassium (K), rubidium (Rb), and alkaline-earth metals like as strontium (Sr) and calcium (Ca) rare-earth metals such as lanthanum (La) and cesium (Ce), and a few elements from group five of the periodic table such as antimony (Sb) and arsenic (As) have been shown to modify or refine the eutectic silicon structure (Zedan et al., 2010). Selection of modifying agents also depends on some features such as ease of dissolution, vapor pressure, stability in the melt.

Modifying agents cause a change in silicon particles from acicular/flake to fibrous morphology. Depending on level of modification it has been categorized to 6 groups (Godowsky, 2007) : 1) unmodified, 2) lamellar, 3) partial modified 4) absence of lamellar

structure, 5) fully modified 6) super modified. It must be noted that microstructure is not always uniform and composed of fibrous silicon, lamellar silicon and acicular silicon. To assess level of modification and illustrate quantitative relationship between variables such as concentration of refiner and modifier elements, cooling rate and holding time and modification standard modification rating system were employed.

According to this classification, morphology of silicon is divided in-to 6 groups: (1) fully unmodified, (2) lamellar, (3) partially modified (4) absence of lamellar (5) fibrous and (6) very fine fibrous silicon. Average modification rating was determined as sum of products of fraction and modification classes as follows:

For example, the modification rate (M.R.) of sample with 30% of class 3, 20% of class 4 and 50% of class 5 would then be calculated as:

M.R= (0.3×3) + (0.2×4) + (0.5×5) =4.2

It means that sample is reasonably well, but not perfectly, modified (Farahany et al., 2011).

2.5 Effect of Additives on Microstructure

2.5.1 Silicon (Si)

Silicon is used with magnesium at levels up to 1.5% to produce Mg_2Si in the series of heat-treatable alloys in wrought alloys. The addition of silicon to aluminum reduces melting temperature and improves fluidity (Moustafa, Samuel, Doty, & Valtierra, 2002). Silicon in combination with magnesium produces a precipitation hardening heat – treatable alloy, while silicon alone in aluminum produce a non-heat-treatable alloy. Consequently, both heat-treatable and non-heat-treatable alloy. Silicon additions to

aluminum are commonly used for the manufacturing of casting. Al/Si particulate composites are increasingly being used for various engineering applications from automotive to aircraft components. Common applications are bearings, automobile pistons, cylinder liners, piston rings connections and rods sliding electrical contacts (Polmear, 2006).

Silicon alone contributes very little to the strength of aluminum casting alloys. However, when combined with magnesium to form Mg_2Si, Si provides a very effective strengthening in aluminum castings (Polmear, 2006). If the silicon content is below 8%, modification is not necessary to achieve acceptable levels of ductility because the primary aluminum phase is present in relatively large amounts. The eutectic composition, which has a high degree of fluidity and low shrinkage on solidification, has particular application for thin-walled castings (Moustafa et al., 2003).

2.5.2 Copper (Cu)

Copper is one of the primary alloying elements for aluminum, based largely on the substantial age hardening response of Al–Cu alloys. The aluminum-copper alloys typically contain between 2 to 10% copper, with smaller additions of other elements. The copper provides substantial increases in strength and facilitates precipitation hardening . The susceptibility to solidification cracking of aluminum-copper alloys is increased; consequently, some of these alloys can be the most challenging aluminum alloys to weld. These alloys include some of the highest strength heat treatable aluminum alloys. The most common applications for theses alloys are aerospace .

The addition of copper to cast Al-Si alloys also promotes age hardening and increases strength. Copper also improves machinability but castability, ductility and corrosion resistance are all decreased (Moustafa et al., 2003). Commercial Al-Si-Cu alloys have been available for many years and compromises have been reached between

these various properties. Compositions lie mostly within the ranges 3–10.5% silicon and 1.5–4.5% copper. The higher silicon alloys (e.g. Al-10Si-2Cu) are used for pressure die castings, whereas alloys with lower silicon and higher copper (e.g. Al–3Si–4Cu) are used for sand and permanent mold castings (Moustafa et al., 2003). In general the Al–Si–Cu alloys are used for many of the applications listed for the binary alloys but where higher strength is needed. One example is the use of Al-6Si-3.5Cu for die cast (permanent mold) automotive engine blocks and cylinder heads in place of cast iron.

2.5.3 Magnesium (Mg)

Magnesium's (Mg) role is also to strengthen and harden aluminum castings. As mentioned earlier in this section, silicon combines with magnesium to form the hardening phase, Mg_2Si that provides the strengthening and heat treatment basis for the popular 356 family of alloys. Magnesium is also the strengthening ingredient in the high-magnesium alloys that contain very little silicon; those alloys too depend on Mg_2Si, but gain additionally from other magnesium-bearing phase (Polmear, 2006). Magnesium reacts with the silicon during heat treatment to form as strengthening compound, magnesium-silicide (Mg_2Si), which precipitates out and resides in the grain boundaries of the alloy.

However, depending on the intended application for the alloy, the strength requirements may vary, which may accordingly necessitate a change in the magnesium content. Mg additions of up to 0.4 wt. % to the Al-11.5% Si alloy increase the yield strength by 94 % and decrease the ductility by 40 % (Moustafa et al., 2003).

2.5.4 Bismuth (Bi)

Bismuth is almost always present in wrought aluminum alloys to improve machinability, promote chip breaking and helps tool lubrication. The presence of 0.5wt. % Bi increases machining speeds and reduces the need for cutting fluids (Dasch et al.,

2009). In addition to those applications in wrought aluminum alloys, slight effect of Bi on silicon morphology of 319-type alloy has been reported. It has been claimed that Bi has a refining effect on the eutectic silicon and its refinement behavior increases with increasing Bi content up to 0.5% for LM25 (Al- 7wt.%Si-0.4wt.%Mg) alloy (Farahany, Orjini, Idris, & Thal, 2011). It has been reported that Bi has a little modifying effect in an Al-11.7wt. % Si alloy. The amount of modification increases with increasing Bi concentration up to 0.3%. They also mentioned that Bi additions to the melt neutralize the modifying effect of Na. It has been found that Bi always precipitates in the form of bismuth oxide due to its high oxygen potential, regardless of the Bi concentration or the chemical composition of the base alloy (Machovec and Zindel , 2000).

It has been determined that the presence of bismuth within the A 319 alloy enhances the lubricity of the alloy by essentially remaining as elemental bismuth within the alloy (Tan, Lee, & Lin, 1995). However, the amount of bismuth must also be limited since it tends to react with magnesium to form Mg_3Bi_2, which reduces the strengthening potential of the alloy. Therefore, it is desirable to limit the bismuth content to 1-2% (by wt.) within the preferred alloy (Tan et al., 1995). This range of bismuth provides the enhanced lubricity while minimizing the loss in strength of the alloy.

2.5.5 Strontium (Sr)

Sr is another modifier which has long-term modifying effect in comparison to Na (Bian et al., 2000). Among the various modifiers, Sr has been used extensively, as it is easier to handle and more resistant to fading and its recovery rate in the melt is usually of the order of 90%. In addition, it has been established that compared with Na, the rate of oxidation and loss from the melt is much slower and apparently Sr does not lead to over-modification (Liao, Sun, & Sun, 2002).

Strontium is added as an Al-Sr or Al-Si-Sr master alloy which also refines the Al-Si eutectic and results in castings having tensile properties comparable with those obtained when using sodium. Loss of strontium through volatilization during melting is much less and the modified microstructure can be retained if alloys are remelted. Another advantage of strontium additions is that they suppress formation of primary silicon in hyper-eutectic compositions which may improve their ductility and toughness. This effect is not observed when sodium is used (Polmear, 2006).

Most master alloys which are used commercially are binary alloys of Al-Sr such as Al-10 wt.% Sr, Al-10 wt.% Sr-14wt.% Si and 90 wt.% Sr-10 wt.% Al (Bian et al., 2000). They have low melting points and dissolve relatively easy in the melt. High Sr-containing master alloys are best used at low liquid temperatures due to exothermic dissolution while low-Sr master alloys are used at higher melt temperatures. (Drouzy, Jacob, & Richard (1980) investigated Al-7%Si alloy and reported that modification level increases with increasing of Sr content. They observed a fully modified structure when the Sr-content used was 0.0056 wt% but when the Sr-concentration is reduced below this level the modification level declined with increasing holding time as shown in Figure 2.6.

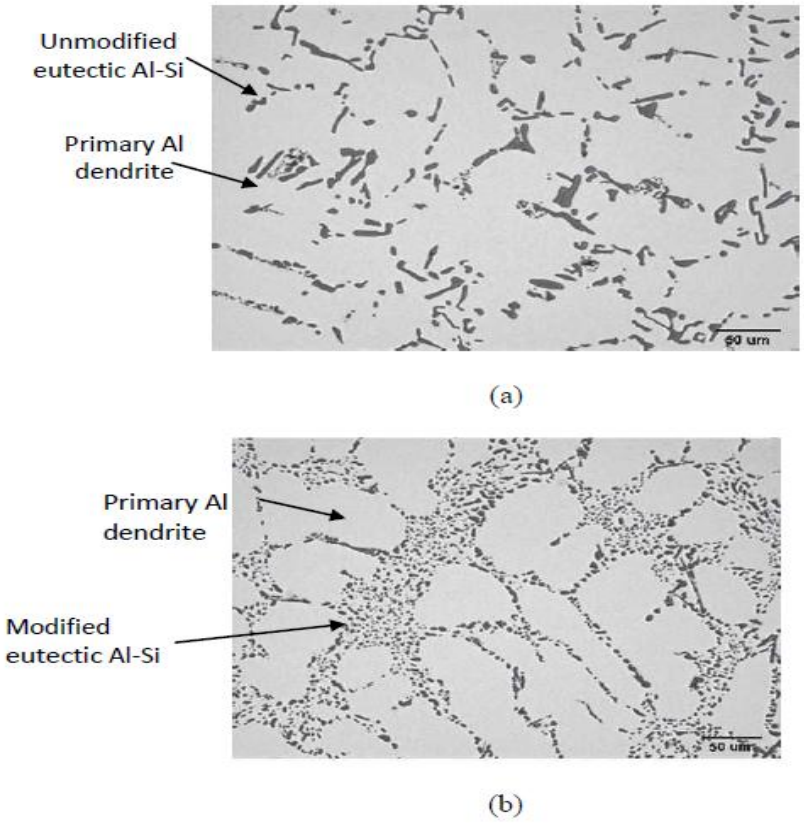

Figure 2.6: Al-7Si alloy (a) without a strontium addition and (b) with a strontium addition to refine the eutectic (Campbell, 2006).

2.5.6 Antimony (Sb)

The tendency toward gas pick-up and porosity formation in Al-Si modified by Na and porosity redistribution by Sr maybe disadvantageous in actual foundry practice (Moustafa et al., 2003). For this reason, Sb was introduced as alternative element for modifying the silicon eutectic (Hegde & Prabhu, 2008). The most important advantage of antimony is that it is stable in the melt and is not affected by holding time, remelting and degassing. Indeed, its losses are approximately zero. One drawback for Sb modification is that it is not compatible with other modifying elements and interacts with them in a negative manner. Moreover, Sb treatment is restricted to permanent mold applications and is not recommended for sand castings. It has been reported that Sb enhances the aggregation of the Si atoms, and promotes the nucleation of Si atom aggregates during the solidification of liquid Al-12.5 wt.%Si alloy, thus modifying the shape and size of the

Si phase in the solid state (Xiufang, Weimin, & Jingyu, 2001). In practice for hypoeutectic Al-Si alloys the optimum content for antimony is 0.10-0.15 wt.% (Tenekedjiev & Gruzleski, 1990).

2.6 Turning

2.6.1 Introduction

Turning is the machining operation that produces cylindrical parts. In its basic form, it can be defined as the machining of an external surface with a rotating workpiece, a single-point cutting tool feeding parallel to the axis of the workpiece and at a distance that will remove the outer surface of the work.

Turning is one type of metal cutting process used to produce cylindrical surface. During turning operation workpiece is rotated and tool will travel along workpiece rotation. The combination between workpiece rotation and tool motion will result in reducing workpiece size or diameter of workpiece. Figure 2.7 shows turning operations.

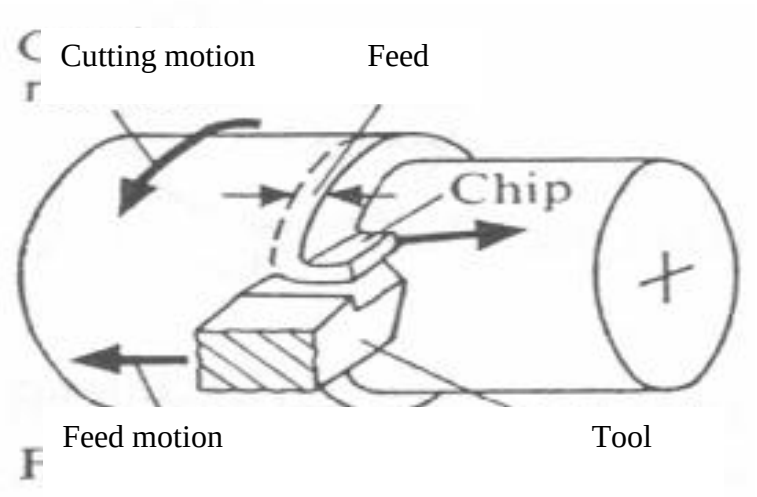

Figure 2.7: Turning operation.

The cutting speed (V) is the rate at which the uncut surface of the work passes the cutting edge of the tool, usually expressed in units of ft/min or m/min. The feed (f) is the distance moved by the tool in an axial direction at each revolution of the work. The depth of cut (w) is the thickness of metal removed from the bar, measured in a radial direction. Figure 2.8 shows the adjustable parameters in machining.

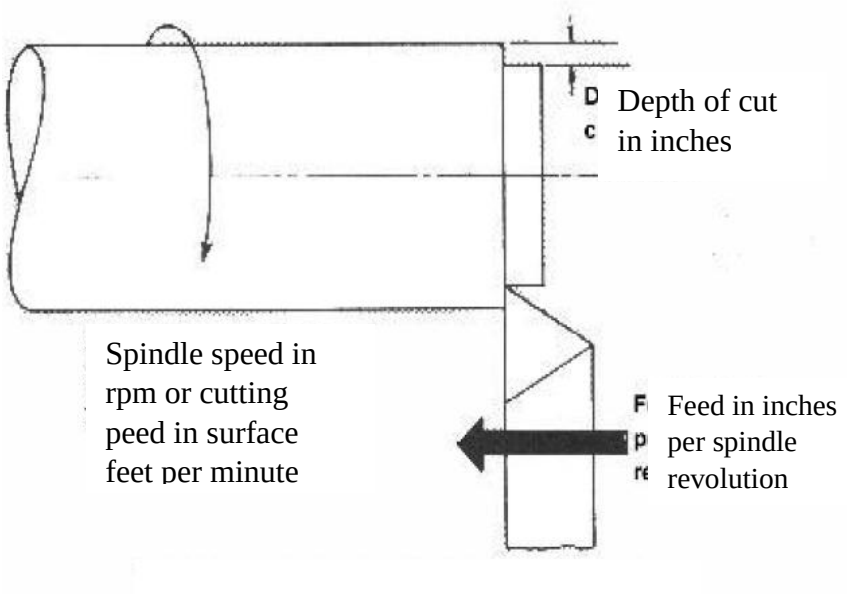

Figure 2.8: Turning and the adjustable parameters (Teti, 2002).

2.6.2 Theory of Metal Cutting

Machining is changing the geometry of work piece to produce desire shape by removing several materials. Generally, metal cutting operation is classified into two types of operation model; orthogonal cutting and oblique cutting, Figure 2.9 shows both orthogonal cutting and oblique cutting. Orthogonal cutting is an idealized case, where the cutting edge is straight and perpendicular with direction of tool travel (Figure 2.10a). When the cutting edge is not perpendicular with direction of tool travel the term oblique cutting is used (Figure 2.10b). Orthogonal cutting is simpler where it represents in two dimensions rather than three dimensions and is widely used in the cutting process analysis (Walker, 1969).

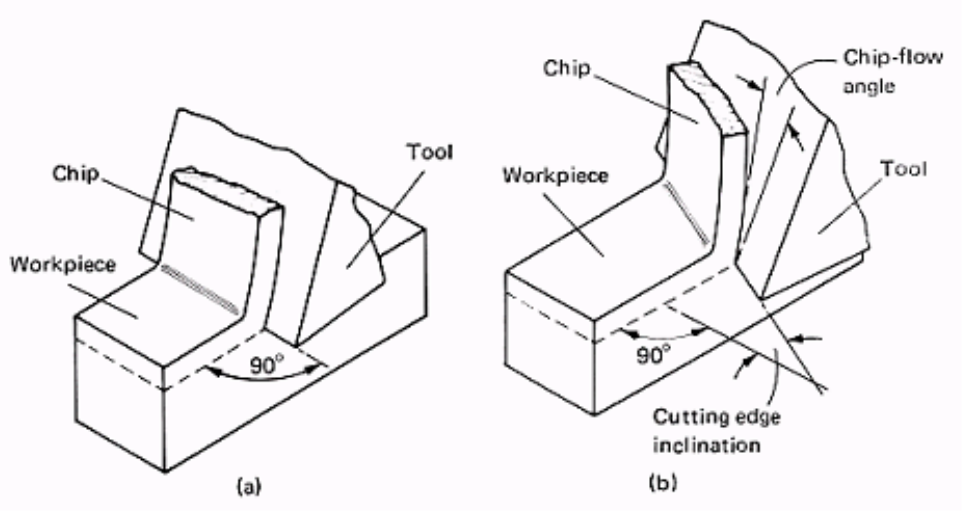

Figure 2.9: Orthogonal and oblique cutting, (a) orthogonal cutting, (b) oblique cutting (Walker, 1969).

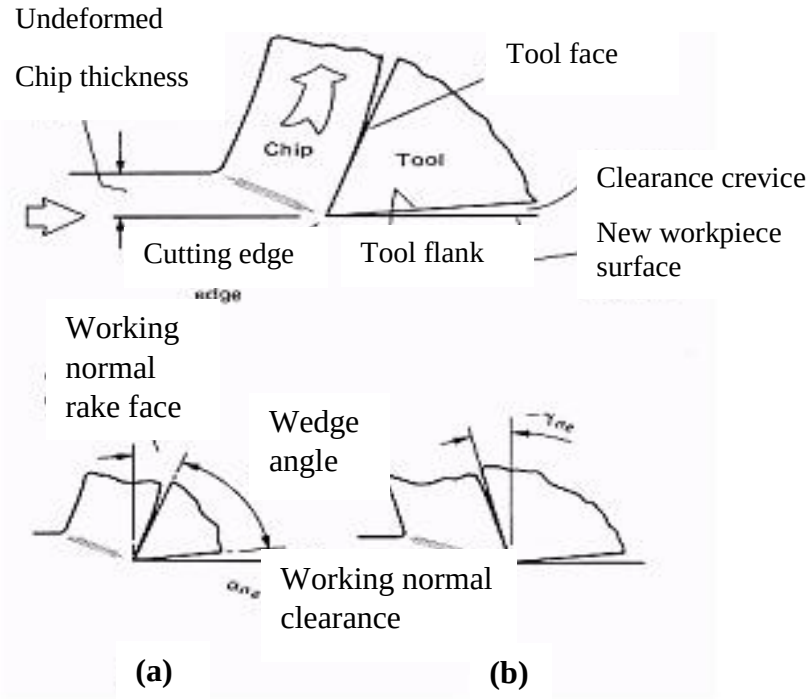

Figure 2.10 : Orthogonal (a) and oblique cutting (b).

The first complete analysis of the cutting process problem was proposed by Ernst and Merchant (Galoppi, Filho, & Batalha, 2006). Their analysis was successfully and more accurate than other analysis carried out by various researchers. Ernst and Merchant analysis is presented in Merchant force diagram (Figure 2.11), while their analysis assumptions used orthogonal cutting.

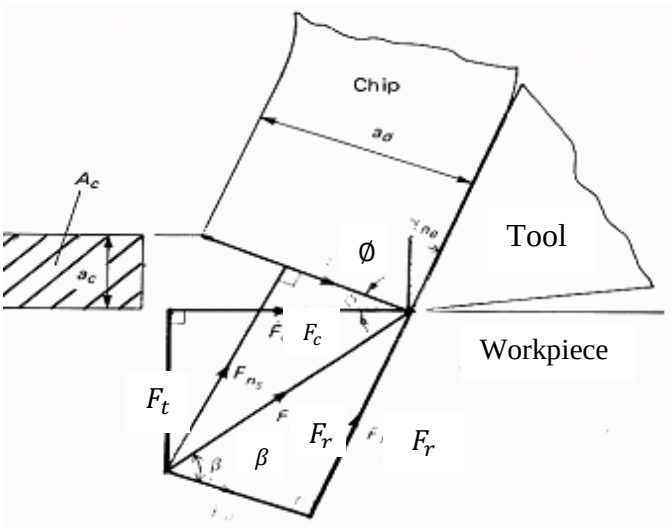

Figure 2.11: Merchant force diagram (Galoppi et al., 2006).

2.7 Cutting Tool Materials

Cutting tool materials in various ranges has been used in the industry for different kinds of applications. A large variety of cutting tool materials have been developed to cater to various programmers such as those found in the nuclear and aerospace industry (Shaw, 2005). Important characteristics expected in cutting tool materials are:

- Hardness higher than the workpiece material.
- Hot hardness where the tool should be able to retain hardness at elevated temperature.

- Wear resistance with high abrasion resistance to improve the effective life of the tool.
- Toughness to withstand the impact loads at beginning of the cut and force fluctuation due to imperfection of workpiece material.
- Low friction to allow lower wear rates and improved chip flow.
- Thermal characteristic where the tool material should have higher thermal conductivity to dissipate heat in shortest time.

These characteristics will give a better cutting performance. The continuous development in cutting tool will help to achieve these characteristic (Figure 2.12).

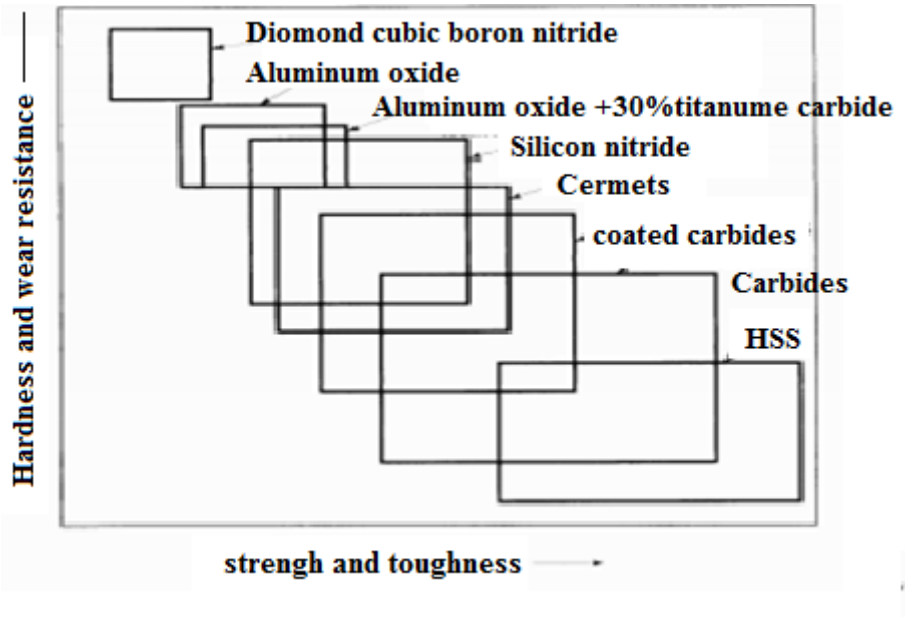

Figure 2.12: Common properties of cutting tool materials (Galoppi et al., 2006).

The various cutting tool materials commercially available today have ability to satisfy the demand of cutting tool properties such as high hot hardness, toughness, and chemical stability. Several cutting tool materials are developed for different applications and have different properties for these applications (Shaw, 2005).

-High speed steel (HSS)

The first HSS produced good wear resistance, toughness resistance to fracture, suitable for positive rake angle, and less expensive than non HSS tools. These tools will lose strength when temperature reach above 6500°C, but the coating development, especially TIN coatings, have several beneficial effects to minimize their weakness. HSS tool is often used for interrupted cutting, drilling, and taps (Stephenson & Agapiou, 2005).

-Carbides

Carbide tool is a compound of hard carbide particles, nitrides, borides, and silicide, bonded together with a binder such as cobalt. Tools have sufficient toughness, impact strength, and high thermal resistance but have limited hardness properties. The hardness of carbide tool drops rapidly in high temperature and as result it cannot be used in high cutting speed hence high temperatures are involved. At present, with the development of technology coated tools can improve the tool life of uncoated carbide tools (Wright, 2000).

-Coated carbides

Coating is believed to improve tool life and productivity as it can be used at higher cutting speeds and feed rates. The high hardness, wear resistance, toughness, and chemical stability of the coating tools offer benefits in term machining performance. With the development of coating technology, carbide tools have become more variant and sophisticated thereby improving the performance of carbide tools in metal cutting. In addition, PVD has three basic types of process, and these are arc evaporation, sputtering, and ion plating. These processes are carried out in a high vacuum with temperature between 2000C- 5000C. In PVD process the particles to be deposited are carried physically to the workpiece rather than chemical reactions as in CVD process (Kalpakjian & Schmid, 2009).

-**Chemical vapor deposition (CVD)**

CVD coated tools are a much newer product and consist of a pure diamond coating over a general purpose carbide substrate. Thin-film diamond coated inserts are deposited on substrates with PVD and CVD technique. Thick films are obtained by growing a large sheet of pure diamond, which is then laser cut to shape and brazed to a carbide shank. Diamond coated tools are particularly affective in machining nonferrous and abrasive material, such as aluminum alloys containing silicon, fiber-reinforced and metal-matrix composite material, and graphite. As much a tenfold improvements in tool life has been obtained compared to coated tools (Hua et al., 2005).

-**Polycrystalline diamond (PCD)**

Polycrystalline diamond has replaced the use of single-crystal diamond. These materials consist of very small synthetic crystals fused by a high-pressure, high-temperature process to a thickness of about 0.5 to 1 mm and bonded to a carbide substrate. The random orientation of the diamond crystals prevents the propagation of cracks through the structure, significantly improving its toughness (Walker, 1969).

2.7.1 Single Point Tools

Single point tools are tools having one cutting part. They are commonly used in lathes. Figure 2.13 shows turning geometry. There are various angles in single cutting tool and each angle has importance during turning operation.

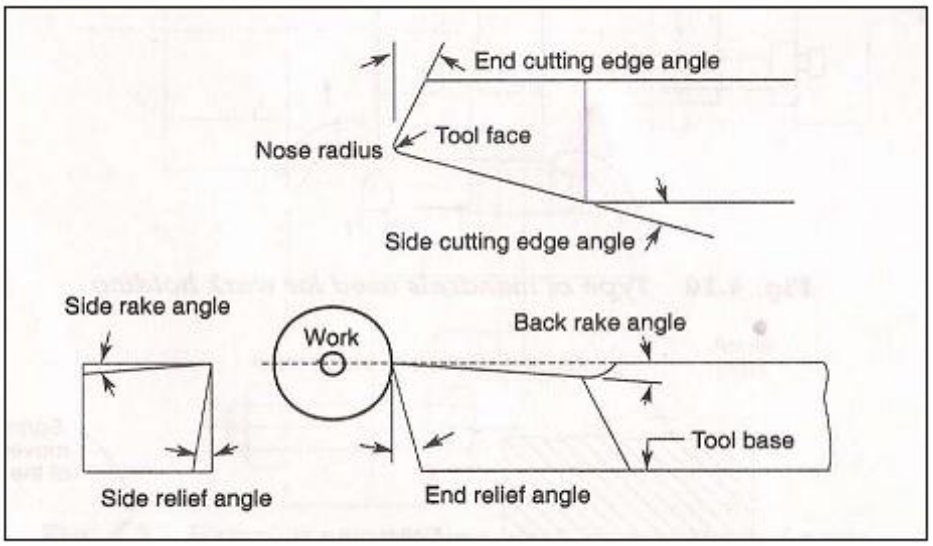

Figure 2.13: Tool designations for single point cutting tool (Jiang, More, Brown, & Malshe, 2006).

Rake angle will determine the direction of chip flow and the strength of the tool tips. While cutting force can be reduced with positive rake angle, the problem is that it will produce a small included angle of the tool tip (Bian et al., 2000). Relief angle will control the interference and rubbing of tool and workpiece. The tool may chip off if the relief angle is large while excessive flank wear will happen in the angle is small (Muthukrishnan, Murugan, & Prahlada Rao, 2008). Chip formation, tool strength and cutting forces are influenced by cutting edge angles. The surface finish is influenced by nose radius. Small value of nose radius will reduce surface roughness and strength of the tool while large nose radius will cause tool to chatter (Muthukrishnan et al., 2008). The tool angles and nose radius are specified in Figure 2.14.

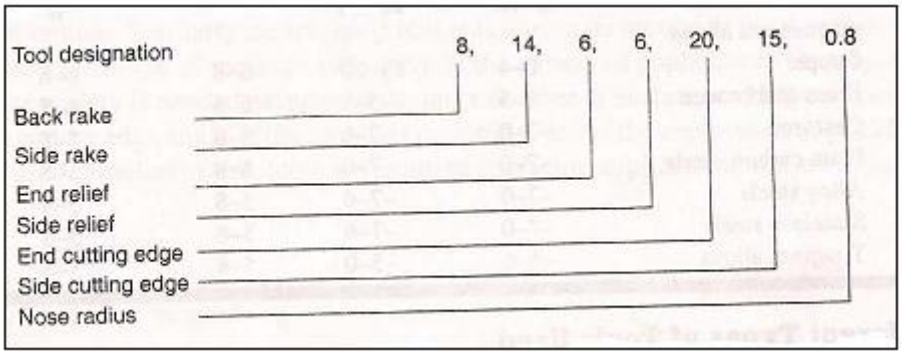

Figure 2.14:Tool designations for single point cutting tool (Zhang, Wang and Zhou, 2000).

2.8 Machinability Criteria

Machinability may be deemed an interactive phenomenon between work piece (material type and form), cutting tool (material type and geometry), and the cutting medium such as air and liquid, in a number of different removal sequences which include turning, milling, sawing, and cutting conditions (speed, feed, and depth of cut). In a collective sense, the significant terms, as related to the subject of machinability are (Davim, 2010) : (i) specific power consumed, cutting forces, and temperature rise; (ii) tool life, wear level, and fracture probability; (iii) chip control including chip breakability, chip shape, and built-up edge; (iv) dimensional tolerances in terms of surface roughness, microstructure; (v) and machining rate. All effort-related parameters are relatively more difficult to evaluate, but can often provide an explanation for good or bad machinability results.

2.8.1 Cutting Force

Cutting force is an important aspect in turning operation. There are three types of force action on cutting tool during turning operation (Figure 2.15). Cutting force F_c, also known as tangential force and the largest force of the three forces, acts in the direction of the cutting velocity. This force is used to determine the power requirement. Thrust force F_t, also known as feed force, acts longitudinally to feed motion. Radial force F_r, is the smallest of the force components and in most cases it is ignored.

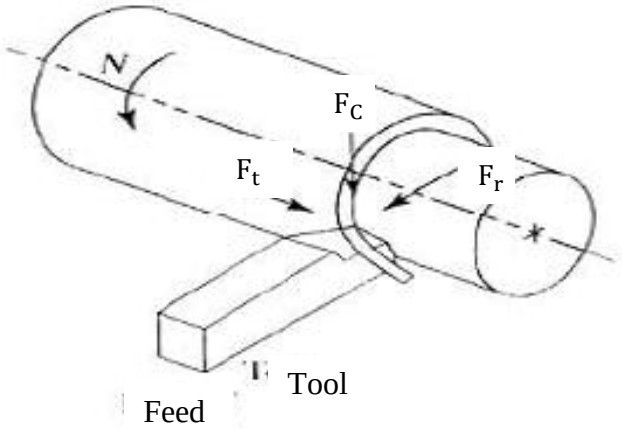

Figure 2.15: Force in turning

There are different theories and mechanical models for continuous and discontinuous chip formation. The behavior of materials during cutting processes in discontinuous chip formation is almost the same as continuous chip formation except that fracture occurs when the shear strain at the end boundary line repeatedly reaches the breaking limit as the cutting proceeds (Senthil Kumar, Raja Durai, & Sornakumar, 2003).

The geometrical resolution of the total cutting force is usually done by assuming that the chip is a solid body in stable mechanical equilibrium under the action of the forces exerted on it at the rake face and at the shear plane as suggested by Merchant on the basis of the following assumptions (Kalpakjian & Schmid, 2009) : (i) the chip is continuous

with no built-up edge, (ii) the tool tip is perfectly sharp, which leads to absolutely no contact between the machined surface and the flank of the tool, (iii) a perfectly planar shear plane, along which shearing occurs as the tool tip pushes into the material, extending from the tool tip to the chip root, (iv) the depth of cut is assumed to be very large with respect to the feed of cut, thus reducing the problem to one of plane strain, and (v) shear stress, strain and strain rates are all assumed to be uniform.

The relationship between the various forces determined by using these force diagrams is as follows (Shaw, 2005) :

$$F_s = F_c \cos\emptyset - F_t \sin\emptyset \quad (2.1)$$

$$N_C = F_c \sin\emptyset + F_t \cos\emptyset \quad (2.2)$$

$$F_f = F_c \sin\alpha + F_t \cos\alpha \quad (2.3)$$

$$N_f = F_c \cos\alpha - F_t \sin\alpha \quad (2.4)$$

where F_s is the shear force on the shear plane, F_c is the cutting force, F_t is the thrust force, N_s is the normal force on the shear plane, F_f is the shear force on rake face, N_f is the normal force on the rake face, $\emptyset$ is the shear angle, and α is the true rake angle of the cutting tool.

The coefficient of friction (μ) at the tool face can be computed as (Shaw, 2005):

$$\mu = \frac{F_f}{N_f} = \frac{F_c \sin\alpha + F_t \cos\alpha}{F_c \cos\alpha - F_t \sin\alpha} = tn\beta$$

Where β is the friction angle. (2.5)

The shear angle in Eqn. 2.1 is determined from a section of the chip by microscopic observations or by using the cutting ratio r, which is the ratio of the feed f (distance moved by the tool-bit along the workpiece revolution axis, per revolution of the

workpiece) to the chip thickness T_c (wall thickness of the tube being machined off) as is shown below (Totten & MacKenzie, 2003).

$$r = \frac{f}{t_c} = \frac{AB\ sin\emptyset}{AB\ \cos(\emptyset - \alpha)} \tag{2.6}$$

And

$$\emptyset = tan^{-1}\left(\frac{r.cos\alpha}{1 - r.sin\alpha}\right) \tag{2.7}$$

Where AB equals the length of the shear plane, and α is the rake angle of the tool.

2.8.2 Surface Integrity

Surface integrity in the engineering sense can be defined as a set of various properties (both, superficial and in-depth) of an engineering surface that affect the performance of this surface in service. These properties primarily include surface finish, texture and profile, fatigue corrosion and wear resistance, adhesion and diffusion properties. In addition, numerous investigations confirm that the quality and especially the lifetime of the dynamically loaded parts are very much dependent on the properties of the material in the surface (Basavakumar et al., 2007).

Severe failures produced by fatigue, creep and stress corrosion cracking invariably start at the surface of components and their origins depend to a great extent on the quality of the surface (Barzani, 2012). Therefore, in machining any component it is first necessary to satisfy the surface integrity requirements. Surface integrity refers to residual stress analysis, microhardness measurements, surface roughness and degree of work hardening in the machined sub-surfaces and they were used as criteria to obtain the optimum machining conditions that give machined surfaces with high integrity. (Janez, Grum & Kisin (2006) have defined surface integrity as the relationship between the

physical properties and the functional behavior of a surface. The surface integrity is built up by the geometrical values of the surface such as surface roughness, and the physical properties such as residual stresses, hardness and structure of the surface layers (Davim, 2010).

In fact, surface quality of the machined surface is one of the most important concerns in a machining operation. Surface roughness measurements and optically observed features on the finished surface give important information about the quality of the surface produced and hence about the machinability of the given alloy under the conditions used for the process. The surface roughness produced in turning depends on the feed rate, tool geometry, tool wear, and the material characteristics of the workpiece and the tool; it can be reduced by decreasing the feed rate and the depth of cut, increasing the cutting speed and the rake angle, and improving the workpiece material by adding free-machining additives or increasing the hardness (Kouam, Songmene, Zedan, Djebara, & Khettabi, 2013).

2.8.3 Tool Wear

Tool wear is a serious concern for manufacturers as it is necessary to avoid damage of the cutting tools, machine and work piece. Many researches have studied machining parameters effect on tool wear, and tool wear prediction. During turning of hard and high strength materials, tool wear becomes more likely and tool life becomes limited. As a result an optimized combination of machining parameters and proper tool material would result in a more efficient turning operation and accurate machining.

Today, there is a continuous struggle for cheaper production and better quality. This can be achieved through optimal utilization of both material and human resources. Machining operations play an important role in the word’s manufacturing infrastructure,

creating more than 20% of the value of all mechanical components manufactured worldwide. Researchers are working on machining operation to optimize cutting process because of its great economic and technical importance (Ren et al., 2010).

One of the most promising techniques for indirect detection of tool wear appears to be the measurement of cutting forces. The force signals are highly sensitive carriers of information about the status of the machining process, and hence are the best alternatives to tool wear monitoring. Tool wear influences machining quality, cutting power, tool life and machining cost. When tool wear reaches a certain value, increasing cutting force, vibration and cutting temperature may cause surface integrity deteriorated after machining process (Ciftci, Turker, & Seker, 2004c). The life of the cutting tool ends, and the cutting tool must be replaced which may interrupt the cutting process. Consequently, the cost and time require for tool replacement and adjustment of machine tools increases cost and decrease productivity. Hence, tool wear related to the economics of machining and prediction of tool wear is of great significance for optimization of the cutting process (Dursun Sedat Kilic, 2008).

2.8.3.1 Cutting Tool Wear and Measurement of Tool Wear

Cutting tool wear may be classified as follows: adhesive wear, abrasive wear, diffusion wear, fatigue, delamination wear, microchipping, gross fracture, and plastic deformation. The most frequently employed tool materials are: high speed steel (HSS), cobalt-enriched high speed steel (HSS-Co), sintered tungsten carbide (WC), polycrystalline cubic boron nitride (PCBN), polycrystalline diamond (PCD), and single crystal natural diamond (Kouam, Djebara, & Songmene, 2014). Diamond is of special interest because its properties are well suited for cutting-tool applications, such as extremely high hardness and high thermal conductivity. Low sliding friction dry

machining is possible for some aluminum alloys and cast irons. New coating materials can play a role in making dry machining practically feasible (Shaw, 2005).

ISO standard 3685:1993 is the standard for measuring wear from the wear experiments when using a single-point turning tool. The word "single-point" refers to the fact that the tool cuts the material with a single point. Figure 2.16 depicts a typical cutting tool use for turning operation (Axinte, Belluco, & De Chiffre, 2001).

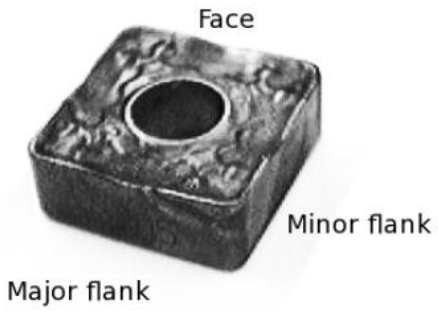

Figure 2.16: A typical cutting tool used for turning operation (Axinte et al., 2001).

From Figure 2.16, it can be seen that the tool consists of three important sides: the major flank, the minor flank and the face at the top. However, the ordering of the sides is dependent on the application. Major flank is the cutting edge, while minor flank faces the newly cut surface and the face receives the material being cut and forms chips. The type of cutting tool presented in Figure 2.16 has four usable cutting edges, one on each side of the tool. The standard also defines four definitions which will be used in most research works as they are defined in the standard (Bardetsky, Attia, & Elbestawi, 2005) :

- Tool wear: The change of shape of the tool from its original shape, during cutting, resulting from the gradual loss of tool material or deformation.

-Tool wear measure: A dimension to be measured to indicate the amount of tool wear.

-Tool-life criterion: A predetermined threshold value of a tool wear measure or the occurrence of a phenomenon.

-Tool life: The cutting time required to reach a tool-life criterion.

According to the ISO standard 3685:1993, there are multiple types of wear and phenomena which can cause tool-life criterion to be fulfilled. Most important of the wear types are flank wear and crater wear (Bardetsky et al., 2005). Flank wear is present in all situations and it is the best known type of wear. It can be found on the major flank of the tool. Crater wear appears on the face of the tool as a crater. Crater wear is the most commonly found wear on the face of the tool. The wear process itself changes under the influence of different conditions. However, three main factors contributing to the wear are known (Davoodi & Eskandari, 2015) : adhesion, abrasion and diffusion. Adhesion occurs when the work material, that the tool is cutting, welds onto the tool. This happens because of the friction between the tool and work material, which generates heat. When these welds are broken, small pieces of the tool are lost (Ciftci, Turker, & Seker, 2004). Abrasion is mechanical wear resulting from the cutting action, where the tool grinds itself on-to the work material. Diffusion wear occurs on a narrow reaction zone between the tool and work material (Ciftci et al., 2004).

In diffusion wear the atoms from the tool move to the work material. This usually accelerates the other two wear processes as the tool material is weakened (Patel & Joshi, 2006). Figure 2.17 shows the general curves of flank wear. The wear is typically characterized by rapid initial wear, a linear increase of the wear in the middle of the tool life and finally a rapid increase of the wear rate before the tool breaks completely (Patel & Joshi, 2006).

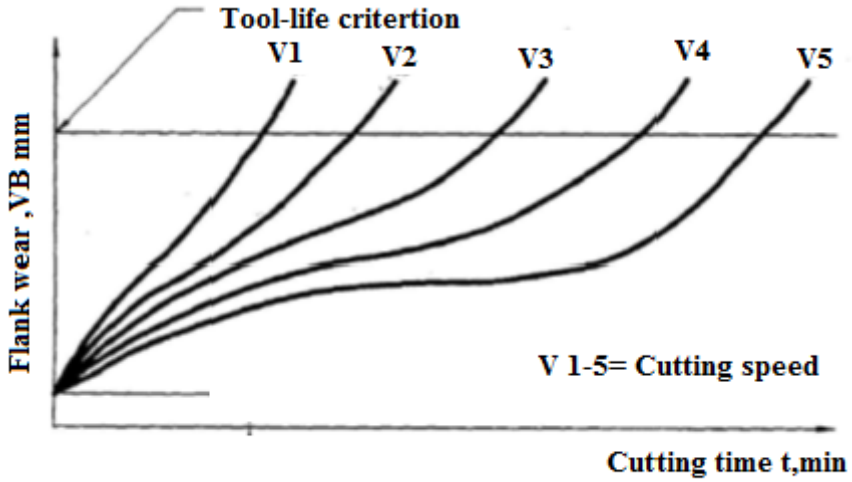

Figure 2.17: Flank wear progress as a function of time (Axinte et al., 2001).

While the general shape of the curve stays the same, cutting conditions or cutting parameters affect the tool life, i.e. the gradient of the curve, especially the linear section. Cutting speed and feed rate are two important parameters in relation to tool wear. The cutting speed is usually expressed in meters per minute and can range up to 500 m/min (Nouri, Fussell, Ziniti, & Linder, 2015). The standard gives a limit to the cutting speeds by limiting the minimum tool life to 5 minutes or to 2 minutes when using a ceramic tool. The cutting feed is expressed as millimeters per revolution, ranging from 0.1 to 0.9 mm/rev (Nouri et al., 2015). Standard has defined the maximum feed to 0.8 times the corner radius of the tool (Songmene, Kouam, Zaghbani, Parson, & Maltais, 2013).

To be able to measure the wear, especially flank wear, a few variables must be known. Most important variables are r_ϵ (corner radius) and b (depth of cut). In Figure 2.18 the tip or nose of the tool viewed from the top is shown.

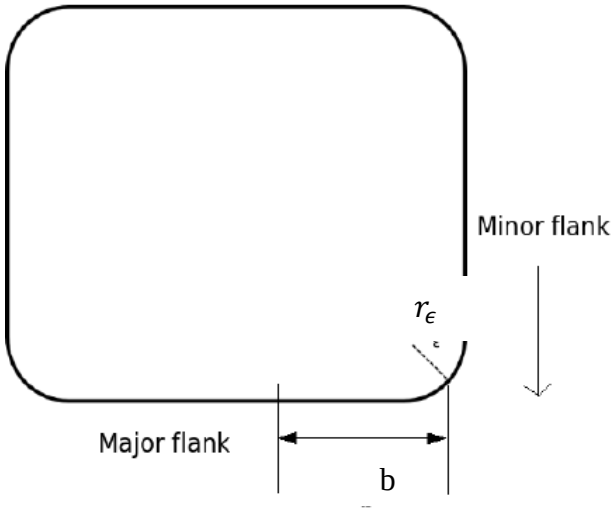

Figure 2.18: Top view of a tool showing the nose section.

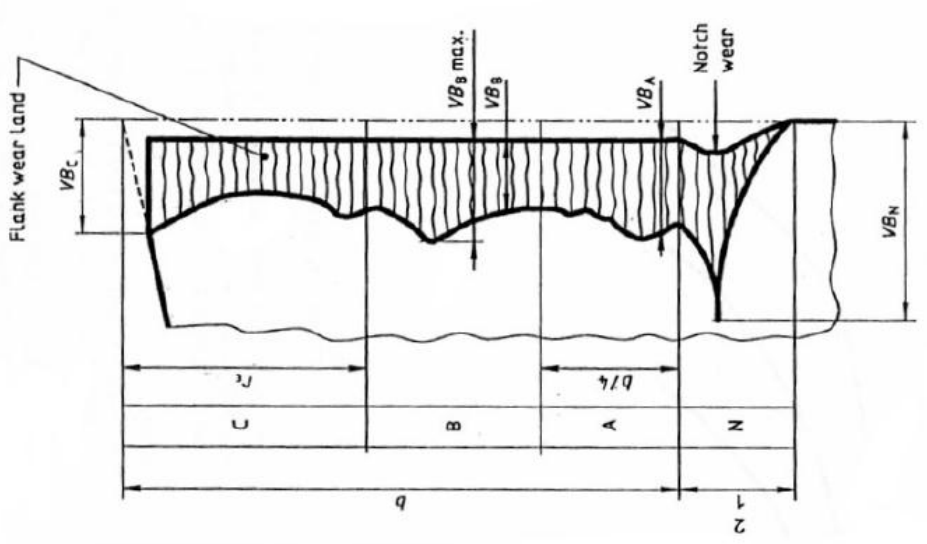

Figure 2.19: Measurement of flank wear (Axinte et al., 2001).

In Figure 2.19, VB_B max and VB_A are the most important factors to measure wear, as they are designated in the standard (Axinte et al., 2001). Besides these most important measures, also VB_C is measured, which is considered to be the maximum wear width in zone C. VB_B and VB_B max show the tool-life by following criteria:

The first is the maximum width of the flank wear land where VB_B max. = 0.6 mm if the flank wear land is not regularly worn in zone B, and the second is the average width of the flank wear land where VB_B = 0.2 mm if the flank wear land is considered regularly

worn in zone B. The measurements are commonly done by hand using a microscope. In the standard manual measurement is defined as the way to measure the wear. It has published that the available methods for tool condition monitoring can be divided into two parts: direct and indirect sensors (Kerr, Pengilley, & Garwood, 2005). Direct sensors are sensors which measure the tool wear directly. These sensors include vision, proximity and radioactive sensors. Proximity sensors estimate the wear by measuring the distance between the workpiece and tool edge. Direct measurements can usually be taken only between the machining runs, because the major flank of the tool is not visible during actual machining. Indirect sensors can only estimate the wear as they have no direct way to measure the actual wear, but instead they rely on secondary effects of the wear, such as increase in cutting forces.

2.8.3.2 Effect of Tool Wear on Technological Performance

Flank wear and chipping of the cutting edge affect the performance of the cutting tool in various ways. The cutting forces are normally increased by wear of the tool. Crater wear may, however, under certain circumstances, reduce forces by effectively increasing the rake angle of the tool. Clearance-face wear and chipping almost invariably increase the cutting forces due to increased rubbing forces (Qin, Zhao, & Zhou, 2008) .

Dimension accuracy flank wear influences the plane geometry of a tool. This may affect the dimensions of the component produced in a machine with set cutting tool position produced in an operation utilizing a form tool. Vibration or chatter is another aspect of the cutting process which may be influenced by flank wear. A cutting operation which is quite free of vibration when the tool is sharp may be subjected to an unacceptable chatter mode when the tool wears (Bardetsky et al., 2005).

2.8.4 Different Chip Formations

Parts manufactured by casting, forming and other shaping processes often need to be machined to its final shape and dimensions with one or more of the processes listed in Table 2.3. Turning, milling and drilling are the three most common types of machining operations. In the turning process, a wedge-shaped cutting tool that consists of two surfaces intersecting to form the straight cutting edge is used. The surface along which the chip flows is termed the rake face, and the surface that contacts the new or machined workpiece surface is known as the flank face.

The turning process is an example of orthogonal cutting, which is a two-dimensional process. Therefore, it has been widely used in theoretical and experimental work (Grzesik, 2008). Turning is the process studied in this research, and thus, the principles of this operation and the factors that determine the orthogonal turning performance will be explained in detail.

Table 2.3: Range of material-removal processes (Stephenson & Agapiou, 2005).

Cutting		Abrasive		Nontraditional
Circular	Various	Bonded	loose	Chemical machining
Turning	Milling	Grinding	Ultrasonic machining	Electrochemical machining
Boring	Planning	Honing	Abrasive-jet machining	Electrical grinding
Drilling	shaping	Coated abrasives	Lapping	Electrical –discharge machining
	Broaching		polishing	Laser-beam machining
	Sawing			Electron-beam machining
	Filing			Hydrodynamic machining

The important process variables of orthogonal turning are the cutting speed (generally expressed in units of m/s), and feed (generally expressed in units of mm/rev). Correspondingly, the force F exerted by a cutting tool has three mutually perpendicular components as shown in Figure 2.20 (a). The coordinate system is oriented along the directions of primary and feed motions, i.e. the total force is resolved into the perpendicular projection of these two directions into the cutting force and feed force denoted by symbols F_c and F_t. Moreover, there is a back force F_p tending to push the tool away from the workpiece in a radial direction perpendicular to the working plane (Grzesik, 2008)This force is usually ignored for orthogonal cutting. As can be seen in Figure 2.20 (b), in orthogonal cutting, the entire force system lies in a single plane and the appropriate force components can be easily calculated by drawing the Merchant circle diagram (Grzesik, 2008).

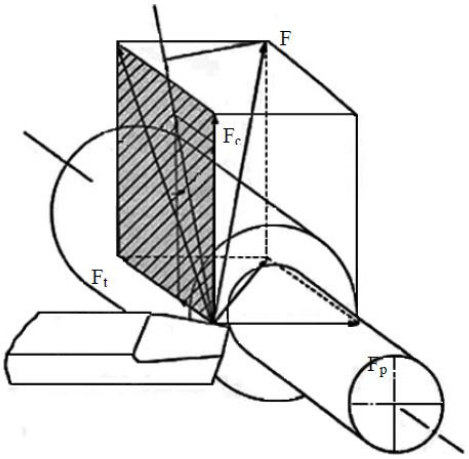

(a)

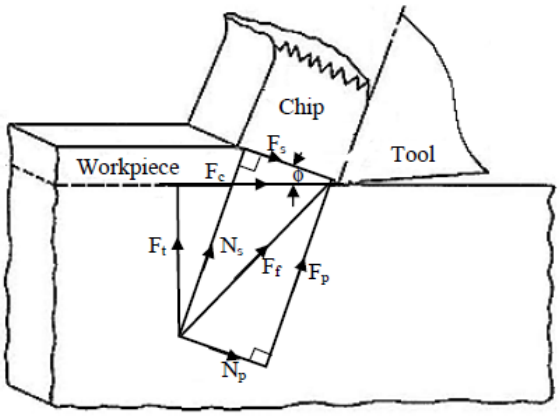

(b)

Figure 2.20: Force resolution in the cutting zone for orthogonal cutting (a) Geometrical force resolution in the cutting zone for orthogonal cutting with a continuous-type chip, (b) physical force resolution in the cutting zone for orthogonal cutting with a continuous Type chip (Grzesik, 2008).

Continuous chips are long and ribbon-like, generally produced during the machining of soft, ductile materials such as 6061 Al and copper (Gallab & Sklad, 2004). These long chips may lead to operational hazards as they may get tangled around the tool or workpiece. High speeds, small feeds and small depths of cut are conditions that favour the generation of continuous chips. Discontinuous chips are fragmented chips formed by the chip breaking into small segments due to cyclic fracturing, generally encountered

during the machining of brittle materials such as cast iron and some Al-Si alloys (Pratibha, 2010).

2.8.5 Discontinuous Chip Formation

The transition from continuous to discontinuous chip formation depends on the thermo-physical properties and the metallurgical state of the workpiece material, as well as on the cutting process (Dabade & Joshi, 2009). Chips become more segmented (discontinuous) with decreasing cutting speeds and increasing feeds (Palanikumar & Karthikeyan, 2007). Low rake angles, rigidity of tool, high feed rates and the presence of in-homogeneities in the workpiece material like second phase particles, lead to the formation of discontinuous chips in metals. For a completely homogeneous material, the transition from continuous to discontinuous chips would be abrupt. However, it would be rather gradual for a non-homogeneous material. At lower speeds, fractures produced in the chips are almost complete and deep, leading to the formation of segmented chips

Kannan & Kishawy (2006) explained the steps in the formation of discontinuous chips based on the single shear plane concept. The chip formation process starts at a high shear angle, which is followed by the sliding of the chip onto the rake face, which in turn leads to an increase in the frictional force deterring the motion of the newly formed chip that causes it to bulge, and there is a simultaneous decrease in the shear angle. The strain along the shear plane increases constantly while the bulging occurs, until it reaches the point of ductile shear fracture, as shown in Figure 2.21. This fracture leads to the formation of segments similar to saw-teeth. This process continues cyclically leading to discontinuous or serrated chip formation.

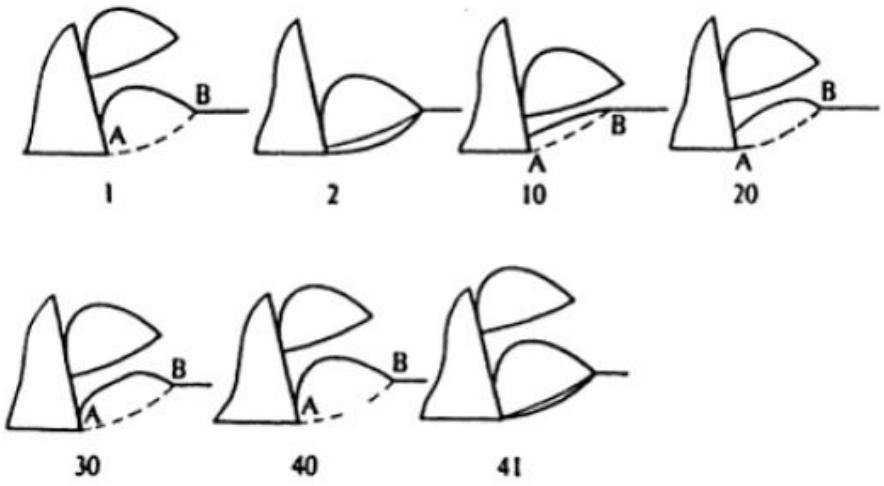

Figure 2.21: Formation of discontinuous chips when cutting brittle material (Kannan & Kishawy, 2008).

Pedersen & Ramulu (2006) presented a review of the several flow localization processes taking place during cutting processes. The adiabatic shear deformation theory of discontinuous chip formation suggests that saw-toothed chips are formed primarily due to a catastrophic thermoplastic instability in the material being cut which is characterized by a decrease in the flow stress due to thermal softening that is associated with an increase in strain, which more than offsets the effects of the associated strain hardening (Seeman, Ganesan, Karthikeyan, & Velayudham, 2009). It was found that during the orthogonal cutting experiments on titanium alloys extremely high temperatures developed in them are due to the substantially high cutting pressure and extremely low thermal properties, which cause the heat to be accumulated in a thin layer at the chip/tool contact (Pérez-Prado, 2001).

2.9 Dry Machining of Cast Aluminum Alloys

Hypoeutectic alloys generally contain less than 12 % silicon and are easy to machine at low speeds, as the silicon present in them is in the eutectic phase, and primary silicon is absent (Barzani, Sarhan, Farahani, & Singh, 2015). However, machining may be accompanied by occurrence of BUE in some cases. Hypereutectic aluminum alloys

have a silicon content of more than 12 %. They have large primary silicon particles, which lead to abrasive wear of the tool used for machining, with the degree of abrasion rising with an increase in the silicon content in the alloy (Roy, Sarangi, Ghosh, & Chattopadhyay, 2009). In addition to the cutting forces being high for these alloys, they cannot be machined using carbide tools, which are more economical than diamond-based PCD tools, because the larger silicon particles lead to faster tool wear. Few results based on the examination of the near-dry machining of aluminum alloys have been reported and these are summarized below.

Gallab & Sklad (2004) studied surface roughness machining of Al/20%Si using polycrystalline diamond tools (PCD) for cutting test. They reported that surface roughness improves with increasing feed rate and cutting speed, but slightly deteriorates with an increase in depth of cut. It is found that machining this type of composite is most economical and safe at a speed of 894 m /min, a depth of cut of 1.5 mm and feed rates as high as 0.45 mm/ rev, when the surface roughness, Rmax, does not exceed 2.5 mm.

Manna & Bhattacharyya (2002) investigated the machinability of Al/SiC. They used uncoated tungsten carbide (wc) and test results show that value of both surface roughness heights Ra and Rt ranged from 0.25 mm/rev to 0.75 mm/rev, the value of surface roughness height Ra increased by 40% whereas when cutting speed is tripled from 60 to 180 m/min the value of surface roughness height Ra decreased by 46%. Hence, it indicates that the cutting speed and feed has equal influence on the surface finish if both are increased simultaneously.

Andrewes, Feng, & Lau (2000) investigated dry machining of the aluminum alloy A380, which produced discontinuous chips during orthogonal machining. The equivalent plastic strain of 1.5 near the shear bands, the shear strain value of 12 in the shear band, and the flow stress of 285 MPa can be regarded as initial failure prediction values. Basavakumar et al. (2007) investigated the influence of melt treatments (grain refinement

and modification) and turning inserts (un-coated, PVD and polished CVD diamond coated) on the cutting force and surface integrity when turning Al-12Si and Al-12Si-3Cu cast alloys under dry conditions using a lathe machine. They found that the combined addition of a grain refiner and a modifier (Al–1Ti–3B-Sr) to the Al–12Si–3Cu cast alloy lowered the cutting forces and improved the surface finish, in contrast to untreated alloys. They also found that the performance of the polished CVD diamond-coated insert (compared to PVD and un-coated inserts) resulted in lower cutting forces and workpiece surface roughness.

It has been published that the natural diamond and polycrystalline diamond (PCD) can be used as a cutting tool when the required shape is attached on the edge/tip for machining non-ferrous materials. However, both are limited for finishing cut because of high cost. Thus, CVD diamond coated tool was a better option to machine these materials, and it was free from built-up edge formation leading to clean cut, low magnitude of cutting forces and improved surface finish of the work-piece (Roy et al., 2009).

Arumugam, Malshe, & Batzer (2006) studied CVD diamond coated cutting tools and PCD tools and uncoated carbide tools in machining. Results have shown that the main advantages were the possibilities of using multiple edges per tool insert and advanced chip breaker technology. Compared to an uncoated carbide tool, the CVD diamond coated insert illustrated much larger abrasive wear resistance, less built-up edge and a lower cutting forces, resulting in a much improved surface finish.

Ozben, Kilickap, & Çakır (2008) analyzed tool wear and surface roughness in machining of homogenized SiC-p reinforced aluminum metal matrix composite. Two types of K10 cutting tool (uncoated and TIN-coated) were used at different cutting speeds (50, 100 and 150 m/min), feed rates (0.1, 0.2 and 0.3 mm/rev) and depths of cut (0.5, 1 and 1.5 mm). Surface roughness influenced cutting speed and feed rate. Higher cutting speeds and lower feed rates produced better surface quality.

Tan et al. (1995) studied cutting forces, wear and surface roughness when machining 52100 bearing steel 64 HRC. The CBN tool with honed edge (0.8 mm nose radius) was used. Three different cutting speeds (44.5, 144.5 and 83 mm/min) and feed rate (0.039, 0.210, 0.216 mm/min) were used. Depth of cut (2 mm) was kept constant. Thrust cutting force on the tool is greater than other cutting forces when depth of cut less than 0.4mm. But at depth of cut greater than 0.4mm, the tangential cutting force was the highest. The main, feed and thrust cutting forces were increase when flank wear increase. All cutting forces reduced with the increased of cutting speeds.

Noordin, Venkatesh, Chan, & Abdullah, (2001) investigated cutting forces when turning automotive AISI 1010 steel with hardness 131 HV. Two types of coated tungsten based cemented carbide inserts (CVD with TICN/ TIC/Al2O3, CVD with TICN/ TIC and PVD with TIN) and an uncoated titanium based cemented carbide insert were tested. All the inserts have identical geometry (0.8 mm nose radius). For Insert 1, the tangential force increased when the cutting speed was increased from low to medium. The force decreased when the cutting speed was at the maximum. For Insert 2, the tangential remained constant when the cutting speed was increased from low to medium and decreased when the cutting speed was at maximum. For insert 3, the tangential force decreased when the cutting speed was increased from low to medium. The force decreased more sharply when the cutting speed was increased to the maximum. They have concluded that the tangential force was much higher than the other forces (feed and radial forces) at any particular experimental test.

Gallab & Sklad, (2004) studied machining of Al-SiC particulate metal-matrix composites using a series of dry high-speed turning tests to select the optimum tool material, tool geometry and cutting parameters for the turning of 20%SiC: Al metal-matrix composites. The results indicated that polycrystalline diamond tools (PCD) provide satisfactory tool life compared to alumina and coated-carbide tools. Furthermore,

the cost of PCD tools could be justified by using dry cutting at feed rates as high as 0.45 mm/rev, cutting speeds of 894 m/min and a depth of cut of 1.5 mm. PCD tools sustained the least tool wear compared to TIN coated carbide tools and Al2O3TiC tools. It was due to PCD's superior hardness and wear resistance, as well as low coefficient of friction, together with high thermal conductivity.

Muthukrishnan et al. (2008) investigated the machinability of Al-SiC metal matrix composites using PCD inserts. It was observed that the 1600 grade PCD inserts performed well from the surface finish and specific power consumption points of view closely followed by the 1500 grade. For all the three grades of PCD inserts and for the chosen cutting conditions, the surface finish was found to be superior at higher cutting speeds and at lower feed rates with compare carbide insert. It has been concluded that dry machining produced the highest degree of aluminum adhesion with a significant amount of the workpiece material adhering to the flank, clearance and rake faces during the milling of 319 Al. On the other hand, in the case of MQL (10 ml/h) milling, moderate adhesion (discontinuous areas) was found on the flank, rake and clearance surfaces.

2.9.1 Selection of Free Machining Constituents in Aluminum Alloys

Free machining Al alloys typically include elements such as lead, tin, and bismuth (Table 2.4) have been used for improved machinability by promoting the formation of shorter chips (Basava Kumar, 2007). The presence of a low melting eutectic constituent in the microstructure of an aluminum alloy seems to be a viable way to form small chips. Although the addition of low melting point elements to aluminum alloys can improve their machinability, this causes hot shortness by the low melting metals (Bardetsky et al., 2005). A hot tear is one of the most serious defects that a casting can suffer. Low-melting second phases could weaken grain boundaries by depressing the solidus temperature of the metal and prolonging liquid film life. Long freezing range alloys are more susceptible

to hot tearing due to the fact that they tend to remain in the semi-solid state for a considerable period after pouring, and thereby permit any tensile/shear stresses arising due to contraction restraints to propagate cracks/tears (Bardetsky et al., 2005).

Table 2.4: Properties of bismuth, indium, lead and tin (Bardetsky et al., 2005).

Element	Atomic number	Atomic weight	Melting point °C	Boiling point °C	Specific gravity
Bi	83	208.98	271.3	1560	9.747
In	49	114.82	156.61	2000	7.31
Pb	82	207.19	327.5	1744	11.35
Sn	50	118.69	231.89	2270	7.31
Cd	48	112.40	320.9	765	8.65

If a low melting point element is to be a suitable chip-breaking additive, it should meet the following requirements (Kalpakjian & Schmid, 2009) :

(i) The solubility of the additive in the solid matrix must be low, and must cause granular micro-segregation in the aluminum alloy.

(ii) It should not form a high melting point intermetallic compound with the base metal nor with the other important alloying element.

(iii) The liquid inclusions must not wet the grain boundaries (their dihedral angle should be larger than 600, otherwise a continuous network of liquid would be present along the grain edges and the alloy would be severely hot-short).

For example, in Al-Pb alloys, the liquid Pb phase wets the grain boundaries during the failure process. In Al-Cd alloys, the liquid Cd at the grain boundaries does not wet and spread, but remains as compact globules (machovec, 2000). These alloys therefore

fail by a more ductile type of fracture. However, Cd cannot be added as an alloying element because of its toxic properties (Kamiya, Yakou, Sasaki, & Nagatsuma, 2008). Also, indium is more expensive than the other low melting point elements, and therefore, bismuth and/or tin are the preferred additives over Pb, In and Cd. Under suitable machining conditions, it has been suggested that the Bi, Sn and Pb act as internal lubricants by forming a viscous layer, and also as a diffusion barrier between the tool and the chip, thereby prolonging tool life and improving productivity (Kamiya et al., 2008). Their globules do not adversely affect the strength or the hardness of the casting but enable surfaces of the casting to be machined without the use of a coolant or a lubricating machining fluid (Dasch et al., 2009).

2.10 Summary

Increasing environmental concerns over the use and disposal of coolants and lubricants, and their high costs, mandate the reduction of coolant and lubricants used during machining. The increasing thrust towards dry machining has seen frequently attempts to machine aluminum alloys without lubricants. However, their high thermal conductivity leads to unwanted deformation of the surface produced and the increased adhesion of workpiece material. This makes the surface characteristics that are obtained without use of lubrication a continued subject of concern for the industry. Modification of eutectic silicon in Al-Si-Cu-Mg alloys is induced by modifier additions to alter the morphology of Si from flake to fibres and enhance the mechanical properties. There is extensive published literature available on addition of modifiers such as Ca, Sr and Ba in Al-Si alloys, however, there is very little data describing the effect of Bi and Sb as well as Sr on mechanical properties and machinability of Al-11Si2Cu-Mg. A thorough understanding of all the metallurgical factors affecting the machinability of aluminum

alloys will promote the optimum machining combinations essential to sustained productivity.

Therefore, having an understanding of these alloys' machinability is imperative when it is necessary to fabricate some industrial products which are produced by casting process. The aim of this study is to investigate the machinability of Al-Si-Cu alloys containing 0.1%wt bismuth (Bi), 0.5%wt antimony (Sb) and 0.04%wt strontium (Sr) subjected to dry turning using coated carbide inserts.

CHAPTER 3: RESEARCH METHODOLOGY

3.1 Introduction

Proper experimental plan is necessary to achieve good results in conducting research. In this chapter, the experimental methods that were used in this work are outlined, namely casting, machining and metallographic analysis. Figure 3.1 shows the summary of the overall methodology. Al-Si alloys which have extended applications in automotive components were cast by permanent mold. The mechanical properties of the alloys were experimentally determined. Dry turning experiments that were performed on these different melts are described here in detail, and the chip morphology, tool wear, surface roughness and the cutting forces during dry turning were systematically measured.

The casting process of the Al-Si alloys that was employed in this work is discussed in Section 3.2. The evaluation of mechanical properties including tensile, impact tests and hardness of selected samples along with examination of the corresponding fracture surfaces are conducted in section 3.3. Cutting parameters and the cutting tools and samples used for the dry turning tests are described in Sections 3.4. The methods used to perform metallographic analysis are discussed in Section 3.5. The method used to measure surface roughness and cutting forces in the dry turning tests are presented in Section 3.6 and 3.7, respectively. The method of measuring tool wear during dry turning is described in Section 3.8. The characterization of the chip morphology and cross-sections of chips are described in Sections 3.9.

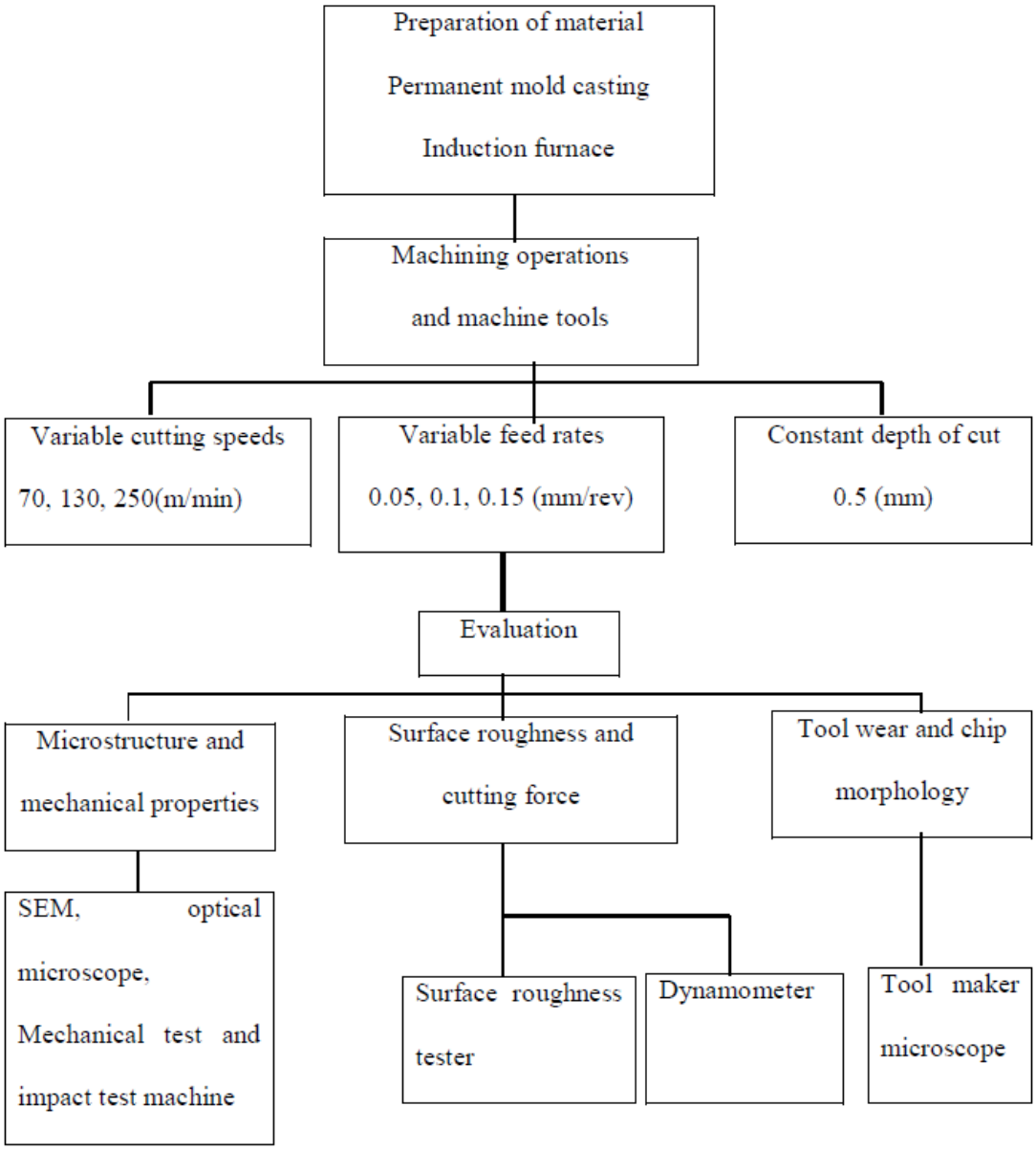

Figure 3.1: Summary of the overall research methodology.

3.2 Casting Process

Tow furnaces were used together, one for preheating the permanent molds, and the other for melting the aluminum alloy, with an induction furnace (Figures 3.2 and 3.3). Initially, the material was cut into small pieces, dried, and melted in a 2 kg SiC crucible using an electric resistance furnace. Then a weighted bismuth, antimony and strontium in the form of pure metallic shots (99.99 wt.%), pure metallic granules (99.99 wt.%, and an Al–10Sr rod master alloy, respectively, were introduced separately into the fully molten alloy. The levels of Bi and Sb were selected based on optimum concentration for each additive and where determined using a combination of microscopic inspection.

The optimal concentration for modifying or refining the eutectic Al–Si phase with Bi and Sb and Sr were 1 wt%, 0.5 wt% and 0.04 wt%, respectively. Addition elements were first wrapped in aluminum foil and then plunged into the melt to ensure that they dissolved properly and evenly throughout the melt before being stirred with zirconia coated steel rod for approximately 30s for better dissolution. Table 3.1 shows Chemical compositions of the fabricated workpieces (wt.%).

After adding the additive elements, the molten metal was kept for 15 min for complete melt homogenization. Prior to casting, the alloys were stirred and the surface was skimmed to remove dross and other impurities. The molten alloy was then poured at a temperature of 730 °C (±5 °C) into cylindrical permanent molds to fabricate workpieces. Four workpieces were prepared as solid bar with 90 mm diameter and 200 mm length. The chemical composition of Al–Si–Cu–Fe die cast alloy is shown in Table 3.1.

Figure 3.2: Firing furnace for preheating the permanent mold

Figure 3.3: Induction furnace for melting ingot

Table 3.1: Chemical compositions of the fabricated workpieces (wt.%).

Element	Si	Cu	Zn	Fe	Mn	Mg	Ni	Cr	Bi	Sb	Sr	Al
Base alloy	11.3	1.99	0.82	0.35	0.33	0.27	0.06	0.036	-	-	-	Bal
Bi-containing	11.2	1.65	0.82	0.41	0.35	0.28	0.04	0.32	0.85	-	-	Bal
Sb-containing	11.3	1.82	0.80	0.43	0.31	0.25	0.6	0.030	-	0.42	-	Bal
Sr-containing	11.2	1.65	0.80	0.43	0.32	0.27	0.6	0.32	-	-	0.45	Bal

3.3 Mechanical Properties Testing

3.3.1 Impact and Tensile Test

Samples for mechanical property testing were produced using gravity permanent metal mold casting technique. Figure 3.4 and 3.5 show Instron universal mechanical testing machine, and Zwick impact testing machine.

Both cylindrical tensile bars corresponding to ASTM B-108 type of impact Charpy test and tensile bars specimens were produced as shown in Figure 3.6(a) and Figure 3.6(b). A high frequency induction furnace was used as the melting unit. The raw materials were melted in a graphite crucible with a maximum capacity of 5 kg and the melt temperature was precisely monitored by a K-type thermocouple. Upon melt homogenization and skimming of the melt surface, the molten metal was poured directly from the crucible to the permanent molds, which were preheated to 600°C for 30 minutes in a firing furnace. All tensile and impact specimens were cast under conditions similar. Each casting provided four impact test bars (Figure 3.7a), and two tensile (Figure 3. 7b).

Tensile testing was carried out on the prepared test bars using an Instron Universal Mechanical Testing Machine (model 5982) as shown in Figure 3.4. Tensile tests were conducted at room temperature at cross-head speed of 1 mm/min and the tensile properties measured included ultimate tensile strength (UTS), 0.2% offset yield strength (YS) and percentage elongation (%El). The reported values are the average of at least two measurements.

Figure 3.4 : Universal mechanical tensile testing machine

The impact test was conducted based on Charpy type using Zwick impact testing machine (D-7900) using 15J hammer to measure the total absorbed energy as shown in Figure 3.5. The fractured surfaces of specimens obtained after tensile and impact tests were examined using FESEM. In addition to tensile and impact tests, hardness measurements were also made using a Vicker's hardness machine (Matsuzawa DVK-2) at an applied load of 5 N. The reported hardness values are the average of five readings

for each sample. The final test bars were then cut and machined with CNC machine according to B557M standard dimensions (Figure 3.8).

Figure 3.5: Zwick impact testing Machine.

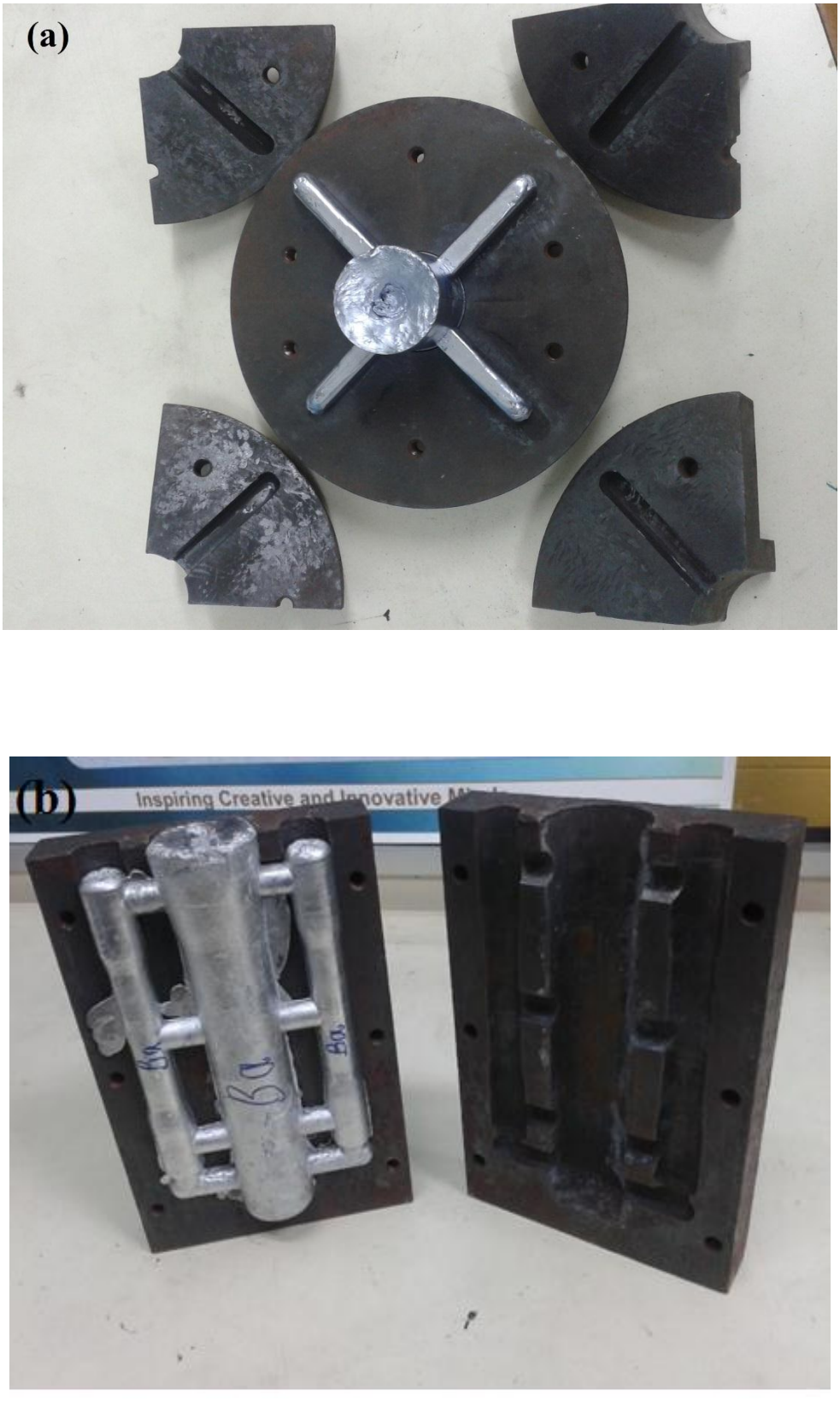

Figure 3.6: (a) Impact test and (b) tensile test samples permanent mold.

Figure 3.7: (a) Impact test and (b) Tensile test samples.

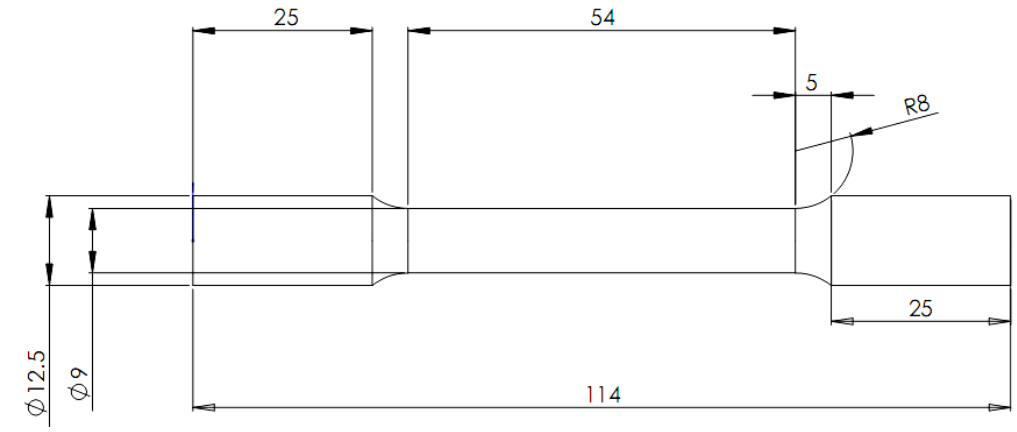

(a)

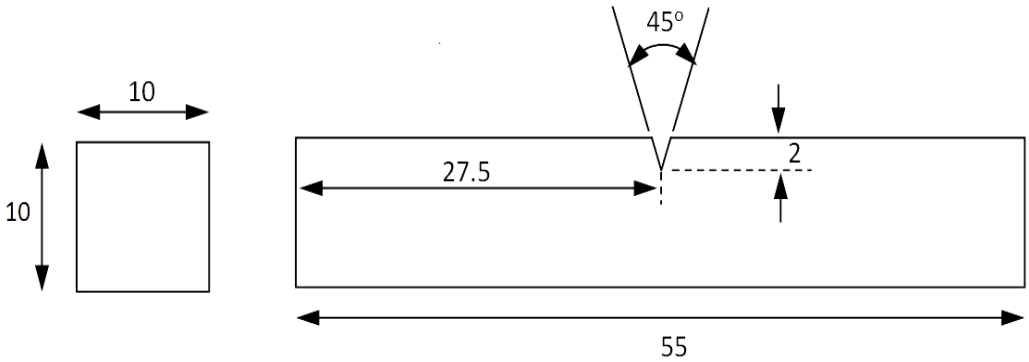

(b)

Figure 3.8 : Dimension of (a) tensile and (b) charpy impact test bar (All dimensions in mm).

3.3.2 Hardness Measurements

A Brinell hardness tester was used to measure the bulk hardness of the Al-Si alloys with a ball of 10 mm diameter, and a load of 500 kg. A microhardness tester, Buehler Micromet II® (Model 1600-9000), with a square-base diamond pyramid indenter (136 ° tip angle), was used to measure the aluminum matrix hardness. The indentation load applied was 10 g. The reported hardness values are the average of 10 measurements each.

3.4 The Turning Lathe

A turning investigation was accomplished on Al–11.3Si–2Cu cast alloy with 80–90 HV hardness using the CNC machine OKUMA LB15-II (Figure 3.9) with 8.3 kW power drive and 6000 rpm maximum spindle speed with various workpieces weighing up to 500 kg (4905 N). The maximum cutting length and diameters were 425 mm and 250 mm, respectively. Preliminary machining (skinning process) of this research was performed on a Manual lathe machine. Four workpieces were casted and firstly prepared by skinning a certain thickness of the outer layer of supplied material to remove the oxidized skin on the layer by using carbide insert at cutting speed 200 m/min.

Figure 3.9: CNC Machin for turning operations

3.4.1 Cutting Condition

The cutting condition were selected based on previous research findings (Basavakumar et al., 2007) and tool manufacturing recommendation, machining tests were conducted and feasible range of cutting speed and feed rate for given cutting tool and workpiece were selected as shown in Table 3.2. The depth of cut was held constant for all tests at 0.5 mm. No cutting fluid was used in machining.

A good surface finish, that is desired in the final machined product and the rigidity of the machine are the main determinants of the feed per revolution used in a given machining process. The final finishing operations were done at light feeds, generally in the range of 0.05 mm to 0.15 mm.

Table 3.2: Machining parameters

Cutting speed (m/min)	*Feed rate (mm/rev)*	*Depth of cut (mm)*
75	*0.05*	*0.5*
130	*0.1*	*0.5*
250	*0.15*	*0.5*

3.4.2 Tool Material

Physical vapor deposition (PVD) coated tool from Kennametal was selected to conduct the machining test. The tool grade is K10U (PVD). The insert material is Carbide-PVD coated (TIAIN/TIN). Table 3.3 shows geometry of insert.

Kennametal inserts with 35rhomboid geometry with nose radius 0.2 mm and Relief angle (α) 5° on a Kennametal holder SVJBL-1616H11 were used. All machining conditions were selected according to the tool maker advice. In Figure 3.10 is shown information about the insert.

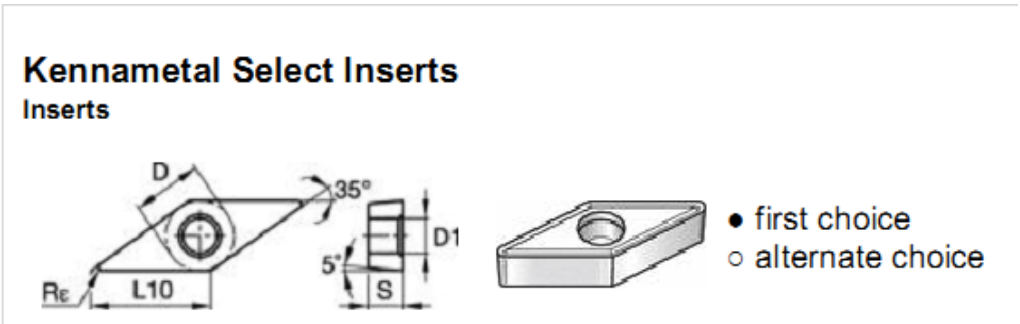

Figure 3.10: Kennametal select insert.

Table 3.3: Geometry of insert

		D		L10		S		Rε		D1								
ISO catalog number	ANSI catalog number	mm	in	mm	in	mm	in	mm	in	mm	in	K10P	K25P	K35P	K10M	K25M	K20K	K10U
VBGT110302F	VBGT2205F	6,35	1/4	11,07	.436	3,18	1/8	0,2	.008	2,80	.110							●

3.5 Metallographic Analysis

Samples for microstructural examination were prepared by conventional grinding and polishing techniques. The samples were wet ground with 240, 400, 800, 1200, 2400 and 4000 P SiC emery papers successively, on a rotating polishing machine (Figure 3.11). After the final grinding, the samples were polished using 3 and 1 μm diamond suspensions, and the final polishing was performed using a 0.1 μm diamond suspension. The samples were cut (Figure 3.12) with wirecut at highest cutting speed (250 m/min) and highest feed rate (0.15 mm/rev) to examine via Field Emission Scanning Electron Microscopy (FESEM) and Atomic Force Microscopy (AFM). Etching for microstructural observations was performed by immersing the samples into a Graff - Sargent solution, which consisted of 84 ml H2O, 15 ml HNO3, 0.5 ml HF, and 3g CrO3, for 5 seconds. Quantitative metallographic measurements of the silicon particle size were conducted using an optical microscope, Axiovert 25, equipped with an image analysis software.

The quantitative microstructual measurements included the measurement of the maximum silicon particle length and width. The particle length was determined by measuring the maximum length of each particle parallel to the maximum length, and the particle width was determined by measuring the widest distance across each particle in a direction perpendicular to the direction of the maximum length. The aspect ratio is defined as the average particle length divided by average particle width.

Figure 3.11: Rotating grinding and polishing machine.

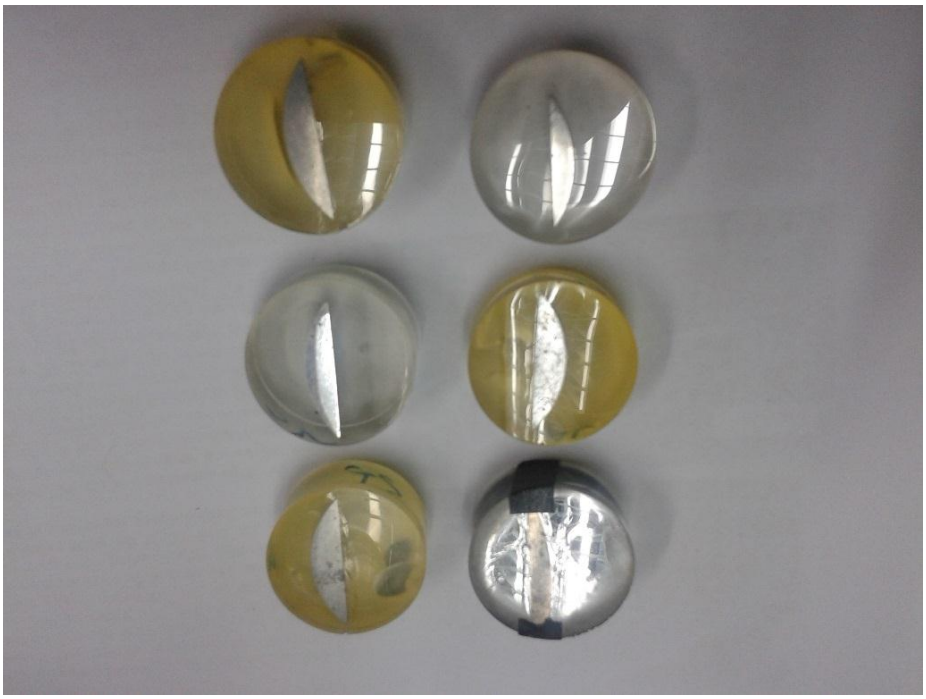

Figure 3.12: Some samples for microstructural examination.

3.6 Measurement of Surface Roughness

Surface roughness of the different Al-Si alloys, machined under different conditions, was measured after the turning experiments, to quantitatively analyze the finish of the surface produced. The average surface roughness of the recorded values (Ra) was calculated and served to investigate workpiece morphology after the machining process. In addition, Ra values were more common than the Rt and Rz values because its considers the averages of peaks and valleys on the surface. The measurements were carried out by using a Mitutoyo-Formtracer CS 5000 with accuracy of ±0.01μm (Figure 3.13). A cut-off length of 0.8 mm was used to compensate for surface waviness. The values were measured perpendicular to the feed marks after each cut. The exact Ra value was obtained by averaging values measured at a minimum of five location points around the circumference of the workpiece. The measurements were taken for each cut. In addition, surface roughness was examined via Field Emission Scanning Electron Microscopy (FESEM, Supra-35VP, Carl Zeiss) and Atomic Force Microscope (AFM) (Model SPM- 9500J2). Figures 3.14 and 3.15 show FESEM and AFM, respectively.

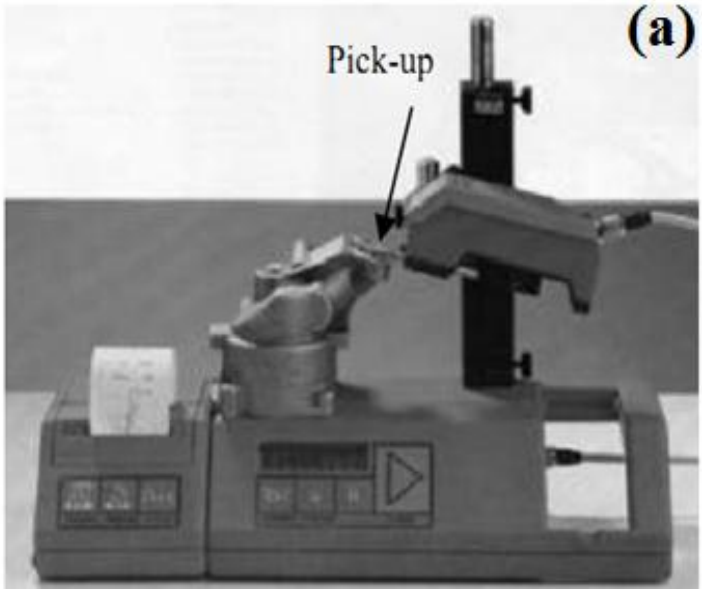

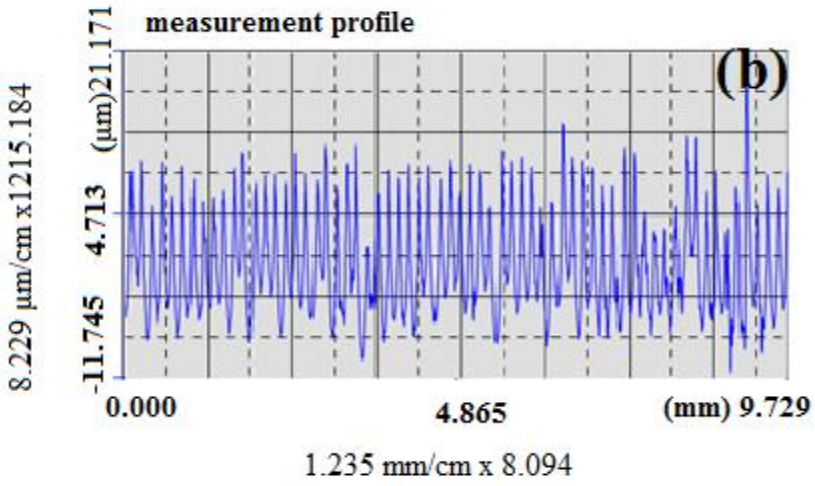

Figure 3.13: (a) Profilometer for measuring surface roughness and (b) Mitutoyo-Formtracer CS 5000 graph

Figure 3.14: Field Emission Scanning Electron Microscopy.

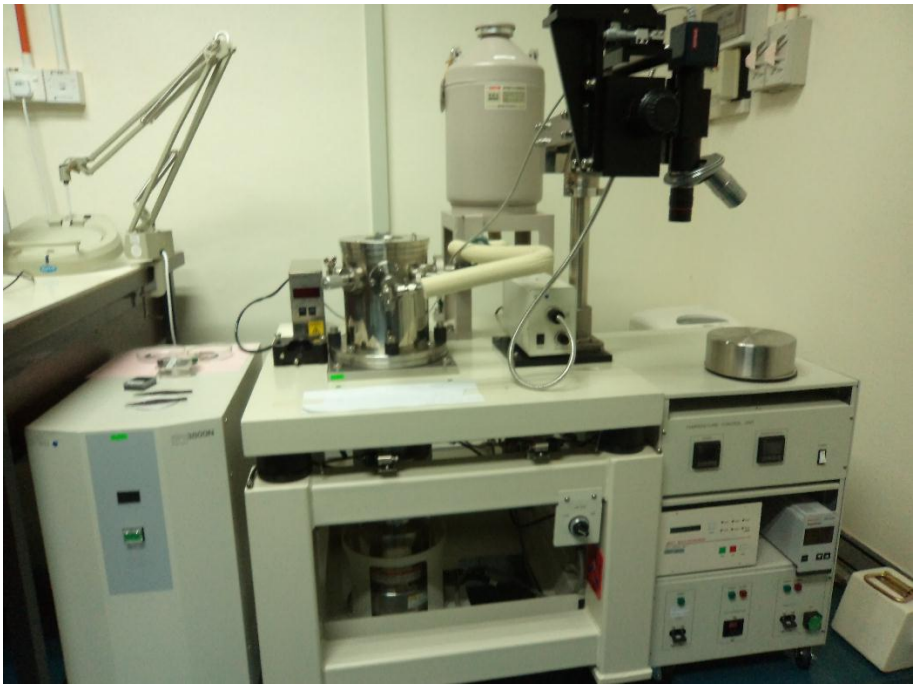

Figure 3.15: Atomic force microscopy.

3.7 Cutting Forces Measurements

The cutting forces were measured with three component force dynamometer. A tool dynamometer (Model 9121, Kistler Instrument AG, and Winterthur, Switzerland) was installed on the turret of the LB15-II (Figure 3.16a and 3.16b). The dynamometer has several quartz-based piezoelectric force transducers in steel housings. When force is acting on the dynamometer, each transducer produces a charge proportional to the force component that is sensitive to that axis. The 9121 model measures force on the X, Y, and Z-axes. The data acquisition system recorded cutting force (F_c) during machining at sampling frequency such that 20 points/cycle could be obtained (Figure 3.17).

(a)

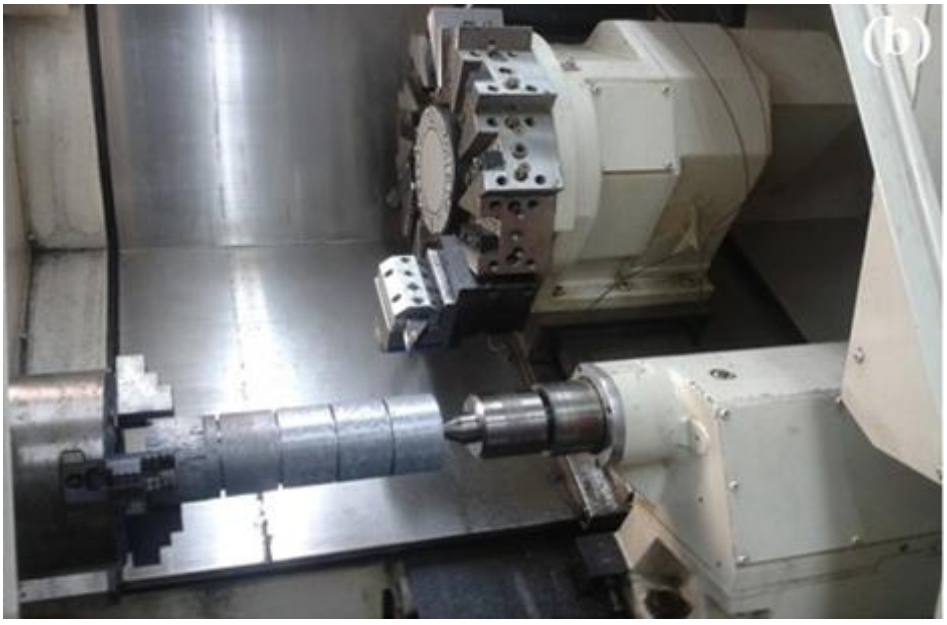

(b)

Figure 3.16 :The data acquisition system and Dynamometer, (Kistler Instrument)

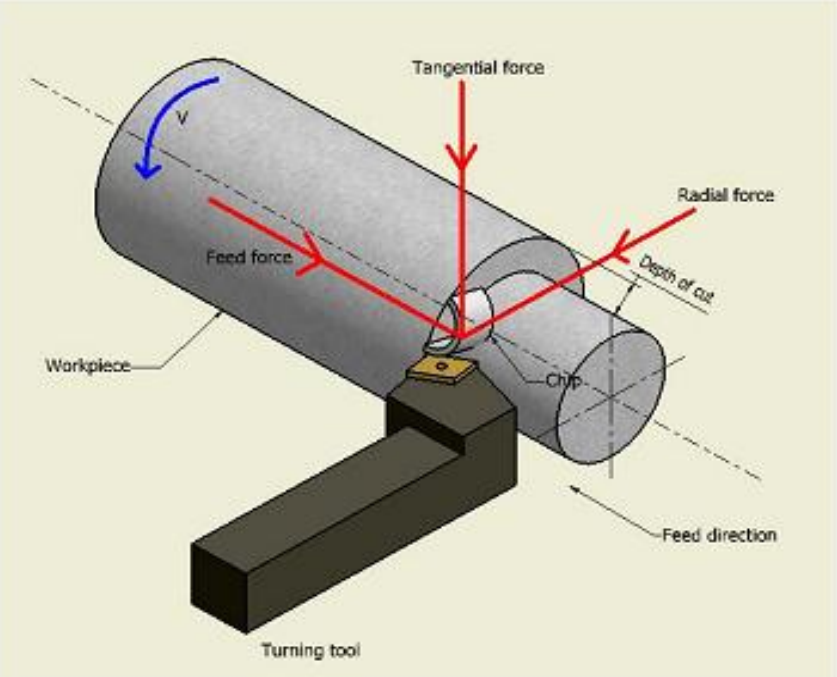

Figure 3.17: Measured cutting force component

3.8 Tool Wear

According to the literature, the tool life criterion on the width of flank wear is VBmax = 0.2 mm (Wright, 2000) and it is measured after each cut using a tool maker microscope. Both the rake and flank faces were subsequently observed using a Zeiss optical microscope. For each condition, a new insert was used. The insets have been cleaned by NAOH (sodium hydroxide) after each pass and checked by optical microscope (model Carl ZeisStemi 2000-c) and magnification: 6.5X-50X (Figure 3.18) to measure flank wear.

Figure 3.18 : Optical Microscope

3.9 Characterization of Chip Morphology

The length and shape of the chips produced from the machining of the alloys with different concentrations of Bi, Sr and Sb were compared. The shapes of the chips were recorded by optical photography. The chips were mounted in some molding cups for grinding and polishing before checking under optical microscope and SEM (Figure 3.19). The free and side surfaces and the cross-section of chips were observed using a scanning electron microscope (JEOL JSM- 5800LV SEM). The distribution of all modifiers in the cross-section of chips was examined using a scanning electron microscope (SEM) equipped (Figure 3.20) with an energy dispersive spectrometer (EDS). Compositional EDS maps of the cross-sections of chips were obtained to determine the bismuth distribution and deformation.

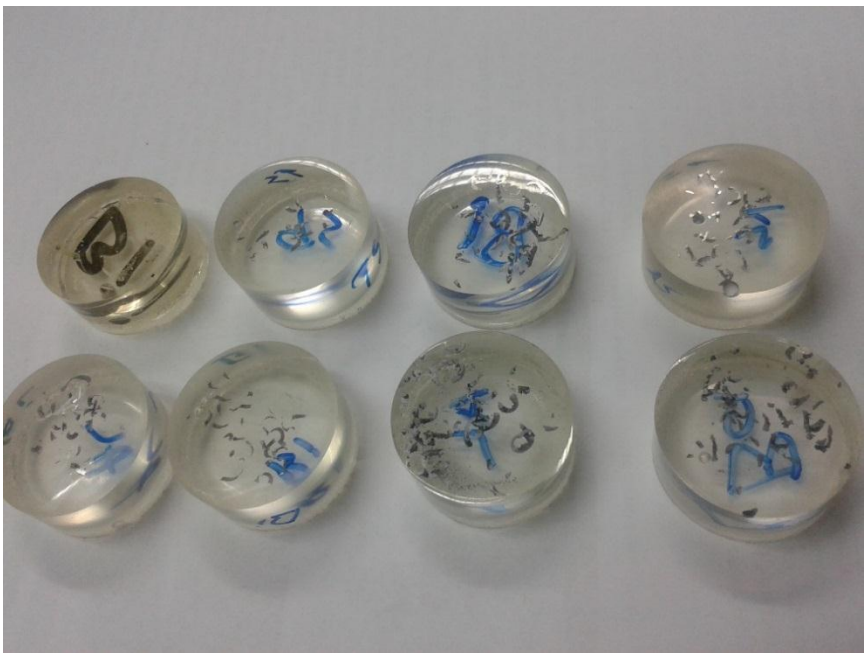

Figure 3.19 : Molding cup samples for chip morphology

Figure 3.20: Scanning electron microscope (SEM)

CHAPTER 4: RESULTS AND DISCUSSIONS

4.1 Introduction

Aluminum-silicon alloys, especially near-eutectic alloys containing 11% Si, are widely used in the automotive industry because of their excellent foundry characteristics and mechanical properties. These alloys have, therefore, replaced iron and steel in many components, including transmission cases and intake manifolds, as well as in more critical components such as engine blocks, cylinder heads and wheels (Moustafa et al., 2003). This extended application of Al-Si alloys for automotive components has created the need for a more in-depth understanding of the effects of microstructure on the machinability of these components.

Modification melt treatment in Al‑Si cast alloys leads to a change in the morphology of eutectic silicon from coarse brittle flake-like to fine fibrous morphology, resulting in improved mechanical properties especially ductility and fatigue life (Farahany et al., 2011). By the addition of certain elements to the melt prior to solidification, chemical modification can be achieve (Barzani, Sarhan, Farahani, et al., 2015). Elements such as Na, Sr, Sb and Bi show marked effect on the eutectic silicon when added to molten Al‑Si alloys by changing its morphology to fibrous appearance.

According to literature, of the various types of Al-Si alloy, near eutectic Al-Si alloys are the most difficult to machine because the silicon phase is almost ten times harder than the aluminium base alloy, thus causing the cutting tools to wear out rapidly. For this reason, consistent attempts have been made to improve the machinability of these alloys. With regard to machinability as one of the characteristics of a given alloy, this study reported on the effect of silicon morphology on mechanical properties and machinability of Al-Si alloy.

Consequently, in view of the above, the purpose of this chapter is to examine the near-eutectic Al-Si cast alloys containing ~11% Si as a basis for understanding the role of alloying elements such as; Sr, Bi, and Sb on the mechanical and machinability properties of these alloys with the aim of examining the effects of silicon morphology on the machining behavior of these alloys for use in industrial applications. A thorough understanding of the role of all these factors in the alloys studied would make it possible to select materials and workpiece designs for obtaining optimum machining combinations critical to maximum productivity.

4.2 Characterization of the Microstructure

The effects of different contents of Bi on the silicon structure are shown in Figure 4.1. Coarse plate-like Si structure was observed in the untreated base alloy (Figure 4.1a) and treated alloy with 0.1 wt.% Bi (Figure 4.1b) which changes to fine lamellar structure with increasing Bi content up to 1 wt% Bi (Figure 4.1c). Beyond this concentration, there was no significant change in the silicon structure in terms of morphology or size (Figure 4.1d). Similar findings that indicated refinement effect of Bi were reported for LM25 (Al-7 wt.%Si-0.4 wt.% Mg) alloy (Farahany et al., 2011).

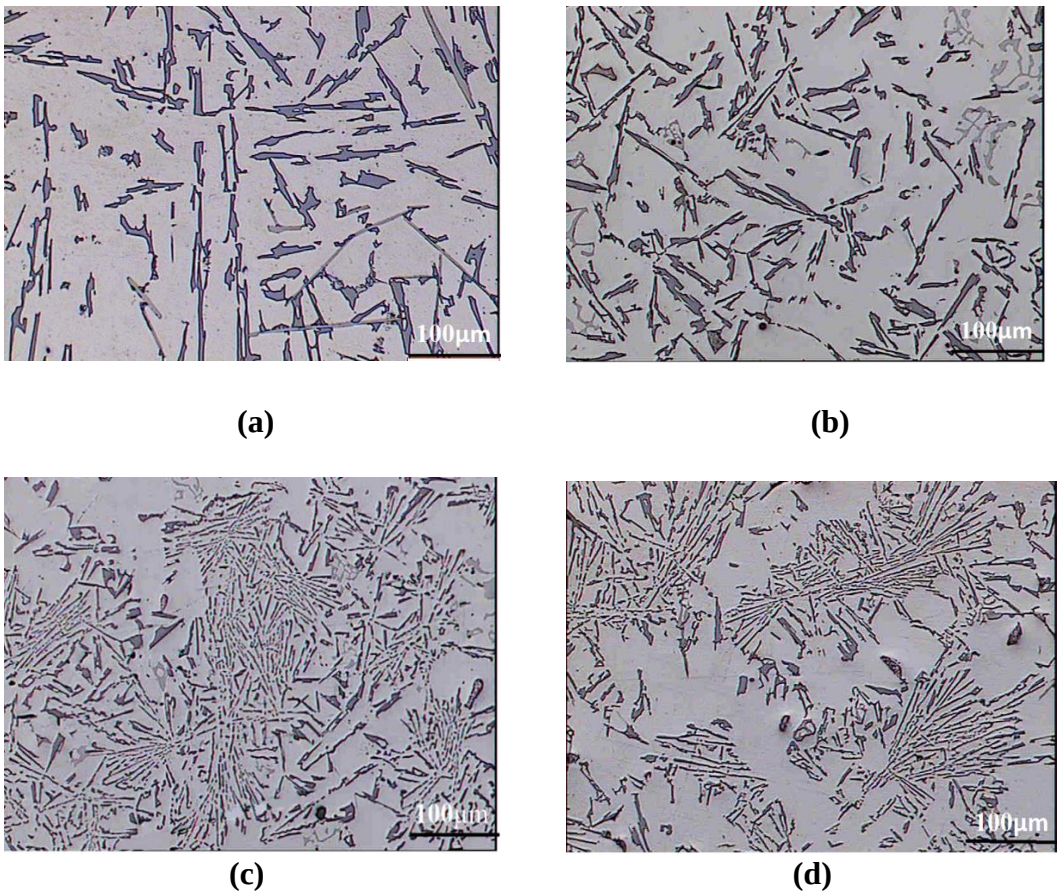

Figure 4.1: Optical micrographs of Si eutectic morphology for samples treated with a) 0, b) 0.1, c) 1 and d) 1.5 wt.% Bi

The influence of various concentration of Sb on eutectic Si morphology is also illustrated in Figure 4.2. It is clear that the coarse flake morphology exhibited by the Si in the untreated base alloy (Figure 4.2a) has transformed gradually into refined lamellar structure with increased addition of Sb up to 0.5 wt.% (Figure 4.2d). It has been published that addition of 0.2 wt.% Sb to Al-12.6 wt.% Si can refine the eutectic structure by reducing the inter-flake spacing without changing its morphology from flake-like or lamellar to fibrous Si (Barzani, Sarhan, Farahany, et al., 2015). Xiufang et al. (2001) used a high-temperature X-ray diffractometer and noted that Sb in liquid Al-Si alloys promotes the aggregation and nucleation of Si atoms and finally modifies the size and shape of the Si phases in the solid state. Muthukrishnan et al. (2008) reported that Al-Sb particles

perhaps enhance the refinement of eutectic silicon by increasing the nucleation of Si particles.

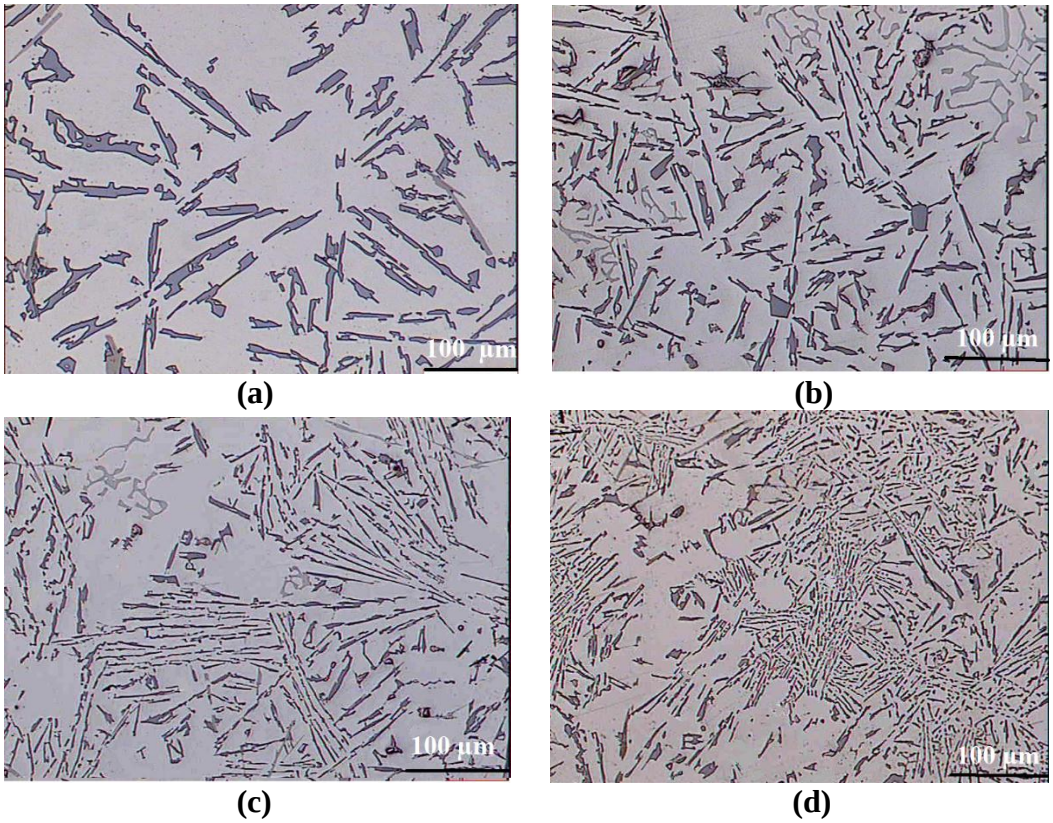

Figure 4.2 : Optical micrographs of Si eutectic morphology for samples treated with a) 0, b) 0.2, c) 0.4 and d) 0.5wt.% Sb.

In contrast to additions of Bi and Sb, however, addition of Sr to the Al-Si alloy represented a completely different behavior. As can be seen in Figure 4.3, the flake Si morphology exhibited by the eutectic Si in the untreated base alloy (Figure 4.3a) has been modified into fibrous-like morphology with addition of Sr. Such modification occurs in several steps depending on the amount of Sr added as shown by the partially modified structure in the alloy treated with 0.01wt% Sr (Figure 4.3b). Subsequent increase of Sr to 0.04 wt.% induced a change to completely modified Si morphology (Figure 4.3c). When the Sr content is higher than 0.04 wt.% fine modified structure was produced but no

significant changes can be observed when compared with alloy modified with 0.04 wt.% Sr, as shown in Figure 4.3(d). It can be deduced that addition of 0.04 wt.% Sr provides sufficient atoms, reduce the potency of the growing surface of silicon, inhibit the growth of Si and produces a modified structure.

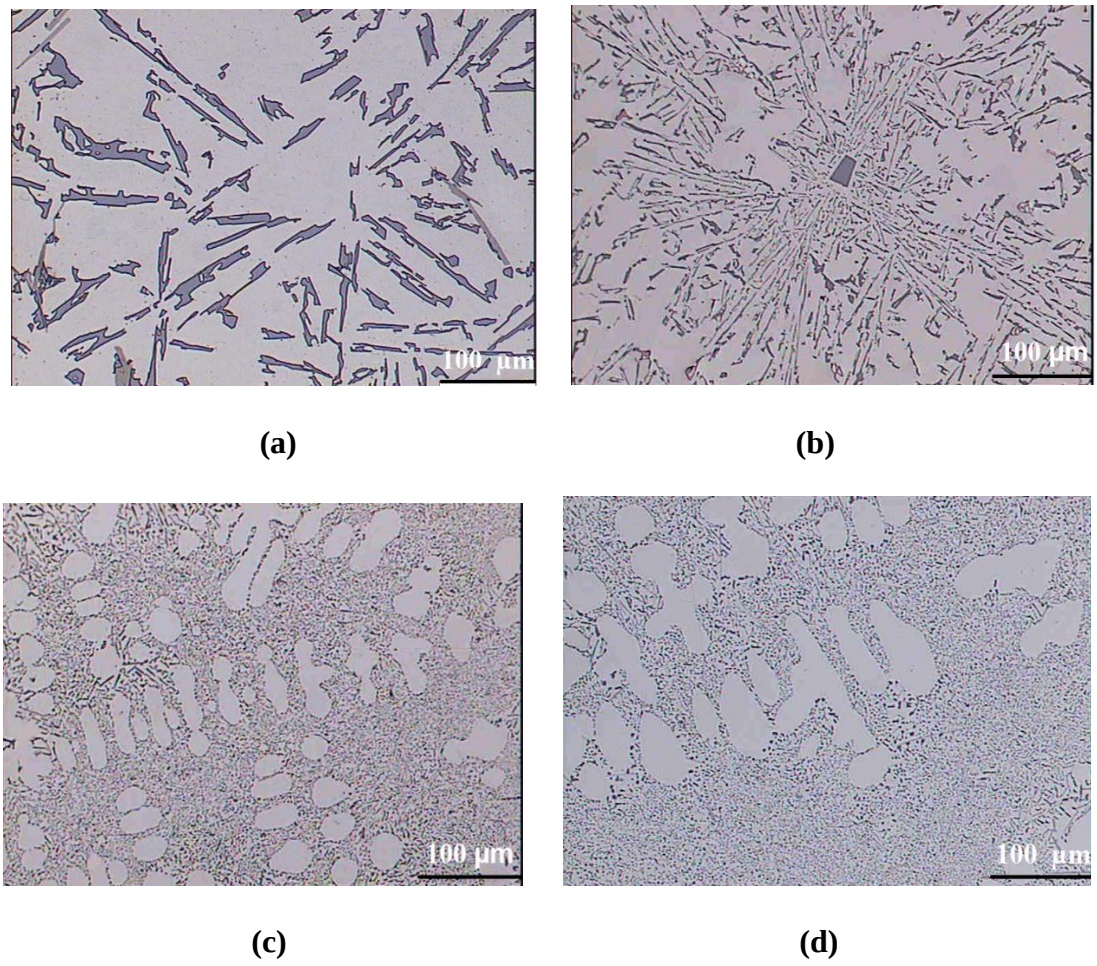

(a) **(b)**

(c) **(d)**

Figure 4.3 : Optical micrographs of Si eutectic morphology for samples treated with a) 0, b) 0.01, c) 0.04 and d) 0.08 wt.% Sr.

4.2.1 Silicon Particle Characteristics

The morphology of eutectic Si plays an important role in determining the machinability characteristics of cast Al-Si near-eutectic alloys. A fine, well-modified eutectic silicon structure is far less detrimental to tool life than heavy element intermetallic phases; tool life will, however, decrease in the presence of a coarse eutectic silicon structure. Table 4.1 summarizes the silicon particle characteristics obtained from quantified measurements of the alloys investigated.

As can be seen in Table 4-1 and Figure 4.4, Si particles are shown in the form of plate like (Figure 4.4a) for unmodified alloy (base alloy) with an aspect ratio of 0.05 and the average particle length of 29.23 μm. The addition of 0.05 Sb transforms the morphology of silicon from plate-like to fibrous (Figure 4.4d). As can be observed, the aspect ratio changed to 0.98 and the average particle length decreased to 5.31 μm. The aspect ratio changed from 0.05 to 0.11 with adding of Bi and the shape of silicon changed from plate like to lamellar (Figure 4.4b) with decreasing the average particle size from 29.23 to 4.65 μm. It is also obvious that the aspect ratio changed from 0.05 (base alloy) to 0.98 for Sb-containing alloy. The shape of silicon for the Sb-containing alloy was the same as Bi- containing alloy with lamellar shape-like (Figure 4.4c). It is interesting to note from table 4.9 that the addition of 0.05%wt Sb, 1%wt Bi and 0.04%Sr has a big influence on changing particle length. In fact, with addition of these elements the average of silicon length decreased and their microstructures are fully modified.

Table 4.1: Summary of eutectic silicon particle measurement for all workpieces

Alloy Name	Particle Length (µm)	Aspect Ratio
Base alloy	29.23	0.05
Sb-containing	5.31	0.98
Bi-containing	4.65	0.11
Sr-containing	2.21	0.62

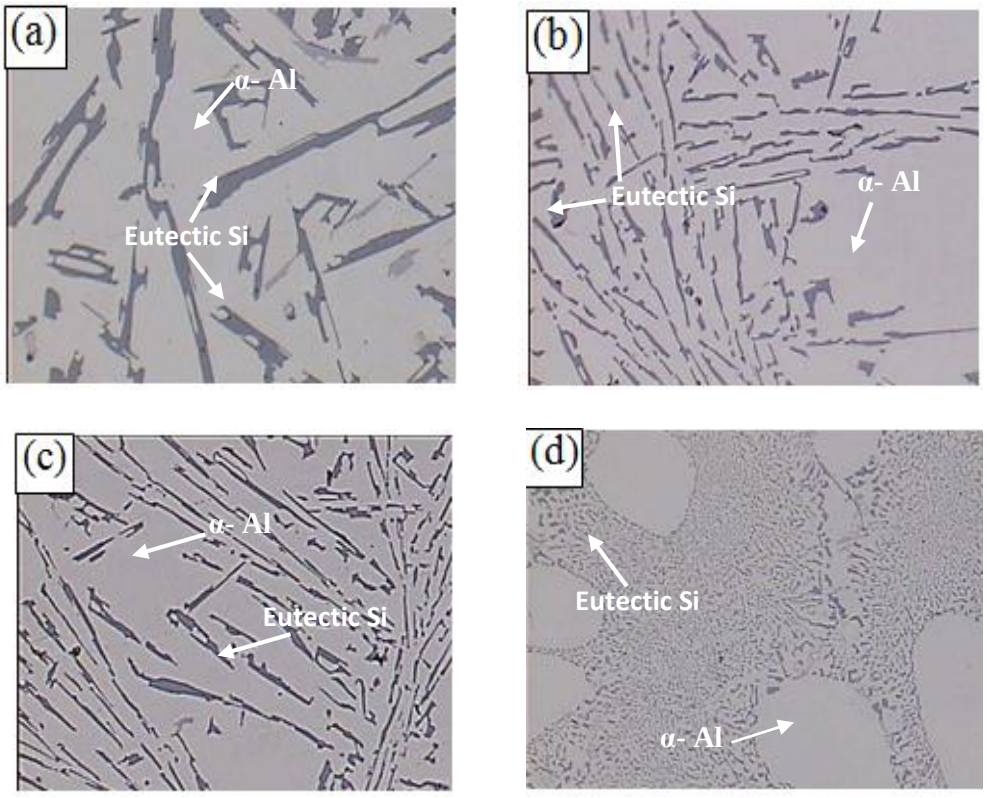

Figure 4.4: Optical micrographs showing the (a) unmodified alloy and effect of (b) Bi-addition, (c) Sb-addition, (d) Sr-addition.

4.3 Mechanical Properties of Al-Si Alloys

4.3.1 Impact Test

The effect of elements having low melting-points on the mechanical properties of Al alloys have been reported in various studies. Mohamed et al. (2008) investigated the effects of trace additions of Sn on the mechanical properties of B319.2 and A356.2 alloys; the results show that the higher ductility of Sn-containing alloy in the as-cast condition may be attributed to the stress-strain state of the matrix material associated with the fine Sn bearing phase. In a study of the effects of Mg on the mechanical properties of secondary Al-Si-Mg alloys containing 0.1% Sn or 0.2% Pb, it was found that, with an increase of the Mg content from 0.2 to 0.5 - 0.8%, the Sn and Pb in the given concentration do not impair the mechanical properties, particularly in the heat-treated condition.

Impact toughness of Al-Si alloys depends mainly on the morphology of Si phase, Al dendrite size and intermetallic phases (Farahany, Ourdjini, Idris, Takaloo, & Thai, 2013). Figure 4.5 shows the relationship between absorbed energy and condition of samples in the form of untreated (base alloy) and treated alloys with optimum concentration of addition elements. The absorbed energy value for the base alloy is 1.15J, whereas it increased to 2.2J for Sr treated alloy. This value is almost two times that of untreated alloy. The measured impact values for Bi-treated and Sb-treated alloys were 1.62 and 1.40J, respectively.

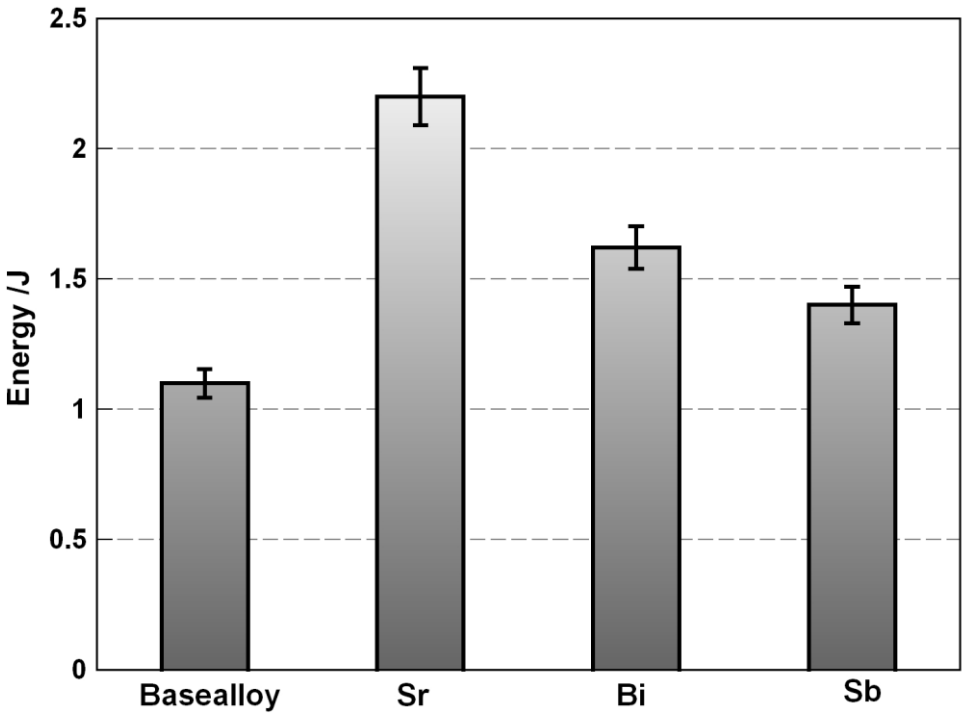

Figure 4.5: Energy absorbed of fracture for base alloy and treated with 1 wt.% Bi, 0.5 wt.% Sb and 0.04 wt.% Sr additions.

In addition to tensile and impact tests, hardness measurements were also made using a Vicker's hardness machine (Matsuzawa DVK-2) at an applied load of 5 N (Table 4.2). The reported hardness values are the average of five readings for each sample. It should be noted that in the present work, the area occupied with Si was selected for hardness measurement. The hardness results for Sr-treated and Sb-treated alloys were found to be closer together and they were lower than base alloy, but it was approximately same for the Bi-treated alloy and base alloy even though the Si eutectic spacing of the Bi-treated alloys was finer than in the base alloy.

Table 4.2: Reporting hardness of workpieces

Name of alloy	Hardness
Base alloy	80+1.20 MPa
Bi- containing	79+1.20 MPa
Sr-containing	77+1.30 MPa
Sb-containing	76+1.50 MPa

The fracture surfaces of failed samples were also investigated to examine the type of failure under FESEM. Figure 4.6(a) shows the fracture surface of base alloy without any addition in which coarse Si planes are observed in the fracture surface indicating brittle fracture. In the Sr-treated alloy, however, as shown in Figure 4.6(b) the fracture surface exhibits fine Si planes associated with ductile fracture. From machinability point of view, therefore, it can be increase built-up edge during machining process and consequently decrease machinability of Al-Si alloy. The fracture surfaces of Bi-treated and Sb-treated samples show a mixed mode of ductile and brittle modes as shown in Figures 4.6(c) and 4.6(d), respectively.

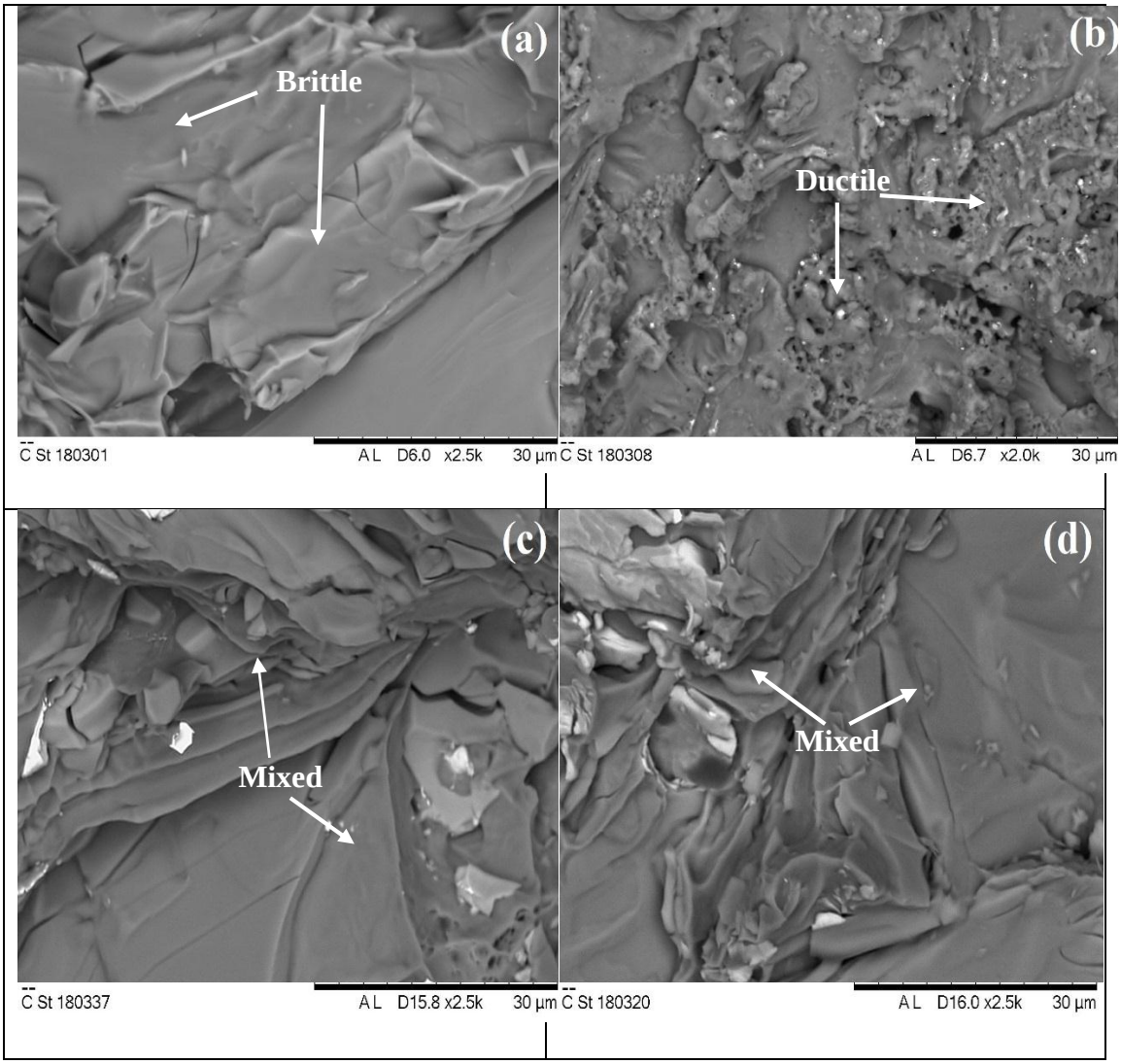

Figure 4.6 : Fractured surface of a) base alloy b) Sr-treated c) Bi-treated and d) Sb-treated alloy subjected to impact test.

Bismuth has modifying effect on Al-11% Si alloys. It has been reported that bismuth in aluminum alloys interacts with such major modifiers as sodium and strontium (Thai, 2006). The Bi-phase is not observed as an intermetallic compound with Al, since it is independently distributed; this phase is thus not uniformly distributed in Al-Si alloy structures and has a tendency to segregate, forming lamellar silicon morphology because of the high wettability of Bi at the grain boundaries. From machinability point of view, therefore, it is able to improve machinability with increase chip break ability during turning process (Zedan et al., 2010).

4.3.2 Tensile Test

The results of ductility of the untreated and treated samples can be reflected in the fracture surfaces. Figure 4.7 shows SEM micrographs of the fracture surfaces of the untreated and treated alloys with Sr, Bi and Sb. Trans-granular quasi-cleavages are very much apparent on the fracture surfaces of the untreated alloys (Figure 4.7a) and these quasi-cleavages occupy a large area indicating that fracture exhibits mostly brittle behaviour, which is attributed to the low ductility of the castings.

From the viewpoint of the machinability characteristics of the alloy, brittle behavior of materials improves machinability of alloys. Therefore, base alloy illustrious a reasonable machinability with lower cutting force and better surface roughness in comparison with Sr- and Sb-containing elements. However, more evidence of plastic deformation can be observed on the fracture surfaces of Sr-treated sample. The surface exhibits the presence of dimples indicating ductile fracture (Figure 4.7b) and plastic deformation is also clearly evident in contrast to the untreated samples. This leads to produce massive BUE during machining process and decrease surface roughness and increase tool life.

In general, the precipitate particle fracture, interface debonding and matrix crack are the main failure modest during a tensile test. The fracture surface of Sr-containing display a few dimples typical of a ductile behavior (4.7b). In addition, more trans-granular features can be seen in Bi and Sb-treated samples as shown in Figures 4.7(c) and 4.7(d), respectively. This indicates that the coarse silicon particles were refined by the addition of Bi and Sb to the melt, and as a result causes ductile fracture and improves ductility. As it has been mentioned, Bi acts as lubricant during machining process and increases chip breakability with decreasing BUE and improve machined surface roughness. This observation is in satisfactory agreement with Koch & Antrekowitsch (2008) who substituted Pb and Pb + Bi with Sn in the standard AA2030 and AA2011 alloys,

respectively. They reported that, as a result of the extremely limited solubility of the Sn particles in the Al-matrix, these particles remain as separate entities dispersed in the matrix; during machining operations, it is believed that the temperature generated in the cutting zone is high enough to soften or even to melt these dispersed entities. Consequently, this melting gives rise to a local loss of material strength and ductility which in turn leads to the formation of broken chips. Moreover, the low-melting elements act as a lubricant during machining, thereby decreasing the friction between chip and tool edge which then results in a reduction in the cutting forces. On the whole, the results clearly show that when the base alloy is modified chemically, the ductility is improved as indicated by the values of elongation to fracture.

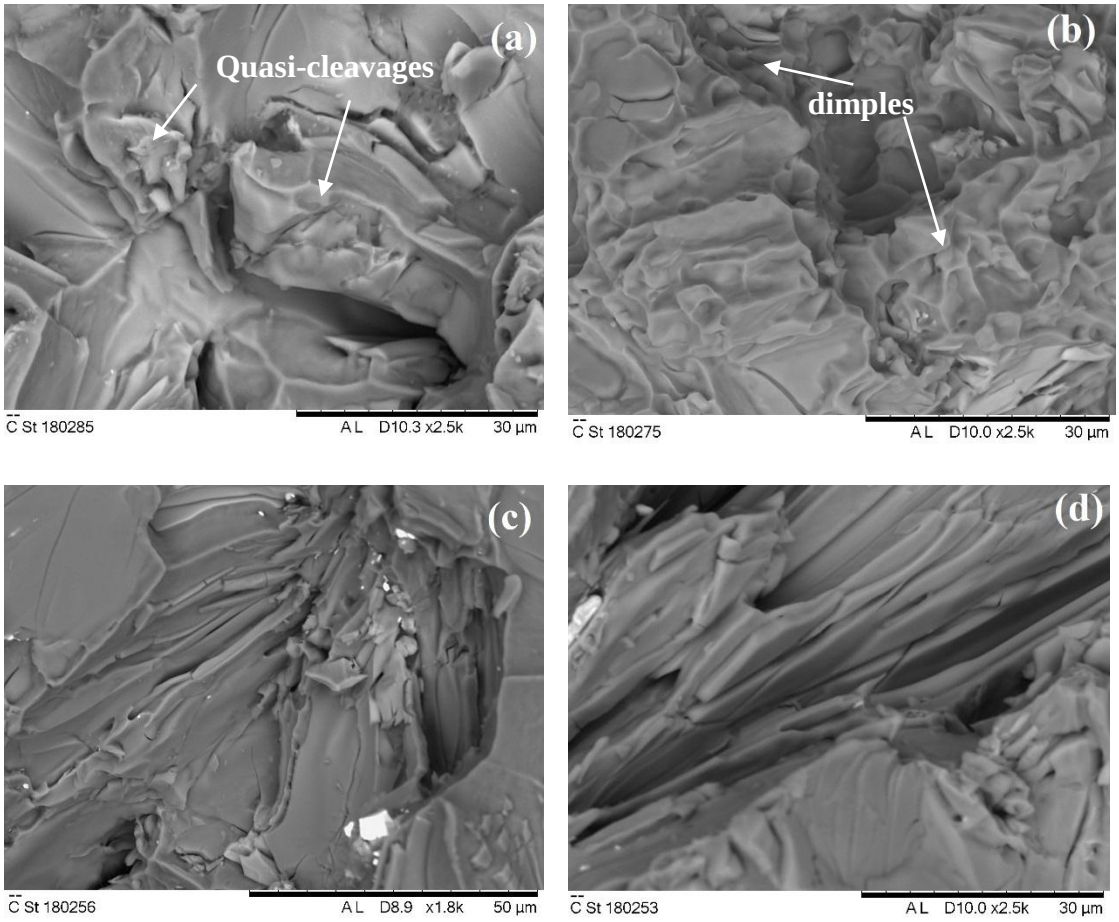

Figure 4.7: Fracture surface of tensile test bar at room temperature: (a) base alloy, (b) Sr-treated, (c) Bi-treated and (d) Sb-treated alloys.

Figure 4.8 shows a summary of tensile test results including yield strength (Y.S), ultimate tensile strength (UTS) and elongation to fracture (El) for base alloy and treated alloy with optimum concentrations of Bi, Sb and Sr additions. The results show that the highest yield strength was obtained in the untreated base alloy (123.9 MPa) compared with the untreated alloys with Sr (116.18 Mpa), Bi (119.17 MPa) and Sb (120.2 MPa). This can be associated with the fact that the yield strength is strongly dependent on α-Al dendrite size rather than silicon morphology.

Unlike the yield strength, however, the values of UTS appear to depend more on the structure of Si rather than Al primary dendrites. For example, the untreated base alloy exhibited the lowest UTS at 131.27 MPa compared with 145 MPa for the Sr-treated and 151.8 MPa for the Bi-treated specimens. The alloys treated with Bi and Sb showed the highest values of UTS, which may be attributed to less potential of these additions for gas pickup and porosity formation than Sr (Kerr et al., 2005) which reported as an advantageous of Sb (Hegde & Prabhu, 2008). Concerning the elongation to fracture the results show that with additions of Bi, Sb and especially Sr the values of elongation have increased by two-fold. The untreated base alloy had elongation percentage of 0.55 compared with 1.2 % after Sr modification. The increase in elongation is likely related to the Si structure and morphology which changes from flake-like to fibrous or lamellar structure with element additions. The large flake-like structure of Si probably raises stress help initiation and growth of cracks.

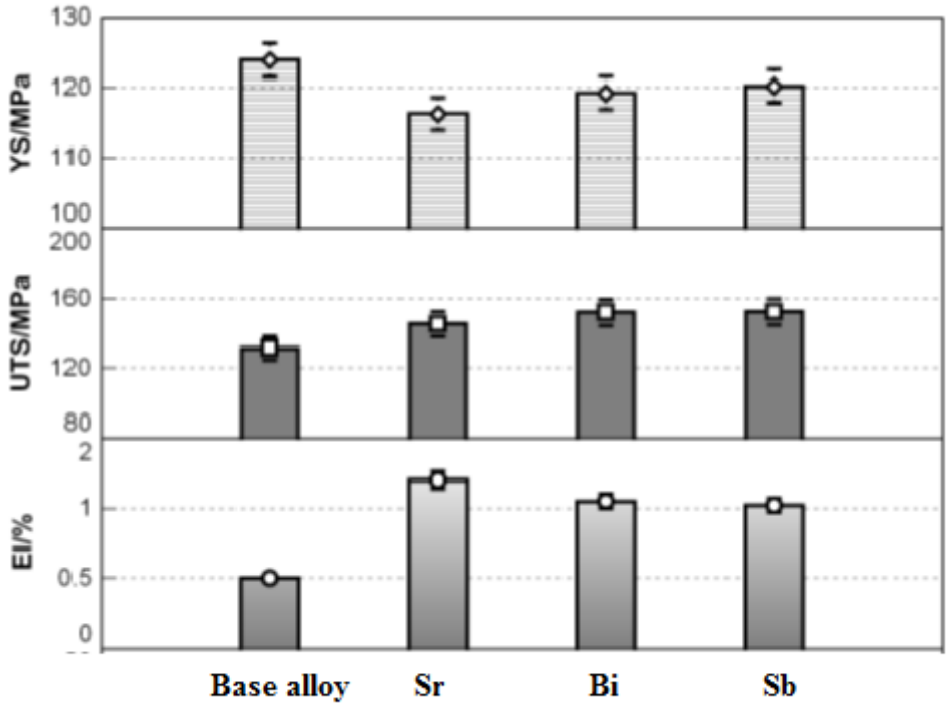

Figure 4.8 : Tensile test results composed of YS, UTS and El% of base alloy with addition of Sr, Bi and Sb.

4.4 Effects of Free Cutting Elements on the Machinability of Al-Si Cast Alloys

The three main aspects of good machinability are prolonged tool life, low cutting force, and chip form. Lower cutting forces result in lower tool-wear rates, better surface finishing, and extended tool life (Koch & Antrekowitsch, 2008). Chip shape is the most important factor in obtaining smoothness of the turning process which will proceed easily if the chips are well-broken (Shaw, 2005). Most ductile materials, however, do not break during turning and form continuous chips instead. The main problems arising in the turning of aluminum cast alloys are considered to be the adhesion, or welding, of the chip to the rake face of insert (Dabade & Joshi, 2009b). All of these problems are closely related to the process of chip formation and chip removal in turning process. Therefore, chip form is often used to assess the machinability of soft, ductile alloys, especially aluminum alloys.

Certain elements known to enhance the wet machinability of aluminum and steel are referred to as free-machining elements. These low melting point elements are added to aluminum alloys to improve their machinability through the formation of insoluble globules which are effective chip breakers resulting in small, easily evacuated chips (Dasch et al., 2009). The most common free-machining elements include bismuth (Bi), tin (Sn), lead (Pb), and indium (In). Due to the harmful effect of Pb on the environment and the high price of In, both Bi and Sn are the most preferable choices as free-machining elements (Ang et al., 2006).

A number of studies on the machinability of alloys containing low melting-point elements which address Al-Si alloy castings have shown that the dry turning performance of a cast Al-Si alloy was improved when these new elements, namely Bi, Sn, and Pb, were added (Ang et al., 2006). Bi was found to be more effective than Sn for improving dry machinability when considering the mechanical properties in the alloy and the hot cracking in the casting.

Previous studies have indicated that the performance of Bi in Al alloys differ in several ways: the solidification of the embedded Bi in an Al alloy is found to take place over a wide temperature range at a contact angle between 72 ° and 80°, and wetting at the Al grain boundaries. In addition, previous research has shown that the presence of Bi in aluminium has a slight effect on the silicon morphology of Al-Si alloys (machovec, 2000). Antimony (Sb) is also present in casting scrap and is added as a grain refiner in order to enhance the mechanical properties by refining the eutectic silicon and changing its morphology into a lamellar structure (Zhang, Fan, Wang, & Zhou, 2000).

4.4.1 Microstructural Analysis of Machined Samples

Aluminium-silicon alloys can have different microstructures and mechanical properties while having the same chemical composition. It can be related to various casting processes or as result of using modifier, and through the selection of a given heat treatment process form the alloy (Palanikumar & Karthikeyan, 2007). This sequence of possibilities show that different processing techniques can result in a whole range of mechanical properties, which then reflects on the characteristics of the machining process itself. The combination of alloying elements and liquid alloy treatments is a satisfactory option for obtaining improved control of the microstructure during solidification, and hence of improving the machinability performance.

The microstructure of Al-Si alloy is typically composed of an aluminium matrix containing eutectic silicon; the silicon can be present in the form of acicular needles, plate shape, depending upon the level of chemical modification and the cooling rate of the cast section. These microstructure constituents also include secondary eutectic phases such as Mg_2Si and Al_2Cu, and other complex intermetallic constituted from the remaining liquid during the final stages of solidification (Moustafa et al., 2002). A number of elements are traditionally thought to provide any given alloy with a certain degree of natural lubricity. Other elements are known to increase matrix hardness, while still others result in the formation of hard intermetallic phases. All of these should be expected to have some effect on alloy machinability. Alloys containing copper, magnesium, or zinc as elements enter readily into solid solution with aluminum, and generally possess the best machining characteristics.

Cast aluminium-silicon alloys contain mainly Cu and Mg as the major alloying elements. In general, copper (Cu) increases the strength and hardness of the aluminium alloy and improves the elevated temperature properties, all of which is accomplished

through heat treating, where the development of the Al_2Cu precipitate occurs; the final properties are dependent upon the precipitate developed (Tash, Samuel, Mucciardi, & Doty, 2007). It has been published that Magnesium (Mg) is normally used to improve the mechanical properties of the alloy through the precipitation of the Mg_2Si intermetallic (Samuel, Samuel, Ouellet, & Doty, 1998). Mg has negative effect on Sr-modification, in other words, it alters the microstructure, causing it to change from being well-modified to only partially modified (Mohamed et al., 2008). Regulating the morphology and distribution of these intermetallics will improve the alloy matrix homogeneity and hence improve its machinability (Tash et al., 2007).

Strontium (Sr) is commonly added to Al-Si casting alloys only in very small amounts to modify the eutectic silicon morphology from coarser, flake like from to a fine fibrous one. The change in the morphology of the Si, in turn, enhances the mechanical properties, particularly ductility (Farahany et al., 2013). It has been published that the presence of Sr also leads to the separation of the copper phase toward areas away from the Al-Si eutectic regions during the solidification process, thereby resulting in a slowing down of its dissolution during solution heat treatment (Zhang et al., 2000).

It has been reported that when an aluminium casting alloy contain both 1% Cu and 5% Mg, the machined surface in the turning process is considerably improved, and there is only a slight effect apparent with regard to tool wear and the cutting force. This improvement in the finished surface maybe attributed to a significant increase in the hardness of the matrix (Gallab & Sklad, 2004). It has been reported that in aluminium alloy containing copper and silicon, a small magnesium addition about 0.3 wt% caused a significant increase in the material work-hardenability and reduced the tendency toward built-up age formation on the cutting tool. Mg leads to increase hardening in matrix and by doing so reduces the friction between tool and workpiece, resulting in shorter and

tighter coiled chip, as well as, providing a better surface finish (Kamia, Yakua, Sasaki, & Nagatsuma, 2007).

Tash et al. (2007) reported that a small amount of Mg added to Al-11%Si alloy, about 0.1wt%, improves alloy machinability and reduces the cutting force, thereby allowing for a high number of holes to be drilled and tapped. It has been reported that copper in Al-Si alloys affords a smoother surface finish, smaller and more tightly coiled chips, and a reduced burring tendency. Dabade & Joshi, (2009) studied the effects of the addition of Cu and Mg on the machinability of hypereutectic Al-Si alloy in relation to tool wear, roughness of the machined surface, cutting forces, and chip formation. They have found that surface finish is significantly improved by adding about 0.5% Cu or 0.3-0.6% Mg to hypereutectic Al-Si alloys. When a sharp cutting tool is used, the addition of Cu or Mg hardly affects the cutting forces at all, although as the tool grows blunt after greater cutting distances, the cutting forces increase as either Cu or Mg are added, and are known as broken type of chips when machining hypereutectic Al-Si.

4.5 Effect of Cutting Conditions on Surface Roughness

Table 4.3 and Figure 4.9 show a summary of the result of experiments. A total of 36 experiments were recorded for the analysis for of four workpieces. From the results of the experiment plans, the highest surface roughness was recorded (in experiment plane No 7) at around 5.542 µm (at cutting speed of 70 m/min and feed rate of 0.15 mm/rev), while the lowest surface roughness was recorded (in experiment plan No3) at around 1.655 µm (at cutting speed of 250 m/min and feed rate of 0.05) for Al-11Si-1.8Cu Non-modified.

Table 4.3: Experimental result for surface roughness Al-11Si-1.8Cu (base alloy)

NO	*Cutting speed (mm/min)*	*Feed rate (Mm/rev)*	*Depth of cut (mm)*	*Surface roughness Ra(µm)*
1	*70*	*0.05*	*0.5*	*2.504*
2	*130*	*0.05*	*0.5*	*2.302*
3	*250*	*0.05*	*0.5*	*1.655*
4	*70*	*0.1*	*0.5*	*5.058*
5	*130*	*0.1*	*0.5*	*3.355*
6	*250*	*0.1*	*0.5*	*1.692*
7	*70*	*0.15*	*0.5*	*5.542*
8	*130*	*0.15*	*0.5*	*3.49*
9	*250*	*0.15*	*0.5*	*3.101*

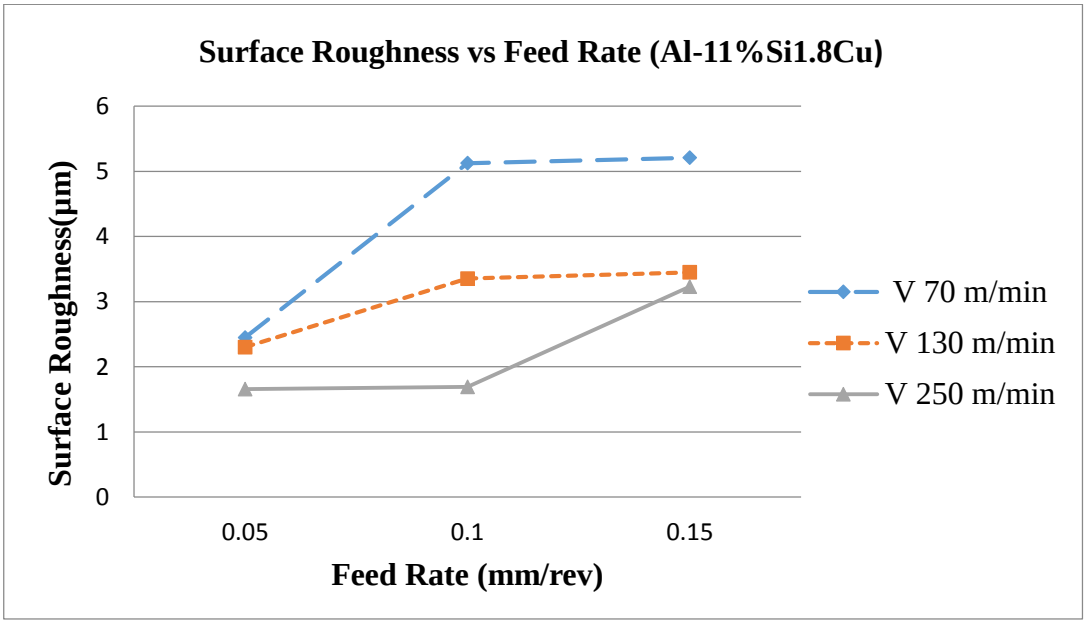

Figure 4.9: Surface roughness and feed rate relationship when turning Al-Si unmodified.

Table 4.4 and Figure 4.10 show the relationship between cutting conditions and surface roughness of Al-11Si-1.8Cu0.5Sb modified. Overall, what stands out from the graphs is that surface roughness increased when feed rated increased from 0.5 to 0.15 mm/rev. Also, the graphs show that surface roughness improved with increasing cutting

speed from 70 to 250 m/min. For instance, the best surface roughness was observed at cutting speed of 250 m/min and lowest feed rate of 0.05 mm/rev, while it was poor in the lowest cutting speed of 70 m/min and highest feed rate 0.15 mm/rev for the all workpieces. It results in a decrease in the BUE during machining workpieces. The temperature increases in cutting area with increasing cutting speed, and at a raised temperature in the cutting zone the strength of the BUE reduced. Therefore, BUE becomes more unstable and needs to be removed from the cutting tool more often. The temperature on the tool face also plays a major role with respect to the size and stability of the BUE (Akdemir, Yazman, Saglam, & Uyaner, 2012).

Table 4.4: Experimental result for surface roughness Al-11Si-1.8Cu Sb modified (0.5wt.% Sb)

NO	***Cutting speed (mm/min)***	***Feed rate (mm/rev)***	***Depth of cut (mm)***	***Surface roughness Ra(µm)***
1	*70*	*0.05*	*0.5*	*2.91*
2	*130*	*0.05*	*0.5*	*3.167*
3	*250*	*0.05*	*0.5*	*2.072*
4	*70*	*0.1*	*0.5*	*5.151*
5	*130*	*0.1*	*0.5*	*3.791*
6	*250*	*0.1*	*0.5*	*1.789*
7	*70*	*0.15*	*0.5*	*6.181*
8	*130*	*0.15*	*0.5*	*4.163*
9	*250*	*0.15*	*0.5*	*4.029*

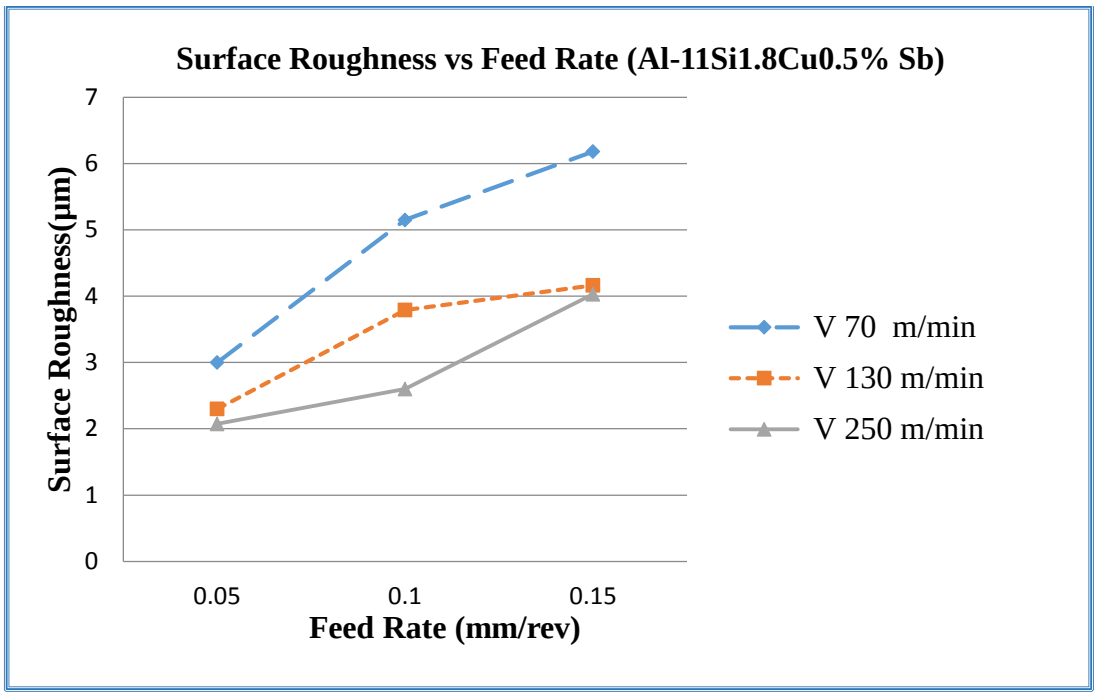

Figure 4.10: Surface roughness and feed rate relationship when turning Al-11Si-1.8Cu0.5 Sb- modified.

As can be seen in Table 4.5 and Figure 4.11, the highest and lowest surface roughness for Al-11Si1.8Cu0.04Sr modified was recorded (in experiment plan No.7) at approximately 5.167 µm (cutting speed of 70 mm/min and feed rate of 0.15 mm/rev) while it was recorded (in experiment plan No. 3) at around 1.665 µm (at cutting speed of 250 mm/min and feed rate of 0.0 mm/rev), respectively. The relationship between cutting conditions and surface roughness of Al-11Si1.8Cu0.04Sr modified was similar to Al-11Si1.8Cu0.0.5Sb modified.

Table 4.5 : Experimental result for surface roughness Al-11Si-1.8Cu0.04Sr-modified

NO	*Cutting speed (mm/min)*	*Feed rate (Mm/rev)*	*Depth of cut (mm)*	*Surface roughness Ra(µm)*
1	*70*	*0.05*	*0.5*	*2.819*
2	*130*	*0.05*	*0.5*	*2.323*
3	*250*	*0.05*	*0.5*	*1.665*
4	*70*	*0.1*	*0.5*	*5.106*
5	*130*	*0.1*	*0.5*	*3.142*
6	*250*	*0.1*	*0.5*	*1.801*
7	*70*	*0.15*	*0.5*	*5.167*
8	*130*	*0.15*	*0.5*	*3.485*
9	*250*	*0.15*	*0.5*	*3.134*

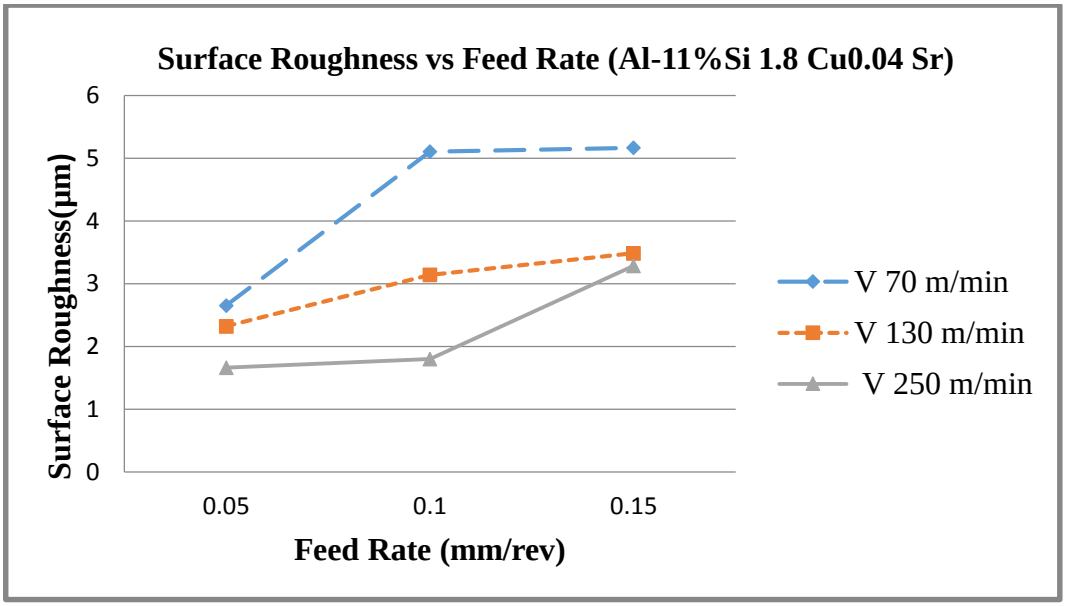

Figure 4.11: Surface roughness and feed rate relationship when turning Al-11Si-1.8Cu 0.06Sr- modified.

It can be seen that the best value of surface roughness was related to Al-11Si-1.8Cu 0.1Bi modified compared to other workpieces. It was recorded around 1µm at feed rate of 0.05 and cutting speed of 70 m/min (Table 4.6 and Figure 4.12).

Table 4.6: Experimental result for surface roughness Al-11Si-1.8Cu Bi modified (0.1wt.%Bi)

NO	*Cutting speed (mm/min)*	*Feed rate (Mm/rev)*	*Depth of cut (mm)*	*Surface roughness Ra(μm)*
1	*70*	*0.05*	*0.5*	*1.501*
2	*130*	*0.05*	*0.5*	*1.323*
3	*250*	*0.05*	*0.5*	*1.000*
4	*70*	*0.1*	*0.5*	*4.501*
5	*130*	*0.1*	*0.5*	*3.122*
6	*250*	*0.1*	*0.5*	*1.801*
7	*70*	*0.15*	*0.5*	*4.990*
8	*130*	*0.15*	*0.5*	*3.785*
9	*250*	*0.15*	*0.5*	*2.434*

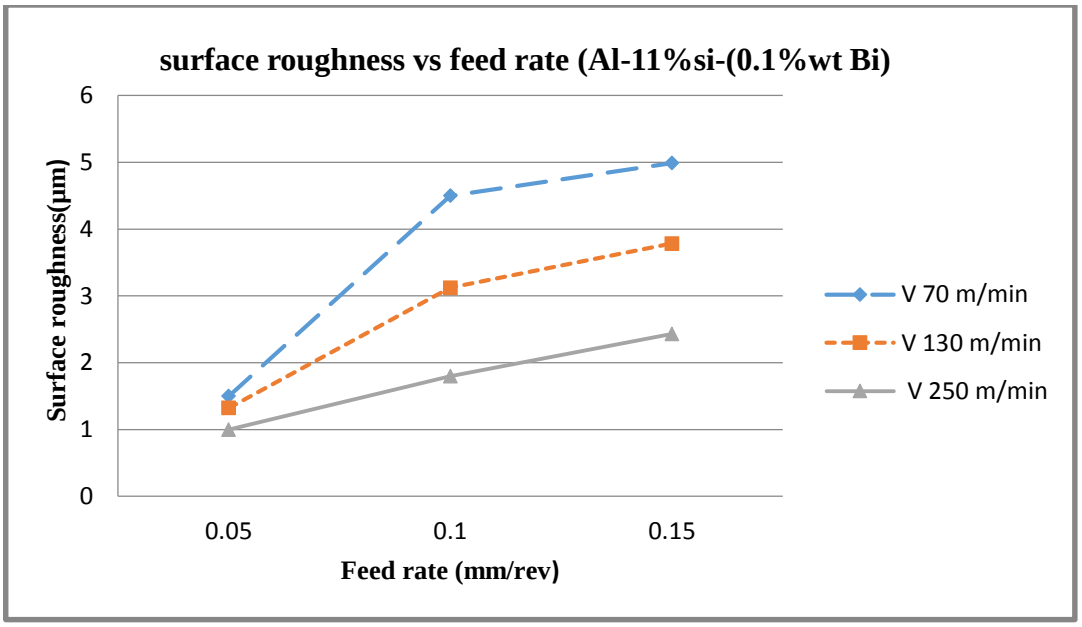

Figure 4.12 :Surface roughness and feed rate relationship when turning Al-11Si-1.8Cu Bi- modified.

Figure 4.13 shows the value of surface roughness as a function of feed rates in different cutting conditions for the base alloy and Bi, Sb, and Sr-containing workpieces. The surface roughness increased with increasing feed rate from 0.05 mm/rev to 0.15

mm/rev at all conditions of machining for all workpieces. It indicates that the increase in surface roughness at higher feed rates is due to the domination of feed mark and increase of distance from peak to valley of the machined surface. Also it can be observed that surface roughness reduced with increasing cutting speed from 70 to 250 m/min for all workpieces.

Strontium-containing alloy showed the highest roughness at about 5 µm at a feed rate of 0.15 mm/rev and cutting speed of 70 m/min, while it was just under 1.5 µm for the Bi-containing at the same feed rate and cutting speed. From the viewpoint of additives, the highest was obtained for strontium-containing alloy and the lowest value was measured for the bismuth containing alloy at the different feed rates and cutting conditions. It is obvious that Bi particles play an important role in improving surface roughness as a free machining element in machining process (Dasch et al., 2009). It may cause to reduce friction between tool and workpiece and improve chip breakability which leads to improve surface roughness (Barzani et al., 2013).

On the other hand, adding Sr increase surface roughness and leads to decreased machinability in comparison with other additives during machining process. It may have caused an increase in ductility of workpiece and an increased in adhesion at high temperature between tool and chip. These changes increase tendency of BUE formation in cutting zone and, consequently, has deteriorating effect on surface roughness after machining process (Barzani, Zalnezhad, Sarhan, Farahany, & Ramesh, 2015). In fact, the change in silicon morphology increases the ductility of the Al-Si phase which changes the tool geometry, resulting in a plastic deformation of the soft phase in the workpiece material and causing an increase in machinability (surface roughness and the cutting force) (Barzani et al., 2013). Moreover, antimony addition, which induced lamellar silicon, increased the ductility of alloy compared to the base alloy and, therefore, it behaves similar to Sr-containing alloy in machining of Al-Si alloy (Barzani et al., 2013).

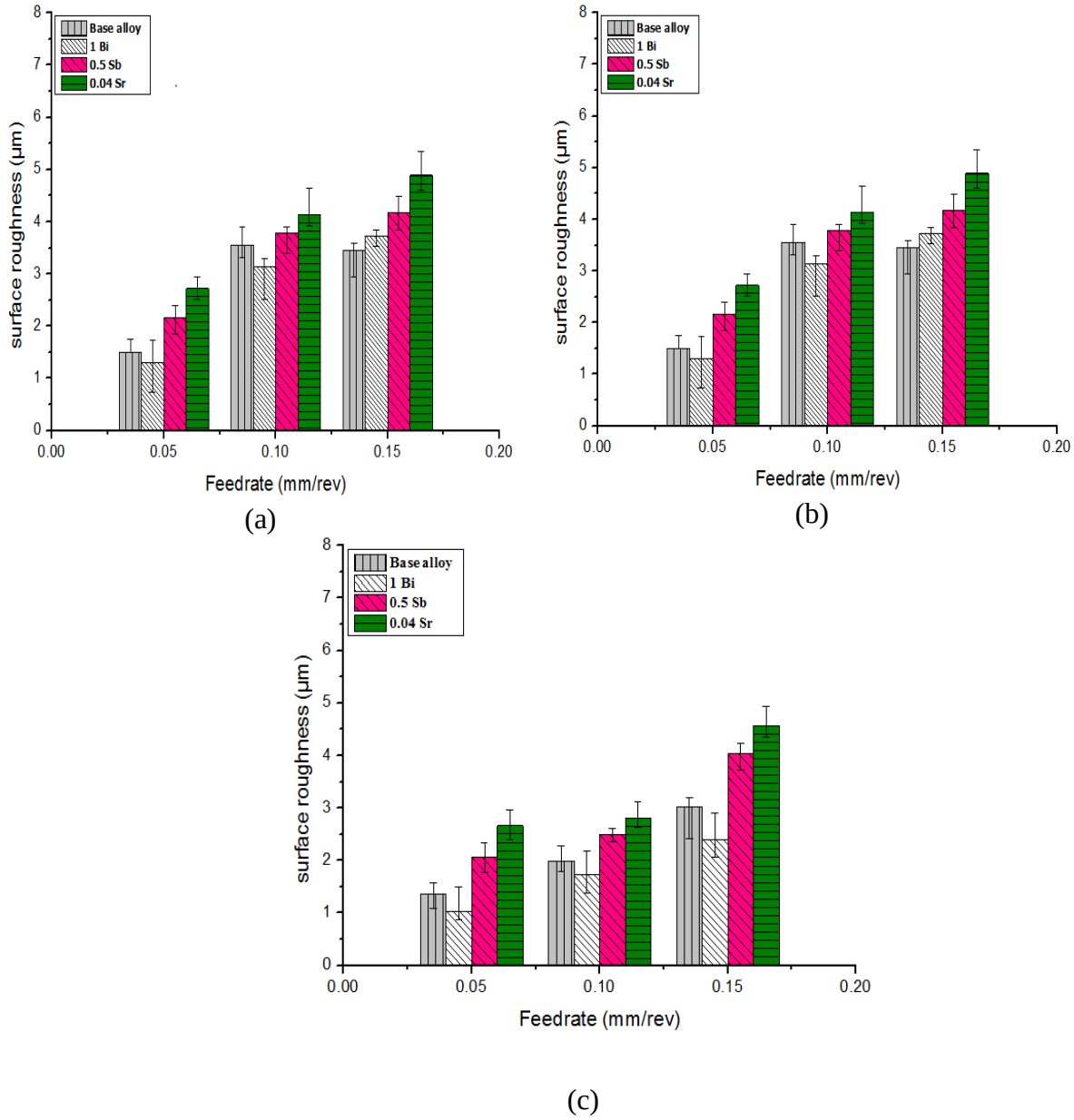

Figure 4.13: The value of surface roughness as a function of feed rates in different cutting conditions for the base alloy and Bi, Sb, and Sr-containing workpieces.(a) cutting speed 70/min, (b)130 m/min and (c) 250m/min

As an example, the plastic deformation near the cutting zone during turning of the antimony-containing workpiece at 250 m/min is shown in Figure 4.14(a). It is evident that the silicon particles were elongated in the machining direction resulting in silicon breakage on the surface of the workpiece and an increase in surface tearing, which produces a change in surface roughness. The cross-sections of the machined surface of

different workpiece materials at highest cutting speed (250 m/min) and highest feed rate (0.15 mm/rev) are shown in Figures 4.14 (b–e). As can be seen, the strontium-containing alloy (Figure. 4.14e), antimony-containing alloy (Figure. 4.14d) and base alloy (Figure. 4.14b) show more surface tearing during turning process, respectively. In contrast, Bi-containing alloy (Figure.4.14c) shows less surface tearing after machining process.

It seems that not only the silicon morphology, but other parameters must also be considered for the bismuth-containing workpiece, which exhibited the lowest surface roughness. It is interesting to note that some bismuth-containing particles were detected under back scattered electron (BSE) as shown in Figure 4.15. The energy dispersive spectroscopy (EDS) spectra confirmed that these particles mainly consist of bismuth. It has been reported that bismuth compounds can partially melt during turning, becoming effective chip-breakers (Basavakumar et al., 2007). Thus, it seems that bismuth acts as lubricant due to its low melting point, thereby decreasing the friction between chip and tool edge which leads to lower cutting forces, less tool wear, a low tendency to form BUE, and a smooth surface finish (Elgallad, Samuel, Samuel, & Doty, 2010). Due to the high atomic number of Bi, it may be detected easily in the form of white particles in the backscattered images.

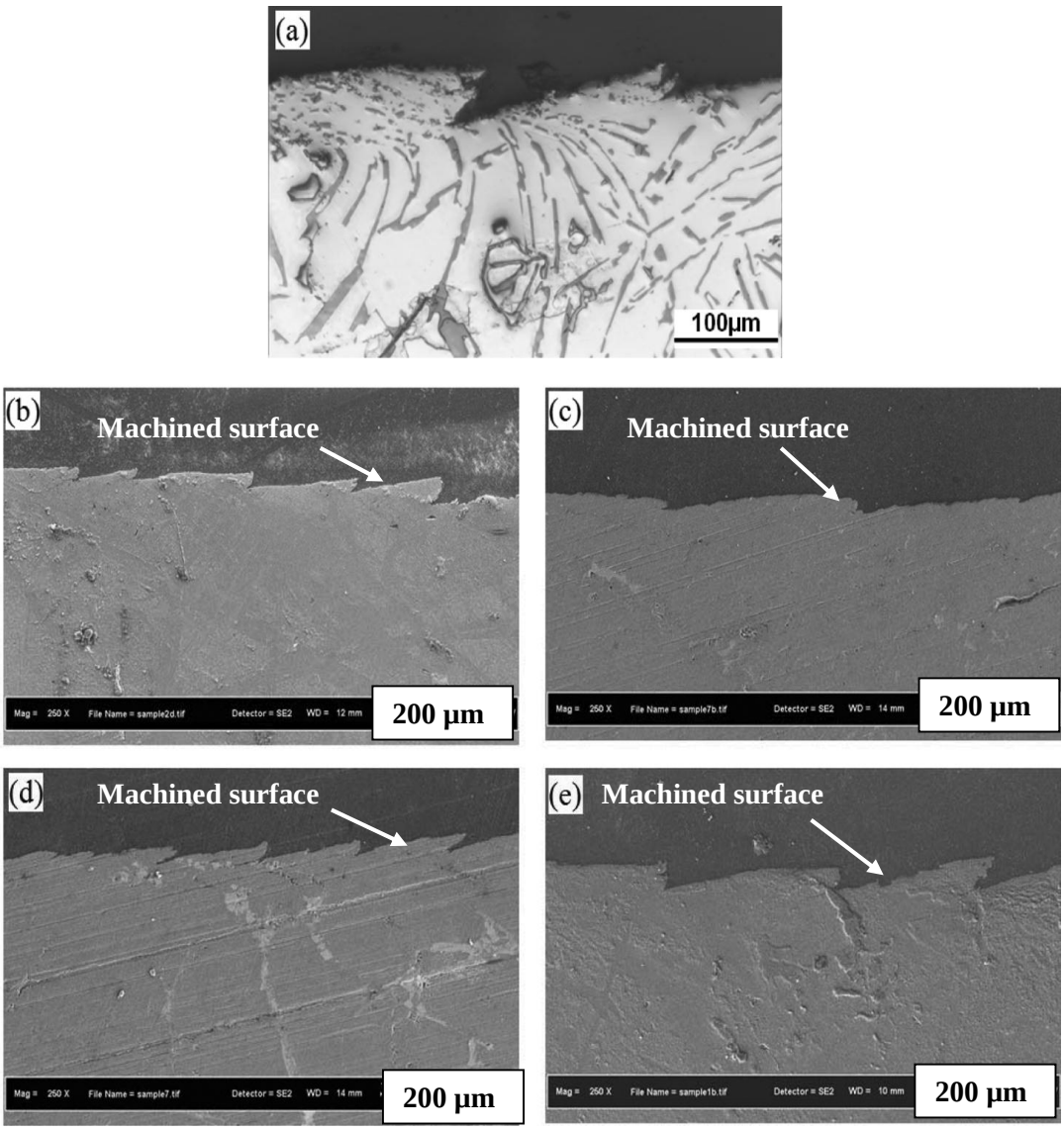

Figure 4.14: (a) Plastic deformation at cutting zone of Sb-containing and FESEM micrographs of machined subsurface of (b) base alloy, (c) 1% Bi-, (d) 0.5% Sb-, and (e) 0.04% Sr-containing workpieces at cutting speed of 250 m/min and feed rate of 0.15mm/rev.

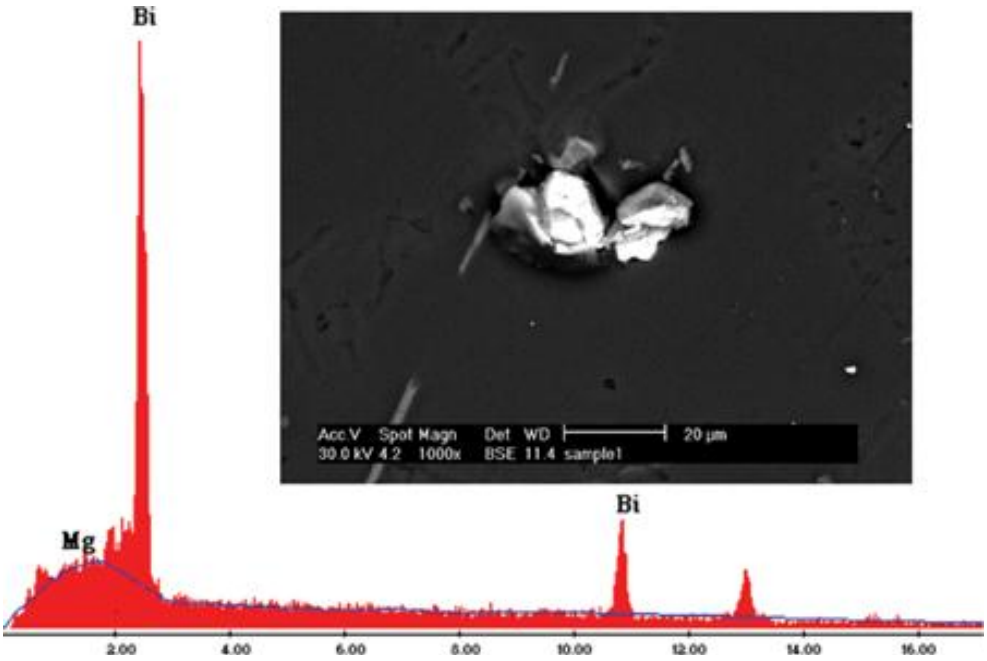

Figure 4.15: BSE image and EDS spectra of Bi-containing particle (white area).

4.5.1 Atomic Force Microstructure Results (AFM)

Feed marks and corresponding AFM images at the cutting speed of 250 m/min and feed rate of 0.15 mm/rev are illustrated in Figure 4.16. It indicates that the increase in surface roughness at higher feed rates is due to the domination of feed mark and increase of distance from peak to valley of the machined surface. In view of the three-dimensional images, hillocks and valleys are observed, and it is clearly shown that the bismuth containing workpiece exhibits the lowest feed mark (Figure. 4.16c) and hillocks in three-dimensional image (Figure 4.16d).

However, the strontium-containing alloy showed the highest feed mark (Figure 4.16g) and exhibited several hillocks and valleys (Figure 4.16h) in comparison to the other workpieces, which can be attributed to the fibrous morphology of the silicon phase. Figure 4.16 (e and f) illustrates the effect of Sb on machinated surface. As can be seen, the distance between peak and valley is much greater than base alloy and Bi-containing

alloy. Therefore, there are some pits on the machined surface which lead to decrease machinability of alloys. It is, therefore, clear that the changes in the topography and surface roughness are related to the change in hard phase morphology.

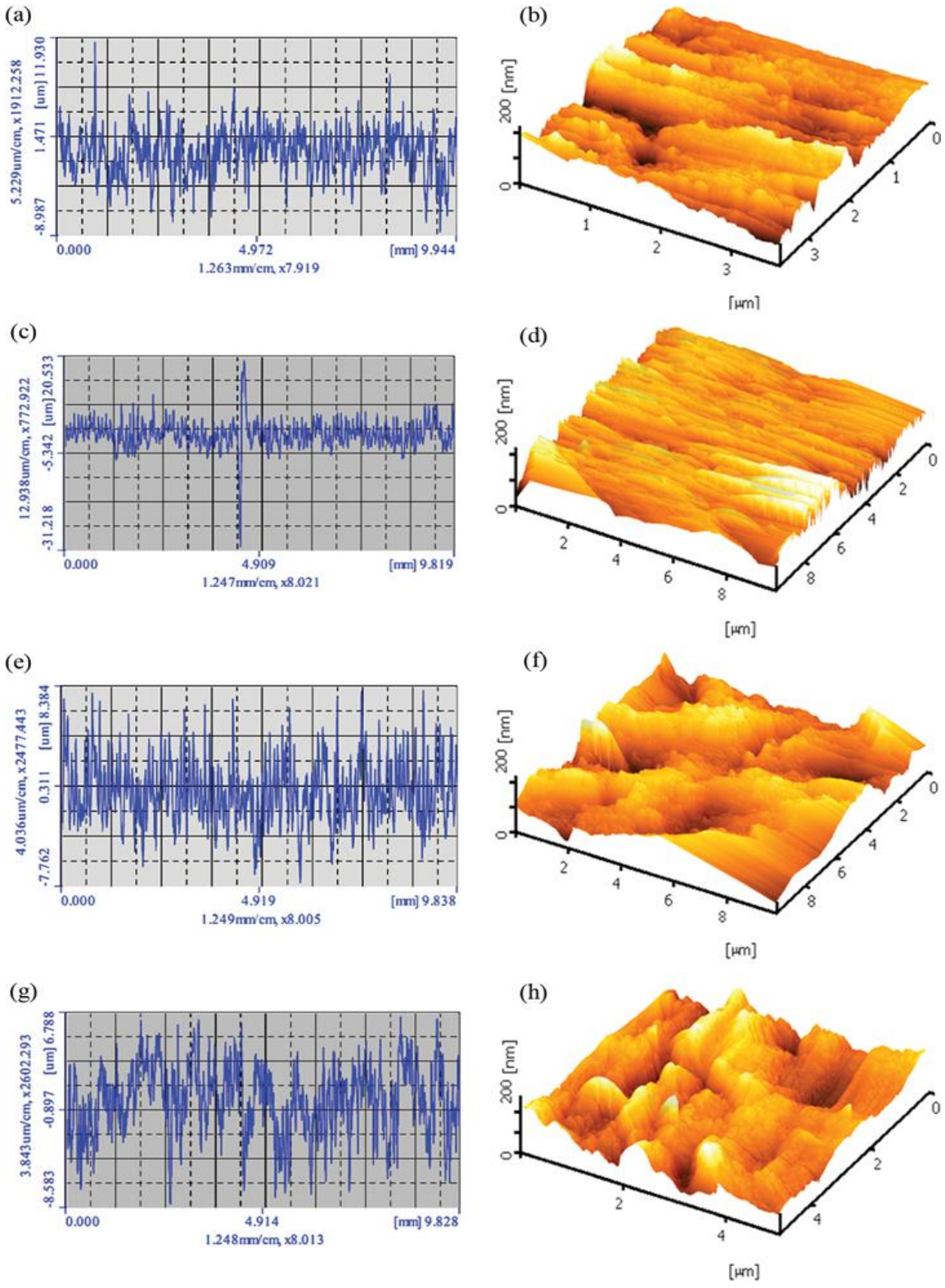

Figure 4.16: Feed mark and atomic force microscopy topographical of machined surface for different workpiece materials: (a), (b) base alloy, (c), (d) 1% Bi, (e), (f) 0.5% Sb, and (g), (h) 0.04% Sr.

4.6 Effect of Cutting Conditions on Cutting Force

One of the most commonly used criteria for evaluating machinability is the cutting force. Cutting force was recorded with three component force Dynamometer (Kistler, type 9265 B 3 axis) mount on the tool holder of 2-Axis CNC Lathe, and PVD coated insert was used throughout the experimental. The tangential force, Fc plays the role of supplying the energy needed for cutting operation. This force acts downward on the tool tip and tends to deflect the tool downward (Kalpakjian & Schmid, 2009). Studying the nature of cutting forces generated during chip formation is the most effective way for understanding the machining characteristics and deformation behavior of materials, and value of cutting force has been changed by shape of silicon during machining process.

Table 4.5 and Figure 4.17 show that the highest cutting force (F_c) was recorded (in experiment plan No.8) at around 80.73 N (at cutting speed of 130 m/min, feed rate of 0.15 mm/rev), while minimum cutting force was recorded (in experiment plan No 3) at about 14.45 N (at cutting speed of 250 m/min, feed rate 0.05 mm/rev) for Al-11%Si (base alloy). As shown in Figure 4.17 cutting force increased when feed rate increased from 0.05 to 0.15 mm/rev. It is clear that cutting force decreased with increasing cutting speed from 70 to 250 m/min. It can be related to amount of built up edge which is less in high cutting speed during machining process. It has been published that in high speed machining, chips are separated from machined surface very fast and, therefore, there is no time for the chips to stick on the rake of insert of composite. Consequently, chip breakability increase and leads to improved machinability in machining (Kalpakjian & Schmid, 2009).

Table 4.7: Experimental results of cutting force Al-11%Si1.8 Cu unmodified

NO	*Cutting Speed (m/min)*	*Feed rate (mm/rev)*	*Depth of cut (mm)*	*Cutting force (Fc) (N)*
1	*70*	*0.05*	*0.5*	*25.40*
2	*130*	*0.05*	*0.5*	*18.43*
3	*250*	*0.05*	*0.5*	*14.45*
4	*70*	*0.1*	*0.5*	*61.41*
5	*130*	*0.1*	*0.5*	*52.41*
6	*250*	*0.1*	*0.5*	*45.49*
7	*70*	*0.15*	*0.5*	*80.58*
8	*130*	*0.15*	*0.5*	*80.73*
9	***250***	***0.15***	***0.5***	***73.84***

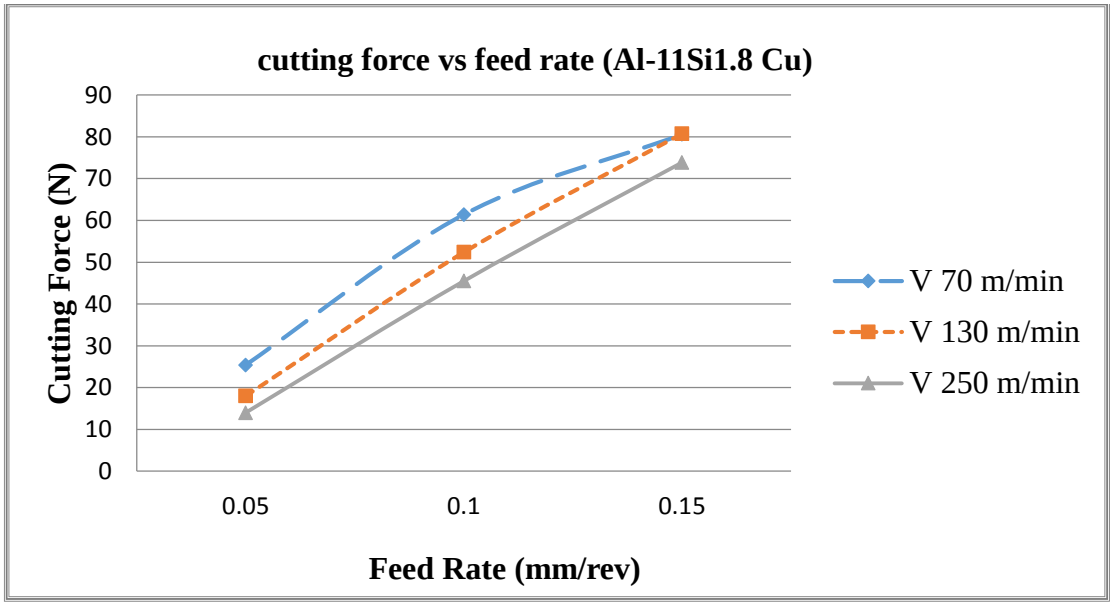

Figure 4.17: Cutting force and feed rate relationship when turning unmodified Al-11%Si1.8Cu.

According to Table 4.8 and Figure 4.18, the highest cutting forces for Al-%11Si1.8Cu0.04Sr modified was recorded (in experimental plan No7) just below 76 N (at cutting speed of 70 m/min and feed rate of 0.15mm/rev), and the lowest cutting force was recorded (in experimental plan No.3) at 15.44 N (at cutting speed 130 m/min and feed rate of 0.05 mm/rev).

Table 4.8: Experimental results of cutting force Al-%11Si1.8Cu0.04Sr modified

NO	*Cutting Speed (m/min)*	*Feed rate (mm/rev)*	*Depth of cut (mm)*	*Cutting force (Fc) (N)*
1	*70*	*0.05*	*0.5*	*24.18*
2	*130*	*0.05*	*0.5*	*18.30*
3	*250*	*0.05*	*0.5*	*15.44*
4	*70*	*0.1*	*0.5*	*57.24*
5	*130*	*0.1*	*0.5*	*53.53*
6	*250*	*0.1*	*0.5*	*50.24*
7	*70*	*0.15*	*0.5*	*75.63*
8	*130*	*0.15*	*0.5*	*74.89*
9	*250*	*0.15*	*0.5*	*66.13*

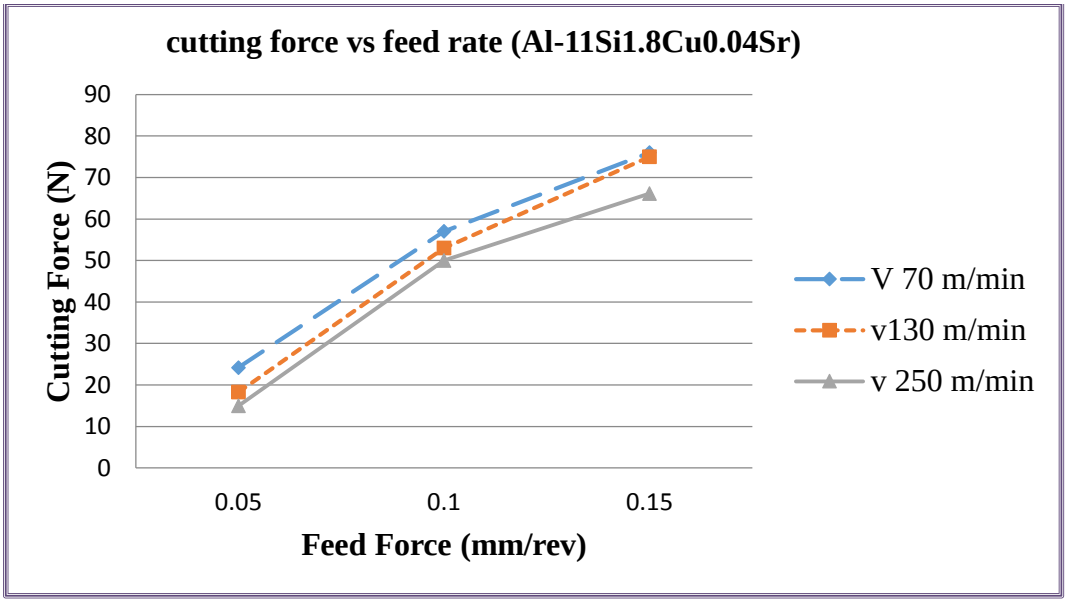

Figure 4.18: Force and feed rate relationship when turning Al-11Si1.8Cu0.04Sr modified.

Table 4.9 and Figure 4.19 show the magnitude of cutting force for Al-11Si1.8Cu0.05Sb modified. The highest cutting force was recorded at approximately 86.34 N (at cutting speed of 250 m/min and feed rate of 0.05 mm/rev). The lowest cutting force was recorded just below 22N at the same cutting speed.

Table 4.9: Experimental result of cutting force Al-11Si1.8Cu0.5Sb modified.

NO	*Cutting speed (m/min)*	*Feed rate (mm/rev)*	*Depth of cut (mm)*	*Cutting force (Fc) (N)*
1	*70*	*0.05*	*0.5*	*31.95*
2	*130*	*0.05*	*0.5*	*25*
3	*250*	*0.05*	*0.5*	*21.95*
4	*70*	*0.1*	*0.5*	*62.92*
5	*130*	*0.1*	*0.5*	*54.91*
6	*250*	*0.1*	*0.5*	*49.55*
7	*70*	*0.15*	*0.5*	*86.34*
8	*130*	*0.15*	*0.5*	*83.04*
9	*250*	*0.15*	*0.5*	*66.35*

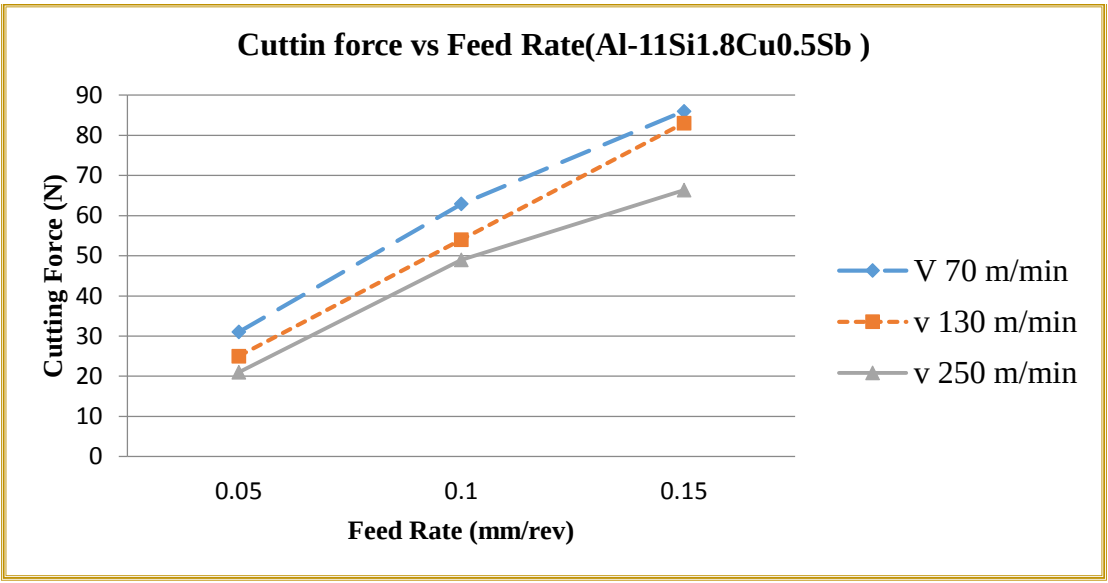

Figure 4.19: Cutting force and feed rate relationship when turning Al-11Si1.8Cu0.5Sb modified.

Table 4.10 and Figure 4.20 show cutting force for Al-11Si-1.8Cu0.1Bi modified. The highest cutting force is around 47.20 N, and the lowest cutting force 21.10 N at cutting speed of 250 m/min and feed rate of 0.05mm/rev.

Table 4.10: Experimental result of cutting force Al-11Si-1.8Cu0.1Bi modified

NO	*Cutting speed (mm/min)*	*Feed rate (Mm/rev)*	*Depth of cut (mm)*	*Cutting force(Fc)N*
1	*70*	*0.05*	*0.5*	*25.10*
2	*130*	*0.05*	*0.5*	*23.40*
3	*250*	*0.05*	*0.5*	*21.10*
4	*70*	*0.1*	*0.5*	*48.80*
5	*130*	*0.1*	*0.5*	*45.20*
6	*250*	*0.1*	*0.5*	*41.10*
7	*70*	*0.15*	*0.5*	*50.10*
8	*130*	*0.15*	*0.5*	*47.20*
9	*250*	*0.15*	*0.5*	*42.20*

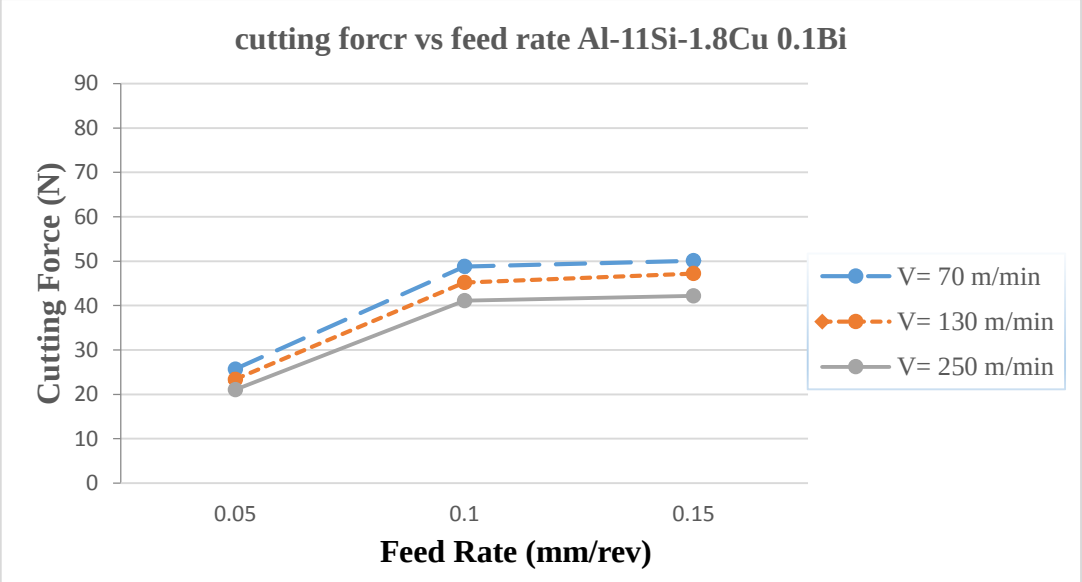

Figure 4.20: Cutting force and feed rate relationship when turning Al-11Si1.8Cu0.1Bi modified.

Average magnitudes of the main cutting forces with different cutting speeds and feed rates during turning process are represented in Figure 4.21. It can be seen that the cutting force increased when the feed rate increased from 0.05 mm/rev to 0.15 mm/rev for all workpieces. In addition, the main cutting force decreased when cutting speed increased from 70 m/min to 250 m/min. These observations are in agreement with the

result obtained for other workpieces during machining. In fact, an increase in the cutting speed increases the shear angle resulting in decreased friction between rake angle and chip, and due to an increase in the temperature, a reduced force is required in the cutting zone (Jiang et al., 2006).

It can be seen in Figure 4.21(a) that the alloy modified with strontium exhibited the highest cutting force at about 90N compared to the base alloy (Figure 4.21a) with 30 N. It has been reported by a number of observers that as the ductility increases, plastic deformation takes place in the cutting zone and consequently cutting resistance becomes greater, causing the cutting force to be higher (Janez Grum & Kisin, 2006). The base alloy which is composed of the brittle flake silicon showed the lower cutting force compared to strontium- and antimony-containing workpieces at the different cutting conditions. From the machinability point of view, a material having high yield strength, *i.e.* the sufficient force required per unit of area to create permanent deformation, necessitates a high level of force to initiate chip formation during machining operations. Thus, the lower the strength of the alloy, the lower the cutting force required during machining since specific cutting pressures decrease with a decrease in tensile strength as depicted during the machining of the base alloy compared to Sr and Sb-containing alloys.

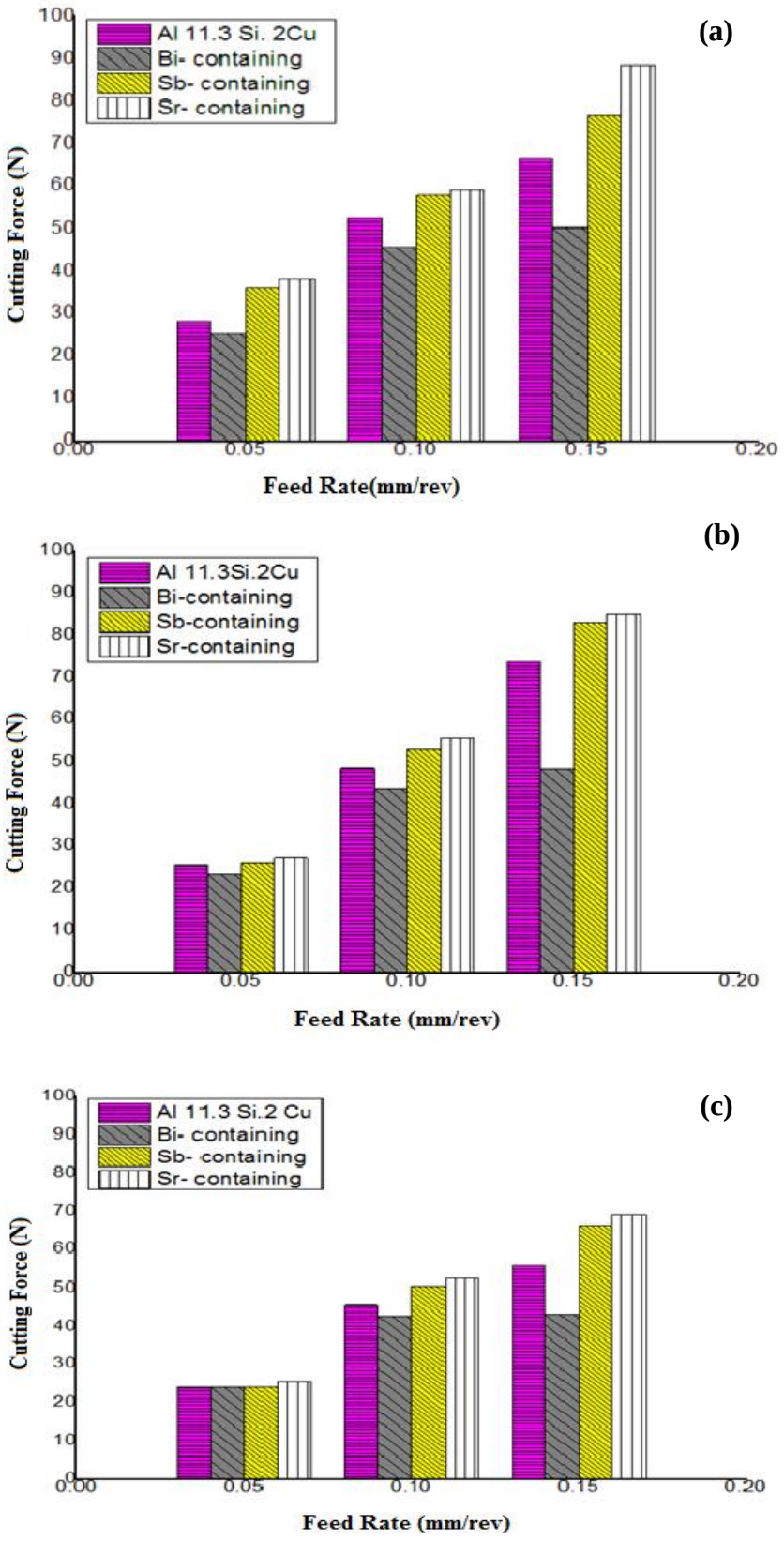

Figure 4.21: Effect of additives and feed rates on cutting force (Fc) at three cutting speeds: (a) 70 m/min, (b) 130 m/min, and (c) 250 m/min.

It is concluded from Figure 4-21 (a-c) that Bi-containing alloy shows the lowest cutting force compared to other workpieces in all machining conditions. It can be explained by providing the least built-up edge (BUE) during turning process which is able to decrease cutting force consequently improving machinability of alloy. Two different behaviors of BUE formation after turning of the Sr-containing alloy and Bi-containing alloy are clearly shown in Figure 4.22. It can be observed that BUE widely covered the rake face of the tool in strontium-containing material and changed the tool geometry.

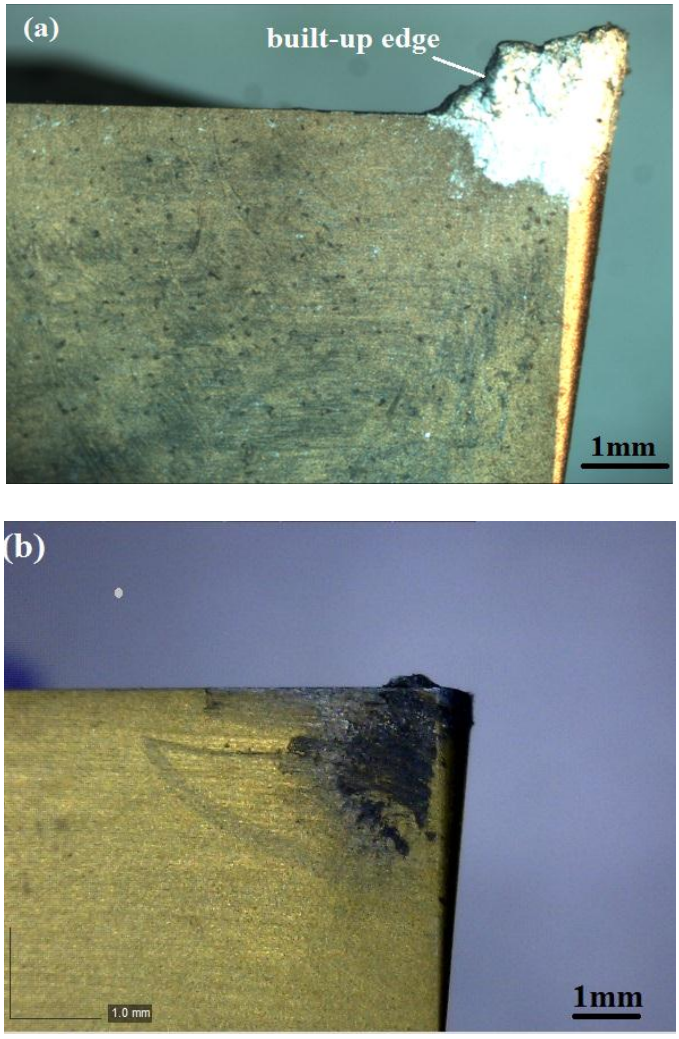

Figure 4.22: Built-up edge (BUE) formation in (a) Sr-containing alloy and (b) Bi-containing alloy.

However, according to microscopic analysis (Figure 4.23), additions of bismuth, antimony and strontium affected the morphology of the hard silicon phase. Therefore, any

changes in machinability parameters are mainly related to the alteration of silicon morphology in the workpieces.

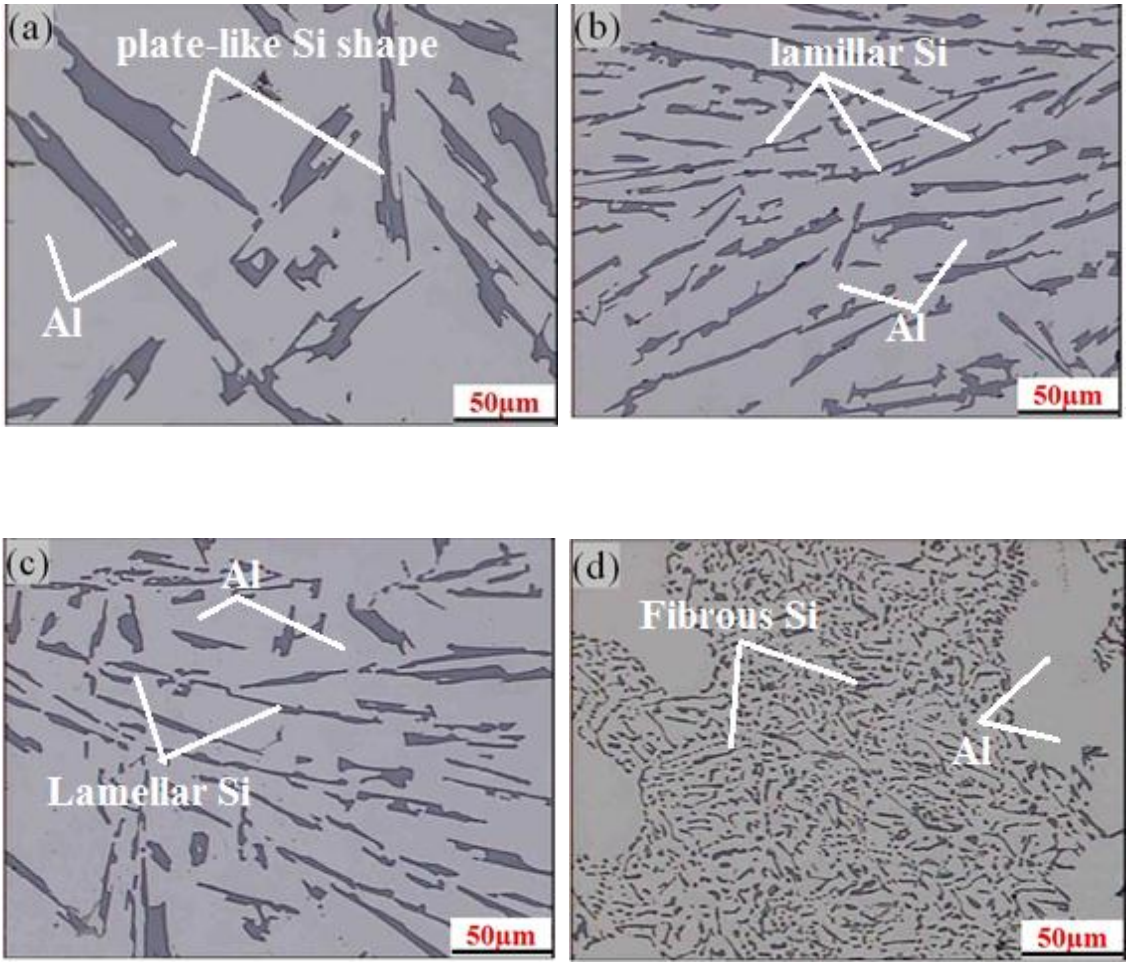

Figure 4.23: Optical microstructures of (a) base alloy, (b) Bi-containing, (c) Sb-containing, and (d) Sr-containing alloys indicating different silicon morphologies.

This result can be related to the change of silicon shape, where fibrous silicon has the highest cutting force value. Moreover, antimony addition, which induced lamellar silicon, increased the ductility compared to the base alloy, and therefore increased the force as well. In fact, the change in silicon morphology increases the ductility of the Al-Si phase which changes the tool geometry, resulting in a plastic deformation of the soft phase of the workpiece material and causing an increase in the cutting force. It is worth

mentioning that bismuth addition, which produces lamellar silicon structure similar to antimony, exhibited the lowest cutting force among all alloys investigated. It may be explained by the fact that Bi particles with low melting point play a lubricant role in machining process causing lower cutting forces, lower tool-wear rates, better dimensional accuracy, and increased machine tool life (Barzani, Sarhan, Farahani, et al., 2015).

4.7 Measure of Flank Wear

With regard to machinability as one of the characteristics of a given alloy, there are studies in the literature reporting the effects of metallurgical characteristics as being important factors in this context; these characteristics comprise the chemical composition, the microstructure, and the morphology of second phase particles of the alloy (Grum & Kisin, 2003). A particular characteristic of the two-phase and multiphase microstructures of Al-Si alloys is the fact that the matrix phase is soft and highly ductile whereas the second phase is considerably harder. In order to obtain a good surface finish, it is important that the particles of the hard phase be fine and uniformly distributed within the soft, aluminum matrix (Basavakumar et al., 2007).

Conversely, most aluminum alloys are fairly soft in relation to cast iron and steel, and are commonly machined by high speed steel (HSS) tools, although an exception to this may be observed with aluminum-silicon alloys. As mentioned before, near-eutectic Al-Si alloys are the most difficult of the various types of Al-Si alloys to machine. This is due to silicon phase which is almost ten times harder than the aluminum base alloy, thus causing the cutting tools to wear out rapidly. For this reason, consistent attempts have been made to optimize the selection of cemented carbide tools, cutting conditions, and tool geometry.

Investigation of the following points was also recommended (Janez Grum & Kisin, 2006): first, the effects of flank built-up on tool wear, second, the effects of cutting fluids on machinability, third, the improvement of machinability through the addition of certain elements. Although Cu and Mg are the main additives used to strengthen the alloys in the Al-Si systems, their effects on the machinability of near-eutectic Al-Si casting alloys has rarely been taken into account. Average flank wear (VB) was taken as tool wear criteria and measurements of it were conducted by using Dino light and optical microscope. Each experiment was repeated two times and two measurements of tool wear were taken from each experiment and the average of tool wear was obtained. As can be seen in Figure 4.24(a) for base alloy, flank wear is just below 0.05 mm in 5 min at cutting speed of 70 m/min, while it is 0.05 and just above 0.05 mm at cutting speed of 130 and 250 m/min, respectively. It can be seen that flank wear increased when cutting speed increased from 70 to 250 m/min.

As shown in Figure 4.24 (a-c) tool wear increased when feed rate increased from 0.05 to 0.15 mm/rev. It is known that friction increases with increasing feed rate which leads to heat built-up edge and tool wear increases especially in the case of aluminum alloys due to their low thermal conductivity and chemical affinity with tool materials at elevated temperatures. Consequently, there is surface integrity problem at the end of product that will reduce product effectiveness, quality and reliability (Basavakumar et al., 2007).

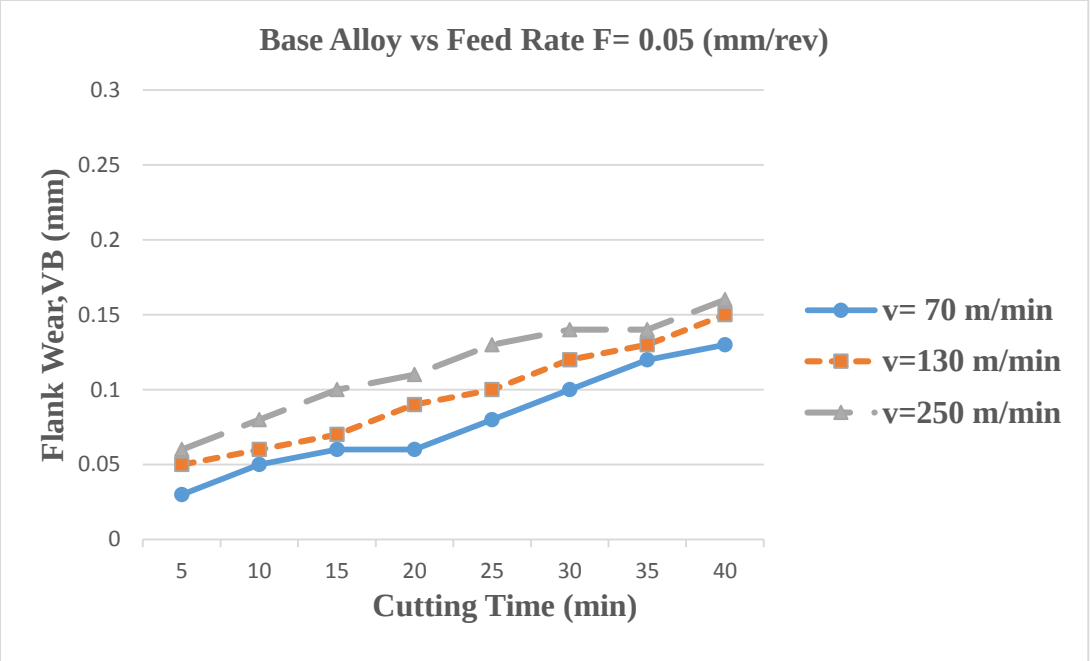

(a)

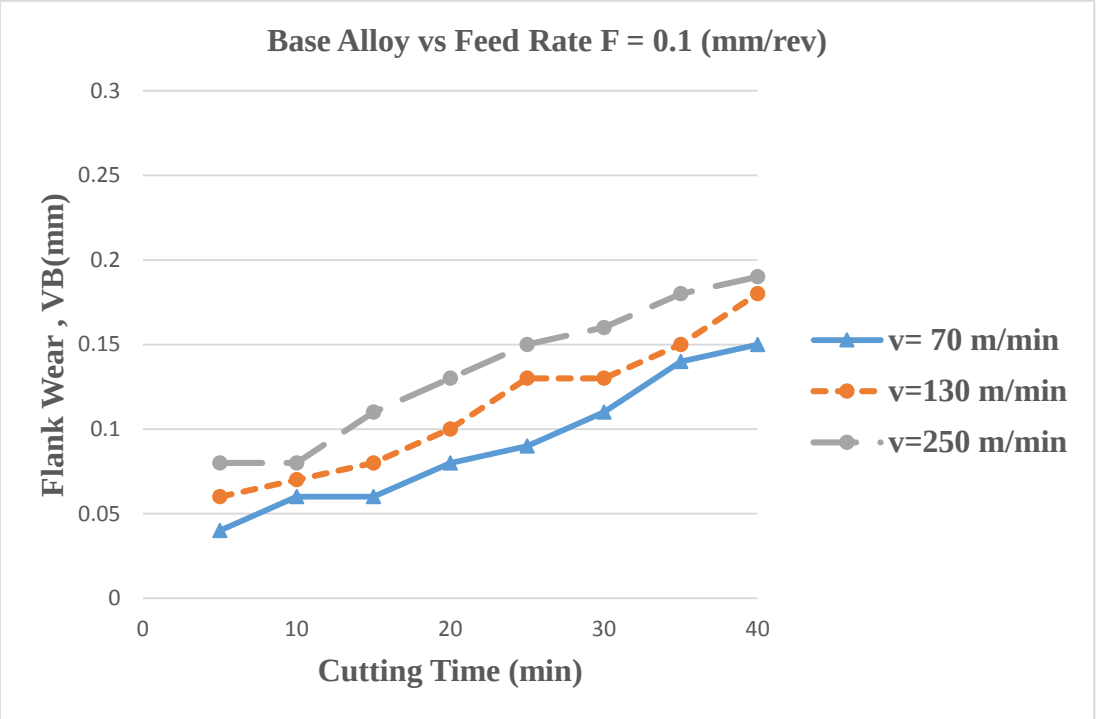

(b)

As can be seen in Figure 4.25(a), tool wear started just above zero in 5 min at cutting speed of 250 m/min for Bi-containing alloy and reached around 0.1 in 40 min (at feed rate of 0.05 mm/rev). As an overall trend, tool wear increased when cutting speed increased from 70 m/min to 250 m/min. Tool wear also increased with rising feed rate

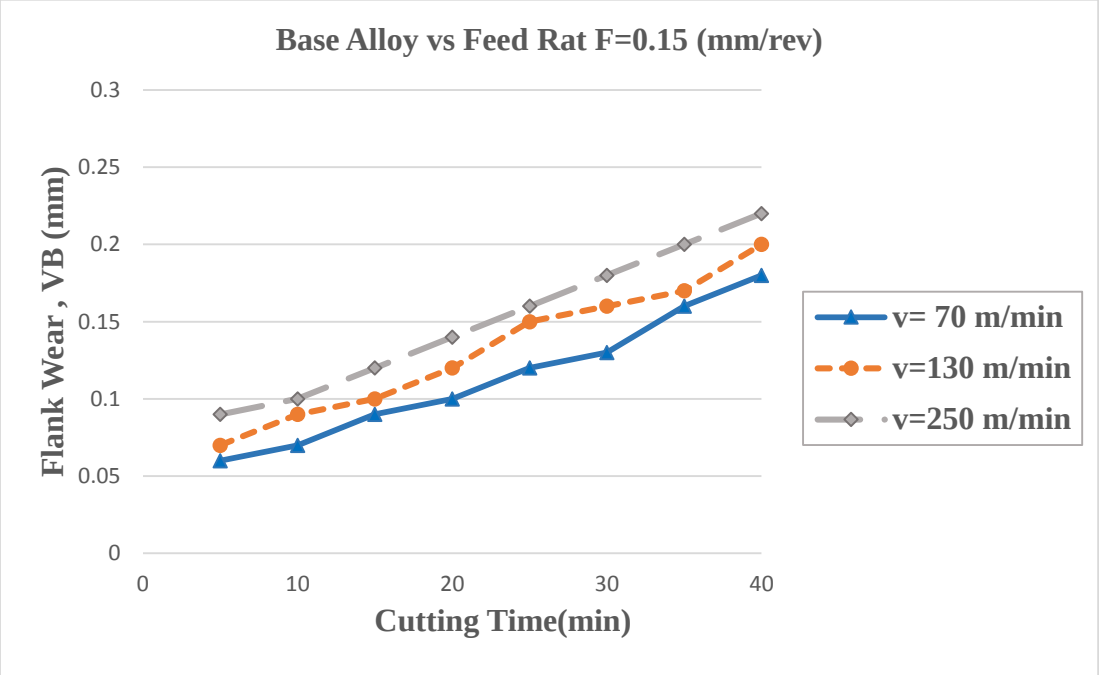

(c)

Figure 4.24: Effect of feed rate and cutting speed on flank wear in base alloy

from 0.5 mm/rev to 0.15 mm/rev. The reason is that the increase in feed rate increases the heat generation, and hence tool wear and decreases the surface roughness value in machining process. It is worth mentioning that Bi decreased tool wear in comparison with other additives in all cutting conditions. In fact, Bi as fine-particle reinforcement plays an important role during turning process. It can decrease BUE which leads to decrease flank wear and improves machinability of Al/Si alloy (Barzani et al., 2013).

As shown in Figure 4.25(c) tool wear reached to just above 0.15 mm at highest feed rate (0.15 mm/rev) and highest cutting speed (250 m/min) which is less than other workpieces. It should also be kept in mind that the Bi-containing alloy has the greatest degree of hardness compared to the other alloys under investigation. Owing to its high hardness and low ductility values, the Bi-containing alloy shows little tendency towards built-up edge formation. It is presumed that tool life is adversely affected by an increase in workpiece hardness, since the cutting loads and temperatures increase with increasing hardness values of the material, thereby reducing tool life even further.

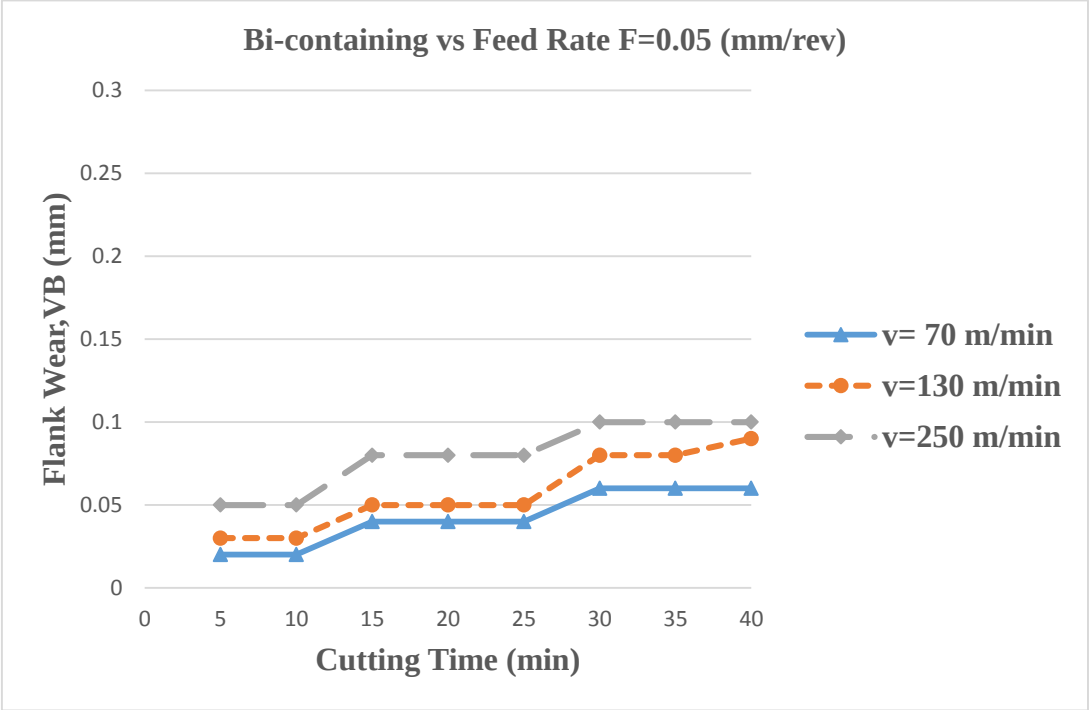
Bi-containing vs Feed Rate F=0.05 (mm/rev)
Flank Wear,VB (mm)
0.3
0.25
0.2
0.15
0.1
0.05
0
0
5
10
15
20
25
30
35
40
Cutting Time (min)
v= 70 m/min
v=130 m/min
v=250 m/min

(a)

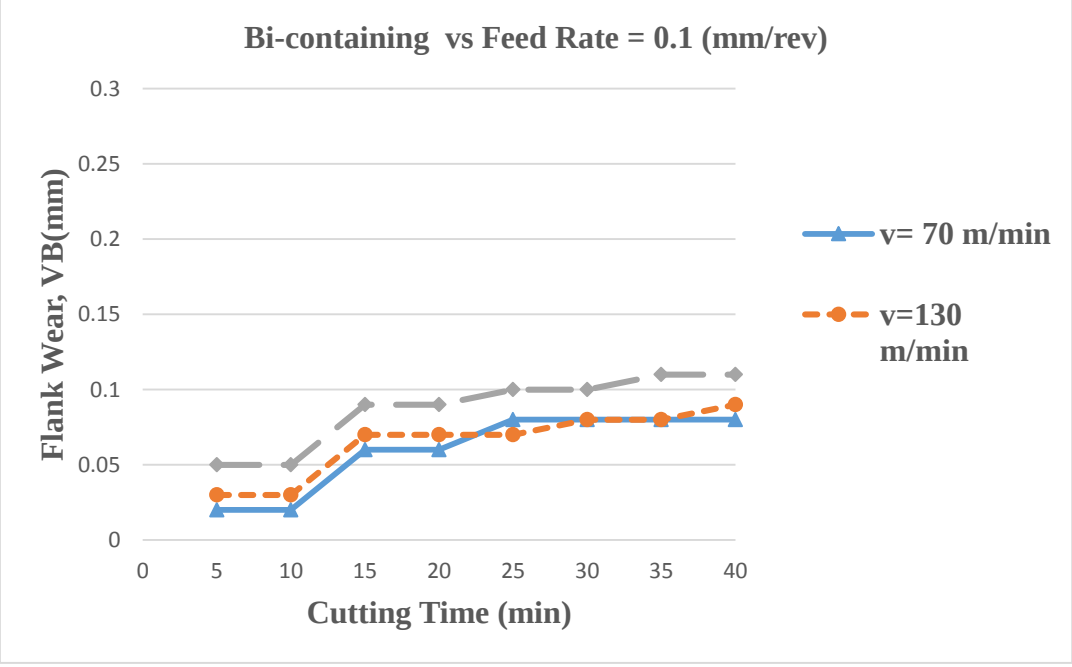
Bi-containing vs Feed Rate = 0.1 (mm/rev)
Flank Wear, VB(mm)
0.3
0.25
0.2
0.15
0.1
0.05
0
0
5
10
15
20
25
30
35
40
Cutting Time (min)
v= 70 m/min
v=130 m/min

(b)

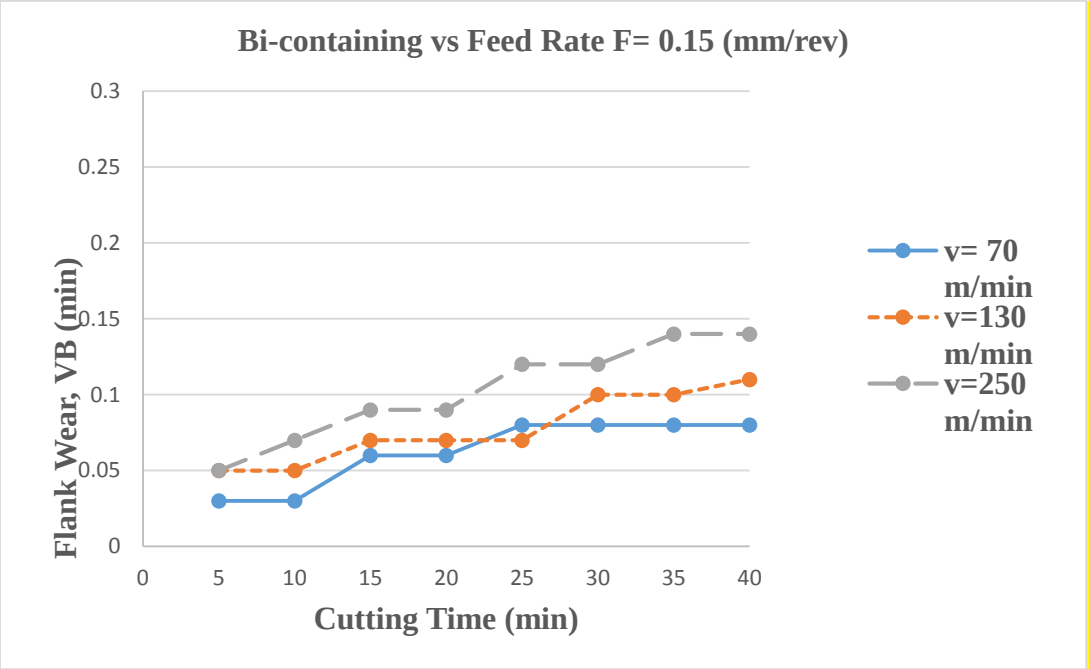

(c)

Figure 4.25: Effect of feed rate and cutting speed on flank wear in Bi-containing alloy.

Figures 4.26 and 4.27 show tool wear for Sb and Sr-containing workpieces with different feed rates (0.05 mm/rev to 0.15 mm/rev), and cutting speeds (70 m/min to 250 m/min), respectively. It is obvious that Sr and Sb alloy elements increased tool wear with increasing built-up edge during machining time. It can be seen that tool wear is around 0.25 mm in Figure 4.26(c) for Sb at highest cutting speed (250 m/min) and highest feed rate (0.015 mm/rev), while it reached 0.3 mm in the same cutting condition for Sr-containing workpiece (Figure 4.27c).

It is clear that Sr has negative effect on machinability of Al-Si alloy. It can provide massive BUE on the rake face of insert (Figure 4.28) which may cause an increase in magnitude of cutting force and decrease surface finish in turning process. It has been published that an increase in the cutting speed caused the cutting tool to be subjected to a high degree of abrasion by some reinforcements in the form of micro cutting along the flank face at higher velocities (Barzani, Sarhan, Farahany, et al., 2015). This mechanism

can be enhanced the ploughing of the cutting tool material by the harder abrasive particles to be more pronounced at higher cutting velocities. The ploughing effect induced several plastic deformation in the metal matrix composite (MMC) material with subsequent increase in the mechanical load of the cutting tool (Kannan & Kishawy, 2006).

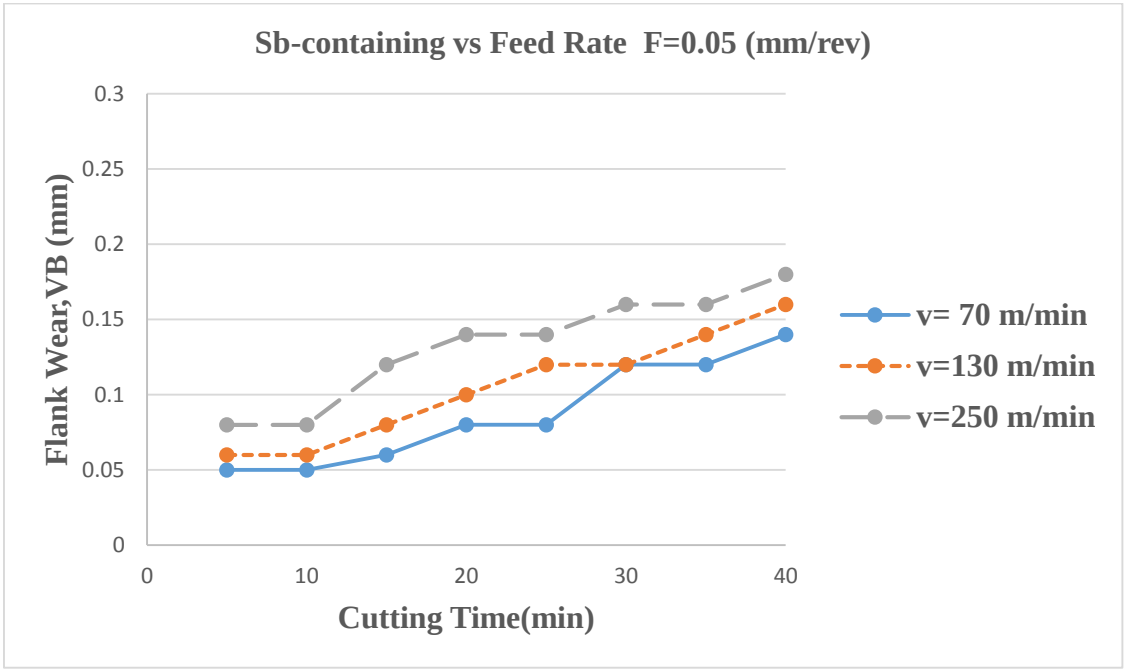

(a)

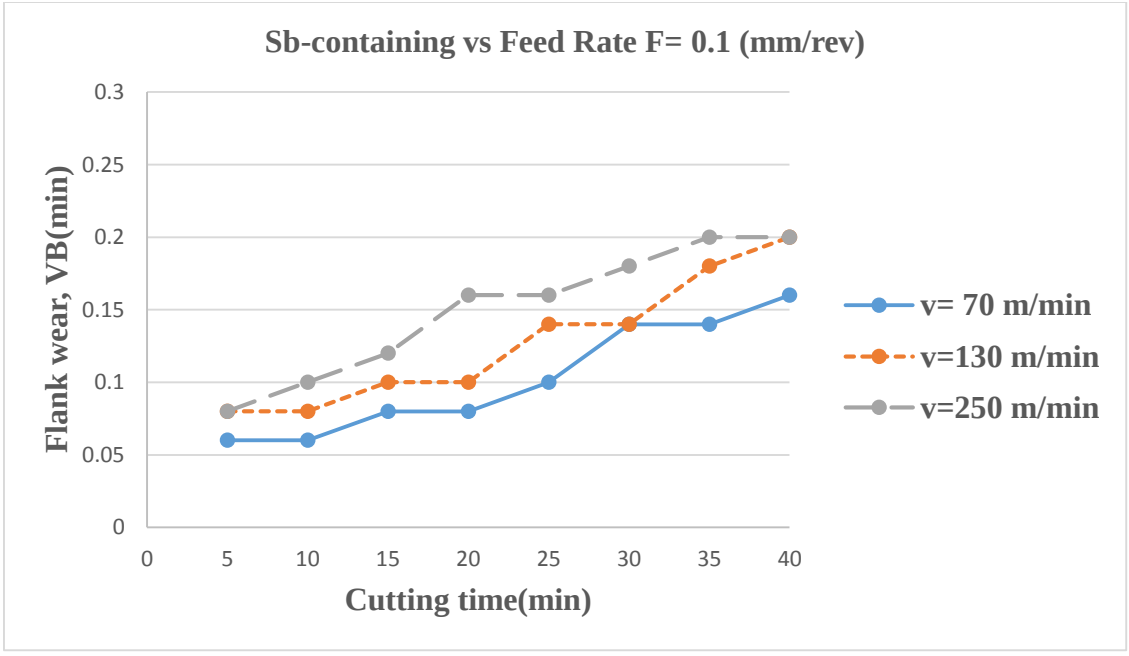

(b)

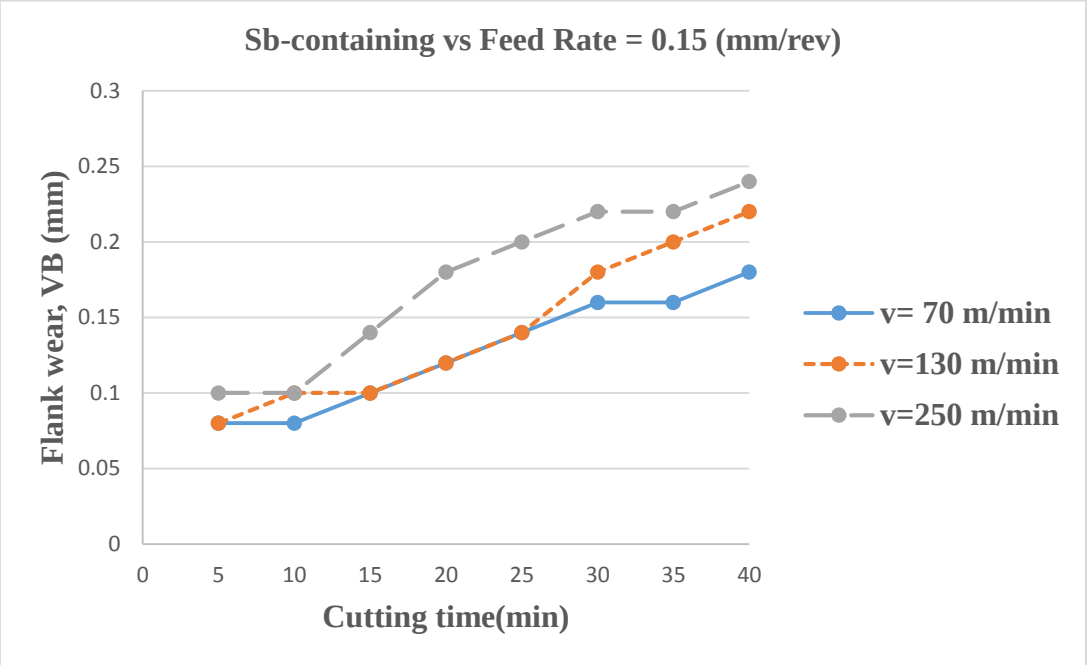

(c)

Figure 4.26: Effect of feed rate and cutting speed on flank wear in Sb-containing alloy.

As can be seen in Figure 4.27 (a-c) tool wear is reached to 0.2 mm in high cutting speeds (130 m/min and 270 m/min) after 40 min machining which is more than other workpieces in the same condition of machining. Although, Sr and Sb are added to alloys to improve mechanical properties, they have deleterious effects on machining of Al-Si alloy with increasing ductility of alloy and changing silicon morphology from plate to fibrous and lamellar shapes, respectively. The trend for increasing tool wear is the same as other workpieces. As an expected result, tool wear increased with changing cutting speed from 70 m/min to 250 m/min and increasing feed rate from 0.05 to 0.15 mm/rev. The increase tool wear in high cutting speed is related to domination of feed mark which is high for Sr-containing alloy. It is presumed that tool life is adversely affected by an increase in workpiece hardness, since the cutting loads and temperatures increase with increasing hardness values of the material, thereby reducing tool life even further.

In contrast, some alloy elements have been used to improve machinability. In this regards, Kılıçkap, Çakır, Aksoy, & İnan (2005) reported that when aluminium casting alloy contain both 1% and 5% Mg, the surface roughness after machining is considerably improved, while there is only a slight effect apparent with regard to tool wear and cutting force .They have found that this improvement is attributed to a significant increase in the hardness of matrix (Ozben et al. (2008) found that a small addition of about 0.3% wt% caused a significant increase in material hardness and drastically reduced the tendency towards built-up edge formation on the cutting tool.

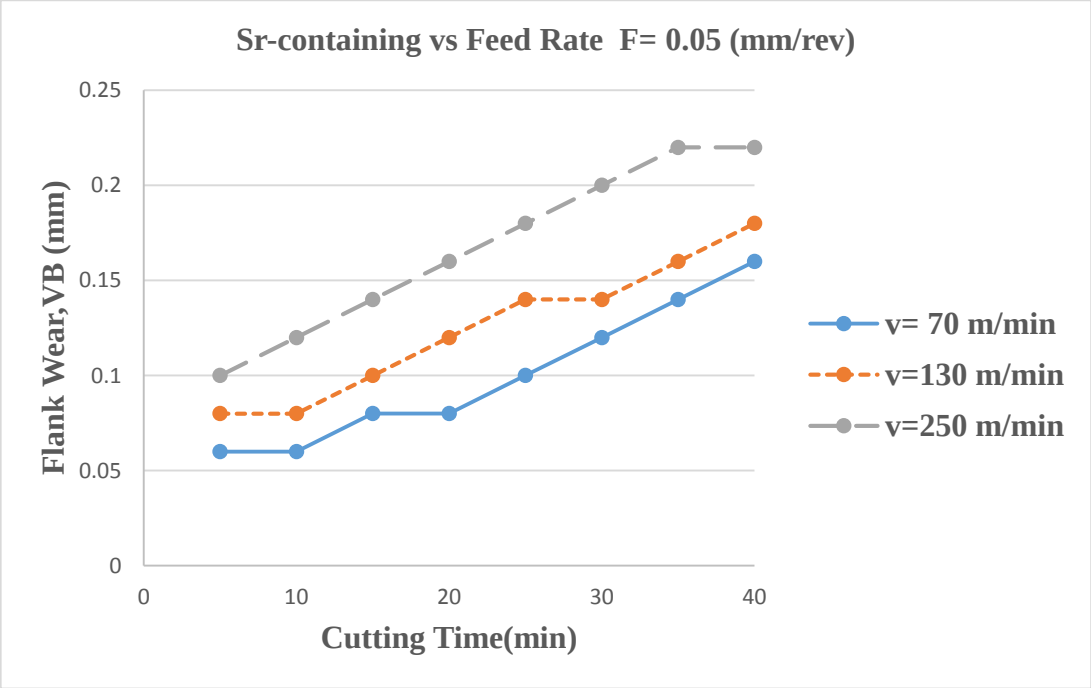

(a)

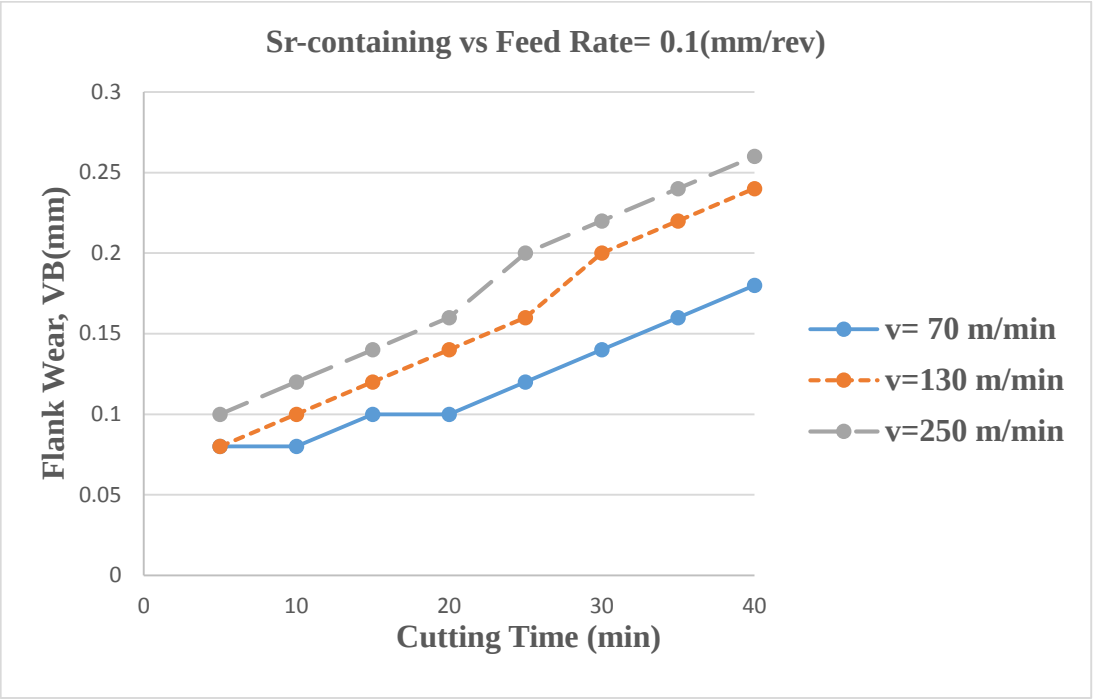

(b)

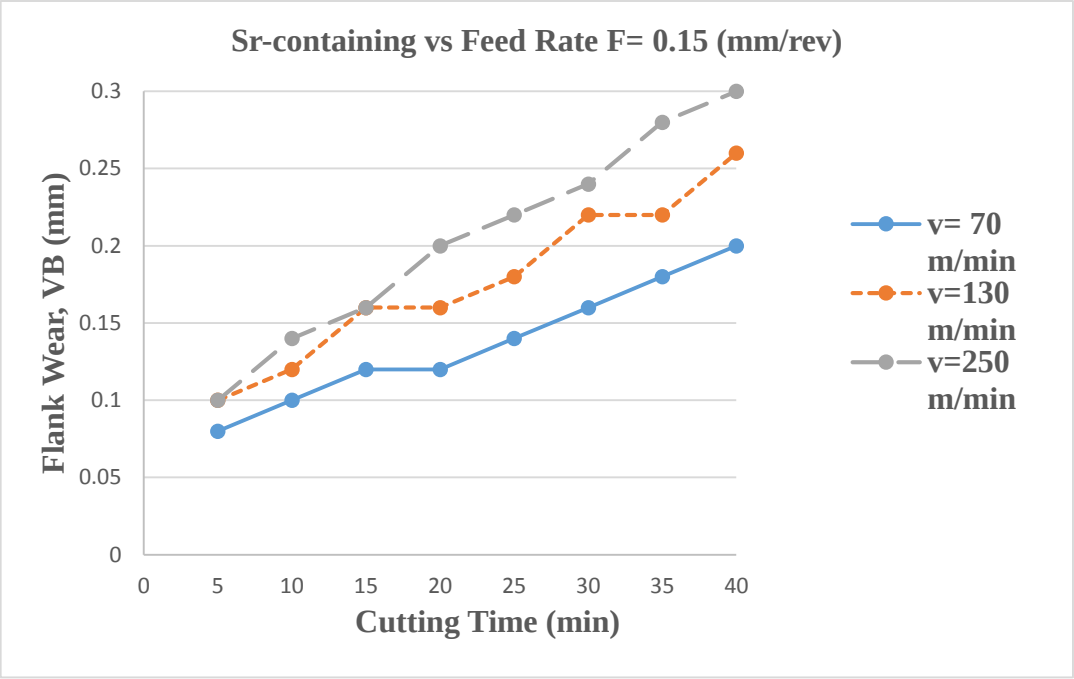

(c)

Figure 4.27: Effect of feed rate and cutting speed on flank wear in Sr-containing alloy.

The better performance of the coated tools could also be explained by a larger and more stable built-up edge (BUE) formation on the coated tools than that on the uncoated

tools. The reason is that the presence of BUE under certain conditions was shown to protect the flank face (Kılıckap, Cakır, Aksoy, & Inan, 2005). BUE is shown on the flank face surface for all workpieces (Figure 4.28). The Sr-containing and Sb-containing alloys present a massive built-up edge in comparison with other workpieces. It is seen in Figure 4.28 for all workpieces that tool wear increases with increasing the cutting speed. This finding is in agreement with the well-known phenomenon that during machining at ambient temperatures, increasing the cutting speed results in an increase in the cutting zone temperature which causes the recrystallization of the highly strained material of the BUE thus reducing hardness and stability (Fang & Liu, 2004).

Pramanik, Zhang, & Arsecularatne (2007) suggested that the introduction of a second phase into a metal structure lowers its ductility, allowing fracture somewhere along the rake face after severe deformation. The occurrence of BUE is also affected by feed rate in uncut chip thickness, rake angle, tool material, and lubrication. For example, the BUE disappears completely at high speeds in accordance with the commercial purity of the aluminum alloy. As shown in Figure 4.28, there is less BUE on the flank face of insert for machining Bi-containing alloy. The most important reason is that Bi particles can penetrate in the machined surface and it may cause decrease in temperature in cutting zone leading to decrease BUE formation during machining process.

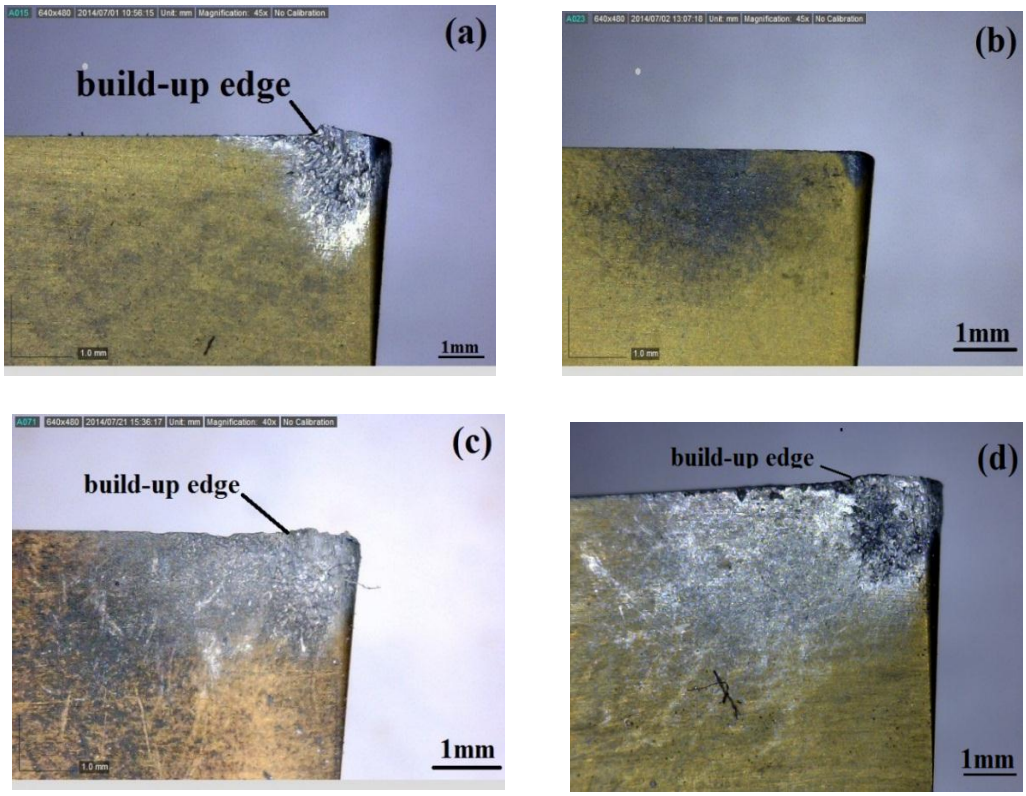

Figure 4.28: BUE formation on the flank face (a) base alloy (b) Bi-containing (c) Sr-containing (d) Sb –containing at cutting speed of 250 m/min an d feed rate of 0.15 mm/rev.

Figure 4.29 shows the effect of cutting condition on flank tool for all workpieces. As an overall trend, tool wear increased with increasing feed rate and cutting speed. It is clear that Bi alloy element shows the lowest tool wear at around 0.05 mm in 5 min to just below 0.15mm in 40 min, while displaying that the tool wear of base alloy element was around 0.1 mm in 5 min to just above 0.2 mm in 40 min. As demonstrated, Sr and Sb increased tool wear with increasing built-up edge and ductility of workpieces. However, tool wear started from 0.1 mm for both Sr and Sb- containing in 5 min, reaching 0.3 mm and 0.25 mm in 40 min for Sr and Sb-containing, respectively.

Lamellar silicon morphology in antimony-containing alloy is shown in Figure 4.23 indicating similar behavior to that observed in bismuth-containing alloy. However, compared to antimony, the addition of bismuth appears to have caused a more refining

effect. Bi plays a lubricate role during machining which decreases friction between workpiece and tool and there is no tendency to BUE formation. As result, Bi element has been used to improve machinability of Al/Si alloy (Dasch et al., 2009). Kılıçkap et al. (2005) reported that the dominant variables influencing tool life and tool wear in the Al-Si alloys are the morphology of eutectic silicon, the in-homogeneities of the alloy structure, and an interrupted regime of cutting resulting from the coarse undissolved particles.

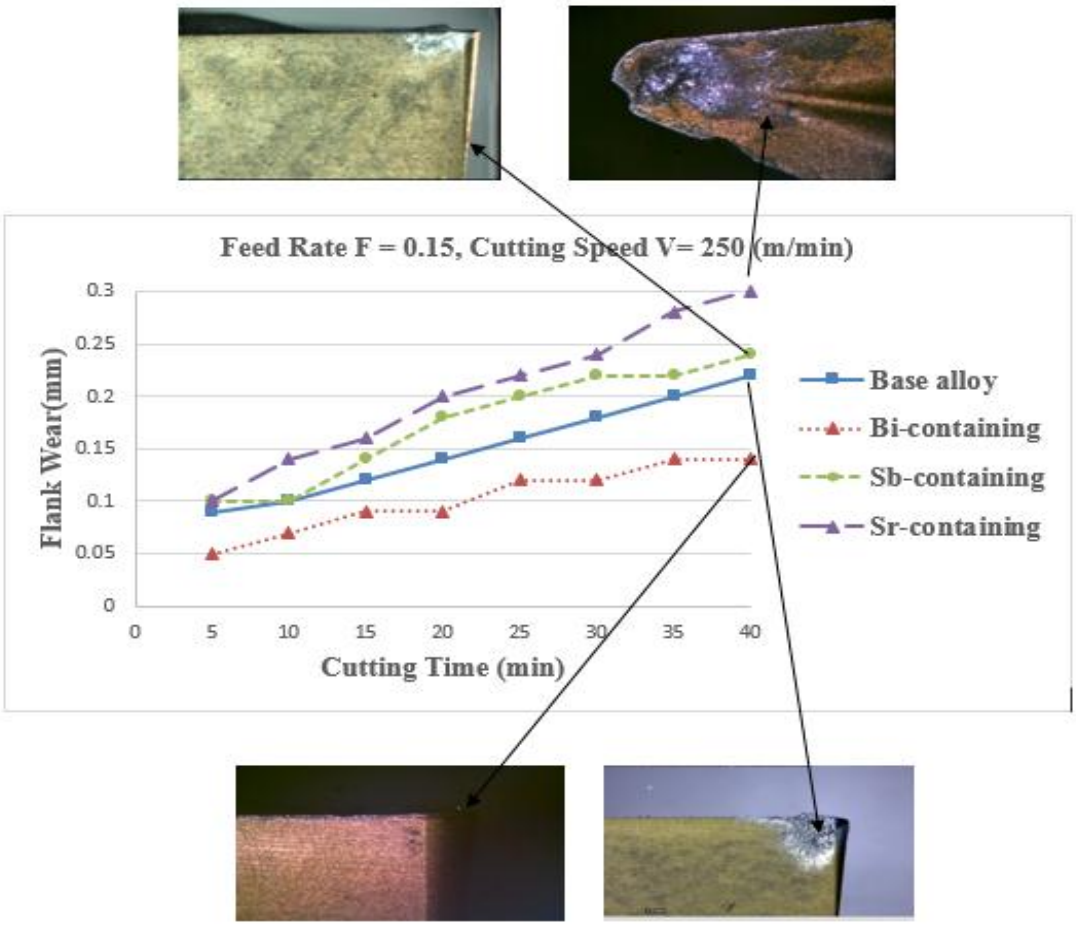

Figure 4.29: Effect of feed rate and cutting speed on flank wear for all workpieces at cutting speed 250 m/min and feed rate 0.15mm/rev

4.8 Chip Morphology

Chip morphology plays an important role in machining Al-Si alloys, and it has a direct effect on the machinability of alloys or composites. It is understood that the variation in the dimensional accuracy and finish of machined surfaces on Al-Si alloys are often a function of changes in processing condition and composition of its constituents (Dabade & Joshi, 2009b). These variations are reflected in the type of chips found during machining beside other variables like surface roughness, cutting force, hardness and residual stress. Therefore, it is clear that a fundamental study of chips and mechanism of their formation could be very useful in analyzing the machining process.

Dabade & Joshi (2009) reported that size and volume fraction of reinforcement are two important reasons to have chip segmentation during machining process. They have found that an increase in volume fraction of reinforcement reduce the number of chip curls due to reduction in strain during machining. Semi- continuous type chips were observed during machining of Al/SiCp composite. It was attributed to reduction in ductility of work material due to addition of SiC reinforcement in composite material. It has been found that elemental and curl type chips were found which was attributed to increase in hardness due to addition of higher volume fracture of Al4C3 reinforcement (Ozcatalbas, 2003).

Iuliano, Settineri, & Gatto (1998) reported that the reinforcement particles pile up along shear planes, which drive the deformed chip in to layers during high-speed turning of metal matrix composite (MMC). However, the types of chip formed were not only related to the nature of the shear zone but are also influenced by material properties such as thermal conductivity, ductility and microstructure. Furthermore, physical phenomena such as instability in the cutting process can change the chip formation mechanism.

4.8.1 Effect of Cutting Speed and Feed Rate on Chip Morphology

Figures 4.30 and 4.31illustrate the effect of cutting speed and feed rate on chip formation at higher and lower cutting speed and feed rate, respectively. As can be seen in Figures 4.30 (a-c), chips have larger radii spring type shape at higher cutting speed and higher feed rate for base alloy, Sr and Sb-containing alloys, respectively. In fact, the change in form of chips from C-type to spring type with increasing cutting speed from 70 m/min to 250 m/min is due to an increased in ductility of workpiece material at high temperature during machining process. At the same time, these reinforcements will have a greater tendency to stick to the tool face for longer duration. This may force the chip to take a longer path by curling through larger diameter.

According to Figure 4.30(d), Bi-containing alloy shows segmentation chips (C-type) after machining in comparison with other workpieces. It may be caused by Bi which acts a lubricant role in machining process and makes the material ideal for producing such C-type chips, which can be easily discarded after machining and improves chip breakability. Thus, it could be beneficial to the machinability aspects.

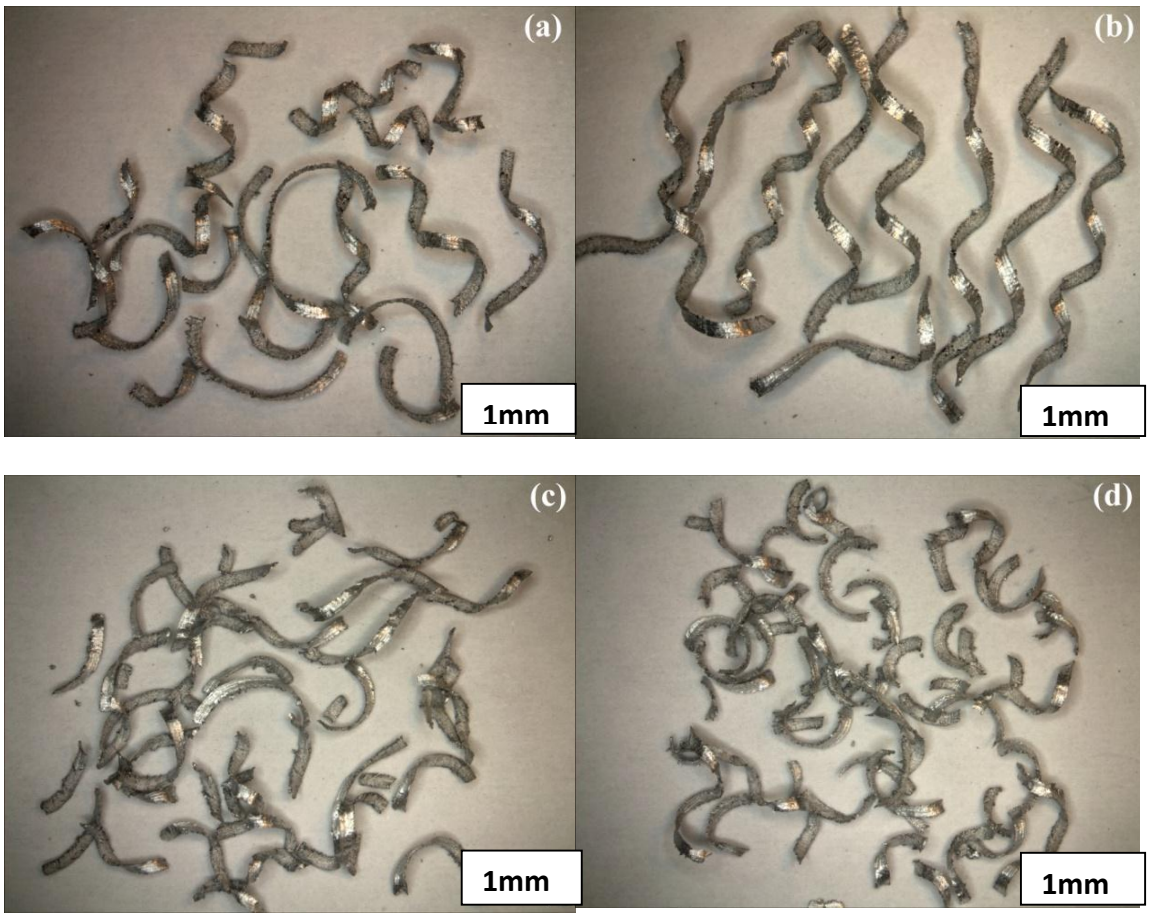

Figure 4.30: Optical micrographs showing different types of chip obtained for (a) base alloy (b) Sr-containing (c) Sb-containing (d) Bi-containing at cutting speed of 250 m/min and feed rate of 0.15 mm/rev.

As shown in Figure 4.30 and 4.31, chips generated are of segmented type. The length and thickness of chip segment reduces with a decrease in feed rate and generated around ½ curled segmented (Figure 4.31 a-d). It has been published that at higher feed rate the number of chip curls observed is more than lower feed rate and is due to the increased deformation volume and tool chip contact length. In fact, it increases the machine temperature, which improves the ductility and increases the number of chip curls. However, at lower feed rate, the chip cross section area is very small due to small radii curled and C-type chips are generated (Figure 4.31). As shown in Figure 4.31(d), Bi-containing workpiece has small C-type chips at lower feed rate too (0.05 mm/rev)

which is due to less built-up edge formation on the rake face of insert during machining process.

It has been published that at the outer radius of the facing cut, the chips were continuous in nature, while at the inner radius, they were almost discontinuous chip. No quantitative data were recorded regarding this phenomenon (Ozcatalbas, 2003). The difference was attributed primarily to greater heating of the matrix in the primary deformation zone at greater cutting speeds which lead to matrix softening and increased ductility. At the inner radius, the cutting speed was slower and therefore thermal softening of the matrix was not so prevalent (Pedersen & Ramulu, 2006). Also, the cutting tool was new at the beginning of the cut (outer radius) and experienced significant wear by the time it reached the inner radius. Rapid tool wear resulted in changing tool geometry throughout the cut which directly affected conditions in the deformation zone which in turn affected whether continuous or semi-continuous chip were prevalent (Figures 4.30 and 4.31).

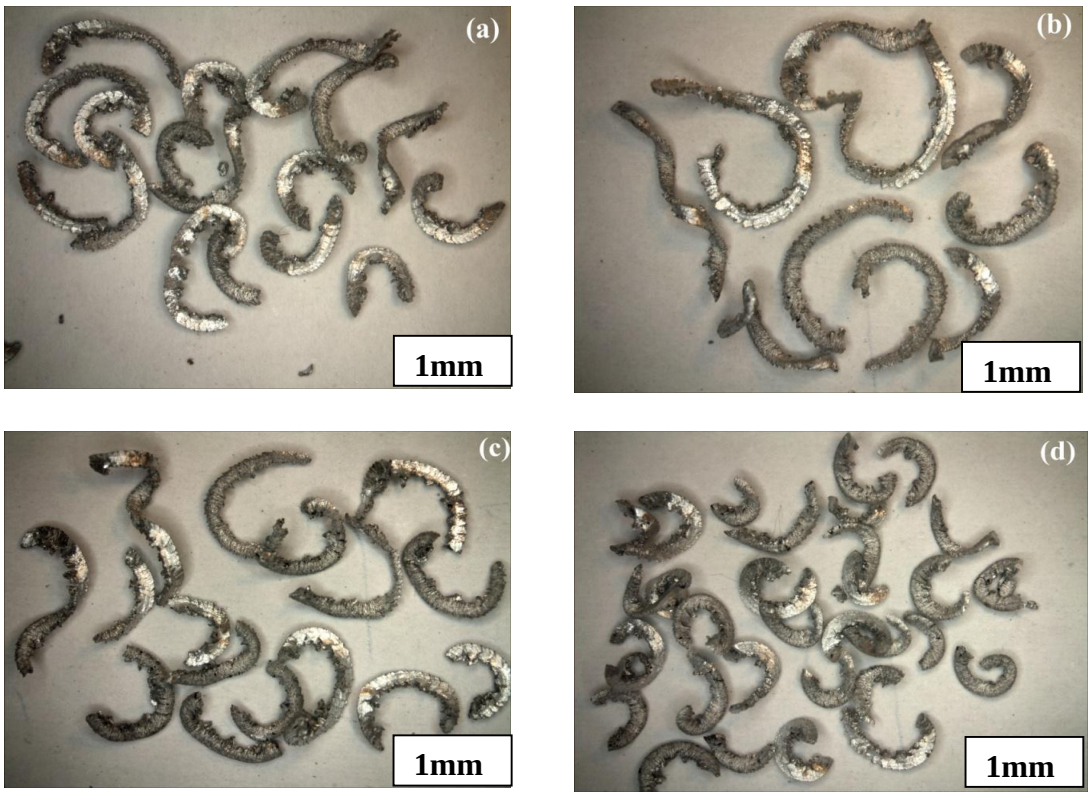

Figure 4.31: Optical micrographs showing different types of chip obtained for (a) base alloy (b) Sr-containing (c) Sb-containing (d) Bi-containing at cutting speed of 70 m/min and feed rate of 0.05 mm/rev.

4.8.2 Cross-Sectional Microstructures of the Chip-Root

It has been reported that the presence of Cu leads to the formation of Al_2Cu particles, which when refined and dispersed, improve machinability by causing a decrease in plasticity, and ultimately result in chip embrittlement (Nishido, Kaneso, Kobayashi, & Toda, 2004). In the research carried out on the relationship between chip breakability and aging treatment in Al-Cu and Al-Cu-Si alloys, chip breakability successfully improved with the increased size of second-phase particles accompanied by advanced aging. In this case, however, it was pointed out that chip breakability was also related to the cracking of the second-phase particles and the ductility of the matrix around them (Nishido et al., 2004). Nevertheless, these facts suggest that the chip breakability of Al alloys is expected to improve with the dispersion of some kind of second-phase particle, since this could be the cause of the chip breaking through cracking during machining (Davim, 2010). The

production of small brittle chips favors intermittent cutting, making chip extraction away from the cutting easier, while at the same time inhibiting the formation of a built-up edge on the cutting edge of the tool.

Figure 4.32 shows the optical picture of chips produced during machining of base alloy and Sr, Sb and Bi-containing alloys at cutting speed of 250 m/min and feed rate of 0.15 mm/rev and constant depth of cut of 0.05 mm. During the machining, it can be observed that when the material underwent shear by the movement of this cutting tool during the chip harming process, crack were initiated from the outside free surface of the chip and some small voids were formed by the separation of reinforcement particles and Al-matrix within the chip (Nishido et al., 2004). As can be seen in Figure 4.32 (a-c) the chips appear to be highly strained, but the segmentation is restricted to the outer (free) surface of the chip. This is related to an increase in ductility of workpieces. Thus, high ductility increase the sticky period at tool-chip interface causing secondary crack formation at inner surface of chips (Figure 4.32 a-c) for Sb- and Sr-containing and base alloy, respectively.

Figure 4.32 (d) shows that once the material was sheared further, the coalescence of the voids caused the crack to grow and propagate in a zigzag manner along the shear plane through the thickness of this chip, and as a result fractures take place and sliding of material formed the saw toothed chips. It has also been published that during machining the propagation of this crack is accelerated by the upward and side curling action of the chip, which from time to time, helps break a long chip into smaller pieces (Nishido et al., 2004). In fact, Bi plays an important role in this process. Bi particles form as a viscous layer between tool and machined surface and may enhance the machinability of alloy. Therefore, Bi can produce small chips which are highly strained leading to separation of chip segments at outer (free) surface, as shown in the optical micrograph of chip in Figure 4.32(d). It is concluded that the segmentation is not complete over an entire chip thickness

and has clear saw –tooth-profile. These chips are also formed while machining of coarser reinforcement composite (Dabade & Joshi, 2009a). However, the observation of inner side of chips shows that the chip segments are joined at bottom chips inner side in Figure 4.32(d).

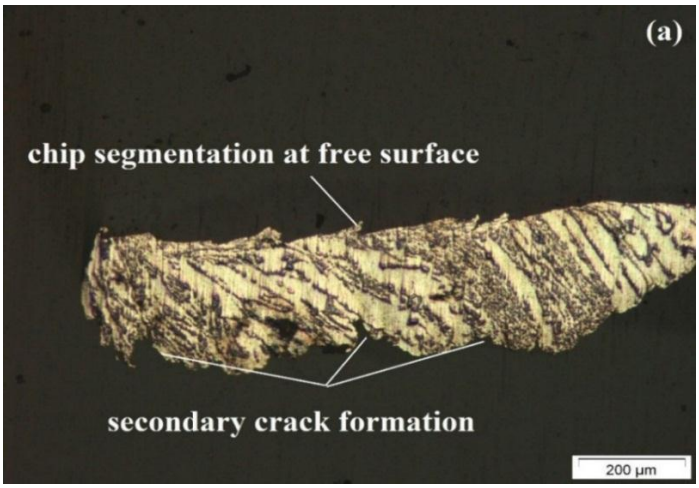

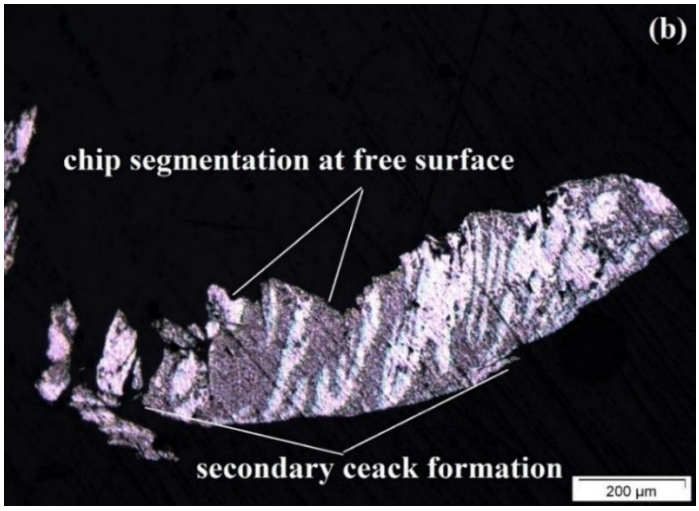

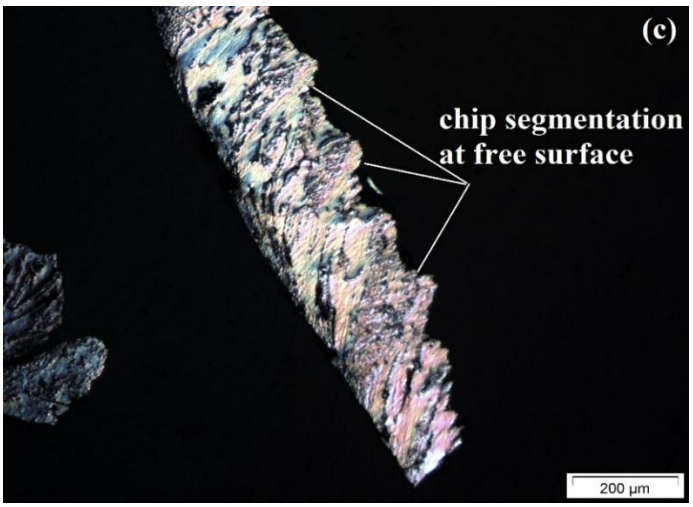

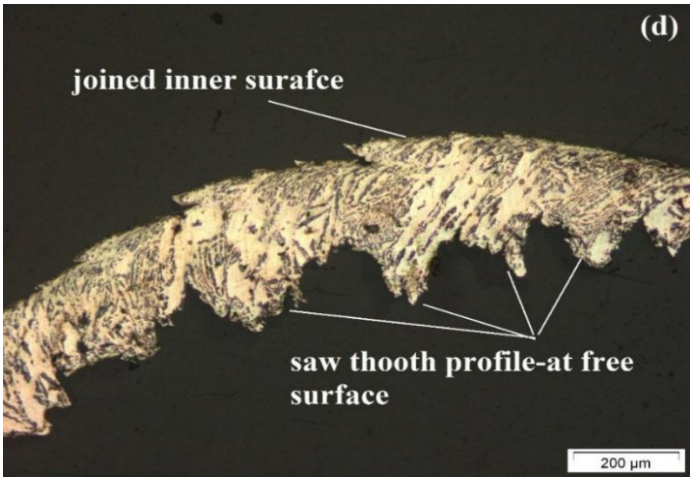

Figure 4.32: Optical microscopy of the chips produced during machining of (a) Sb-containing, (b) Sr –containing,(c) base alloy and (d) Bi-containing.

Figure 4.33 shows SEM of chip morphology and EDS spectrum and corresponding elemental mapping analysis of Al-Si alloy (base alloy). As can be seen in Figure 4.33(a) there are two elements (aluminium and silicon) in mapping for the base alloy. Figures 4.34 and 4.35 demonstrate elements such as aluminum, silicon, antimony and strontium by mapping analysis, respectively. As mentioned, these two elements (strontium and antimony) increase ductility of workpieces and consequently decrease machinability of workpieces. Figure 4.36 demonstrates SEM of chip morphology and

EDS spectrum and corresponding elemental mapping analysis of Bi-containing alloy. Elements such as aluminum, silicon and bismuth are presented.

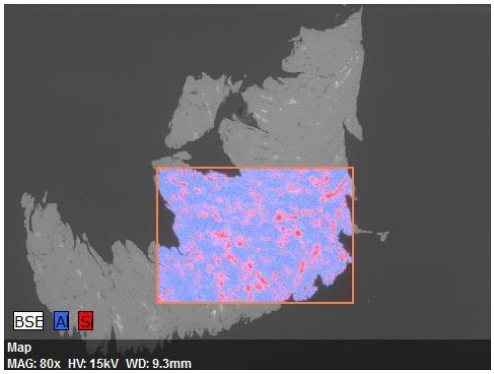

(a)

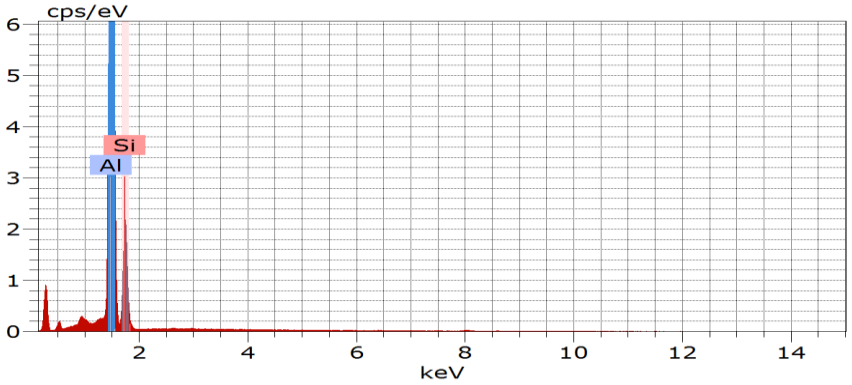

(b)

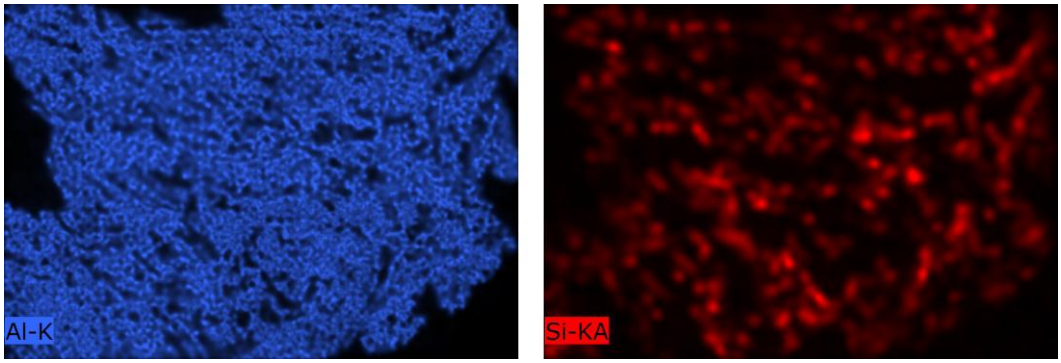

(c)

Figure 4.33: (a) SEM of chip morphology, (b) EDS spectrum and (c) corresponding elemental mapping analysis of Al-11Si (base alloy).

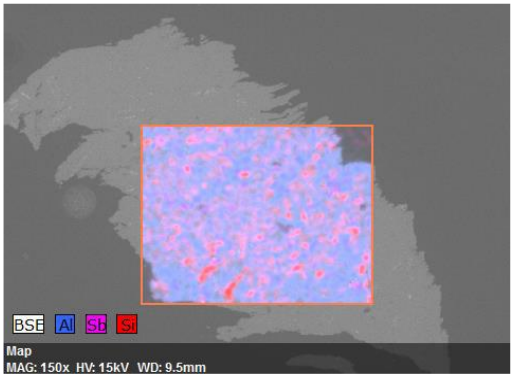

(a)

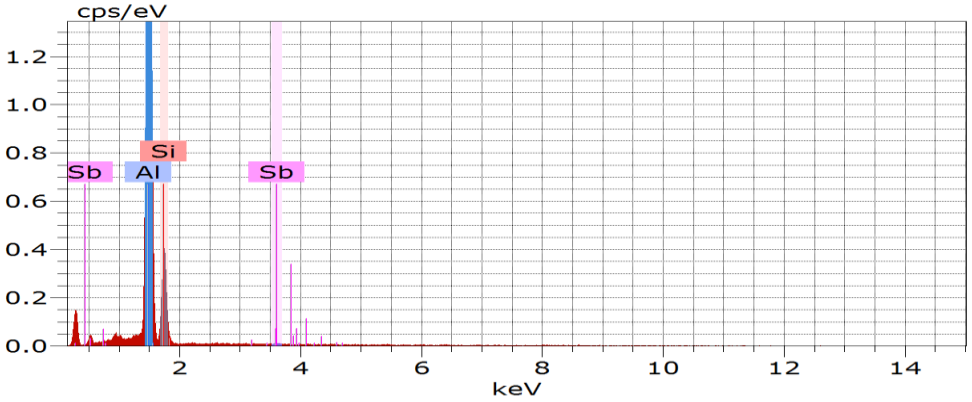

(b)

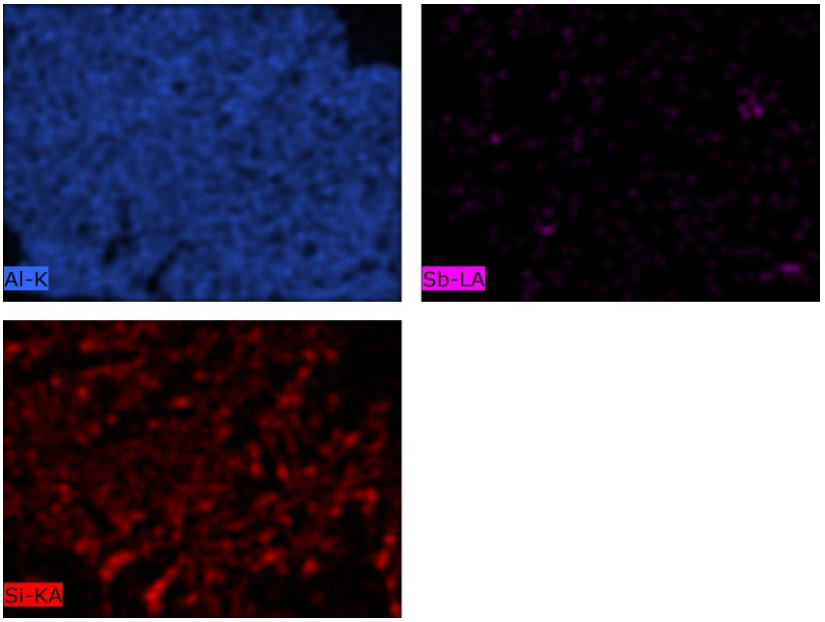

(c)

Figure 4.34: (a) SEM of chip morphology, (b) EDS spectrum and (c) corresponding elemental mapping analysis of Sb-containing.

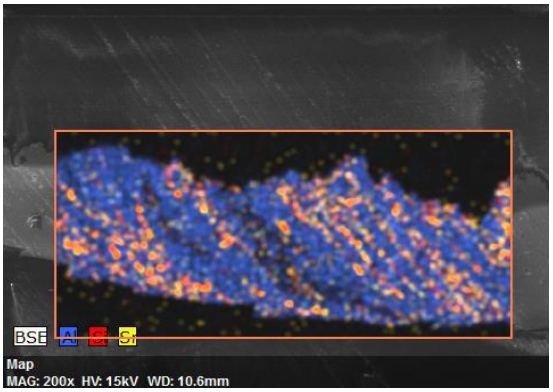

(a)

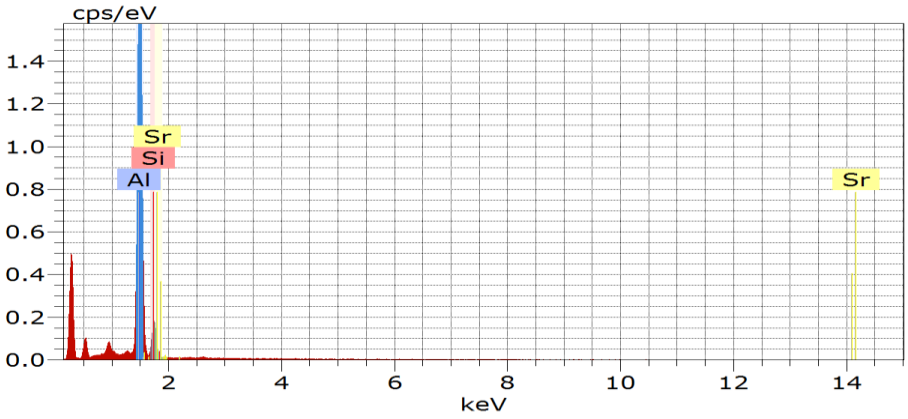

(b)

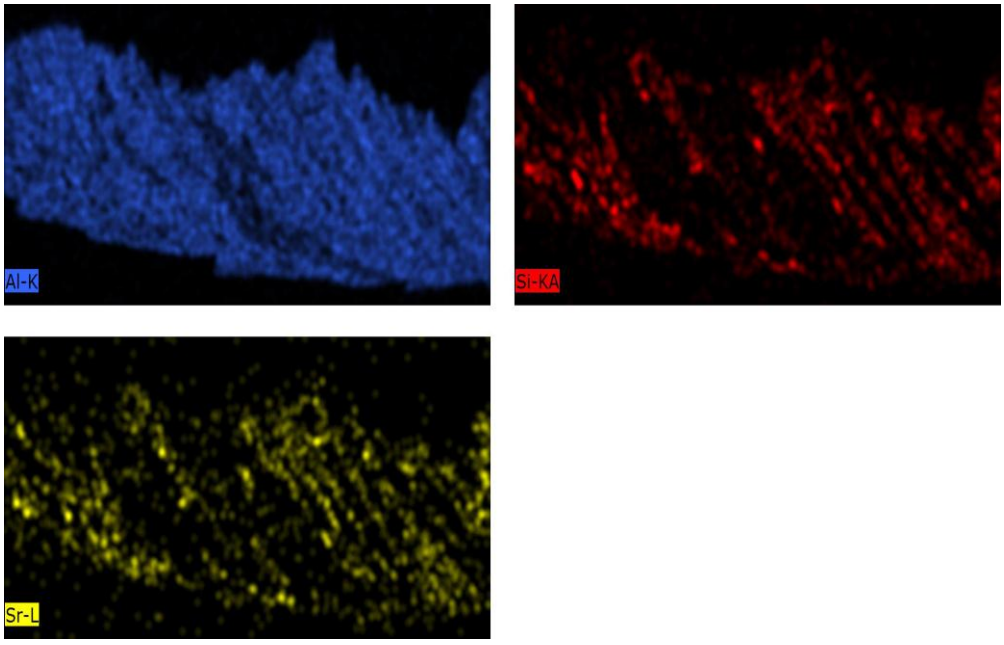

(c)

Figure 4.35 : (a) SEM of chip morphology, (b) EDS spectrum and (c) corresponding elemental mapping analysis of Sr-containing.

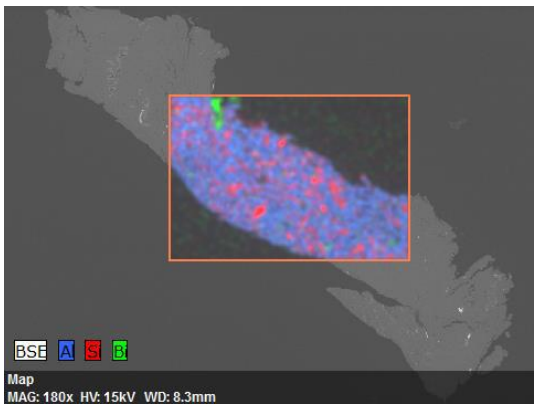

(a)

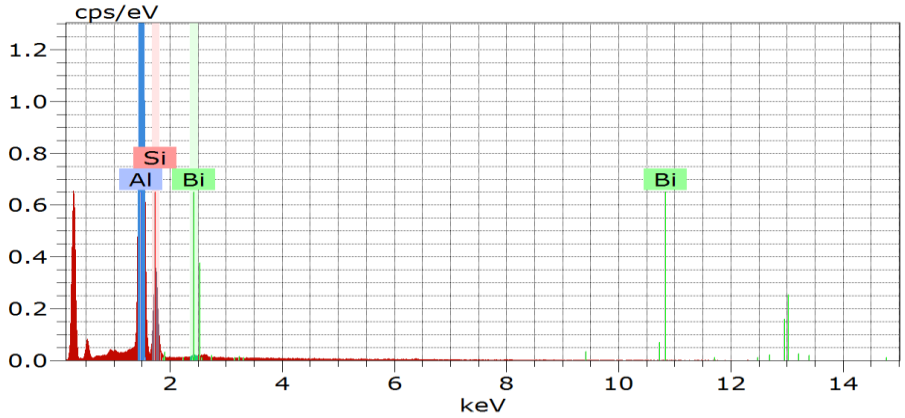

(b)

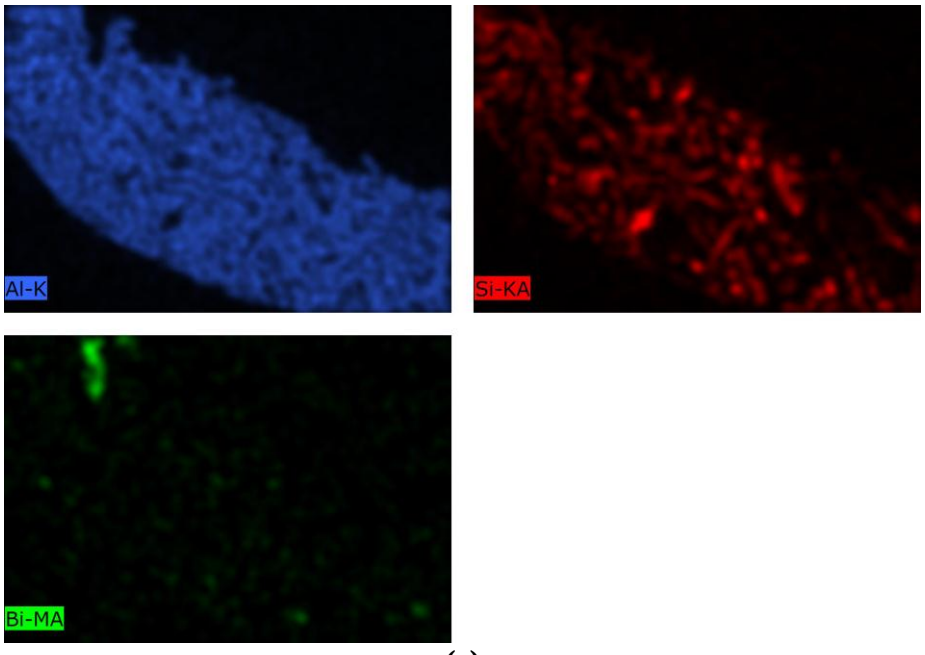

(c)

Figure 4.36: (a) SEM of chip morphology, (b) EDS spectrum and (c) corresponding elemental mapping analysis of Bi-containing.

4.9 Built-up Edge Formation

Built-up edge (BUE) is caused by the incidence of some strain hardened workpiece material welding itself to the rake face and becoming a new cutting surface. As a result of high temperatures, small particles of metal tend to adhere to the edge of the cutting tool thereby leading to built-up. The presence of built-up edge is capable of inducing a number of effects including an alteration in tool geometry, thereby reducing the contact area of the chip with the rake face, consequently, the shear plane angle increases while the cutting and feed forces diminish (Vernaza-Peña, Mason, & Li, 2002).

The fragments of BUE, which are constantly breaking away, leave a very rough surface finish. In order to overcome this issue, high cutting speeds must be applied if surface quality is important. In practice, the size and shape of the BUE vary greatly with the work material and the prevailing cutting conditions (Sahin, 2003). For any material with its cutting conditions, the built-up edge seems to reach an equilibrium size and shape fairly early on. Built-up edge should be capable of supporting the high compressive force and shear stress imposed by the cutting process thereby rendering it unable to grow indefinitely. As the BUE grows in height and changes in shape, the stress system also changes and parts of the built-up edge are broken away.

Ciftci, Turker, & Seker (2004) suggested that the introduction of a second phase into a metal structure lowers its ductility, allowing fracture somewhere along the rake face after severe deformation. The occurrence of BUE is also affected by feed rate in uncut chip thickness, rake angle, tool material, and lubrication. For example, the BUE disappears completely at high speeds in accordance with the commercial purity of the aluminum alloy.

In practice, the size and the shape of the BUE vary greatly with the work material and with the cutting conditions (Ciftci et al., 2004). In general, BUE results in the

deterioration of the chip size, tool life, surface finish, and part dimensional control (Dandekar & Shin, 2012). Figure 4.37 shows the chip formation and the corresponding adhesion of chips onto the rake of tools for all workpieces. The types of chips formed vary, which may be attributed to the material properties and cutting parameters (Pramanik et al., 2007). The interface frictional conditions cause the tool-chip content to lead to the deformation and curling-away of the chips from the tool-rake face. Since chip formation influences tool design, it is crucial to consider tool material and cutting parameter selection in machining (Debnath, Reddy, & Yi, 2014).

Benga & Abrao (2003) reported that plastic deformation of the soft phase in the cutting zone and BUE at the cutting tool edge are pronounced and the tool geometry changes are noticeable through an increase in surface roughness Type of Si shapes (flake or lamellar shape) has a major effect but cutting speed slightly affects chip shape. As can be seen in Figure 4.37 (a), the chips formed during base alloy machining at cutting speed of 250 m/min and feed rate of 0.15 mm/rev are long, while Bi-containing alloy exhibits chip disposability and shorter chips in the same condition (Figure 4.37c). Cracking of some additional particles during turning could be attributed to the enhanced chip breakability of Al–11.3Si–2Cu alloy. However, chip formed for Sr and Sb-containing alloys were longer than others, and was less breakable and free from the formation of cracks (Figure 4.37 e and g). It has been published that short chips are commonly desired to obtain undamaged surface that can translate to better surface roughness and machinability (Benga & Abrao, 2003).

In spite of increasing the cutting speed, BUE was found on the rake face of the tools; hence cracks were seen on the surface of the machining sample. However, at high cutting speed, the depth of crack was shallow with a large distance between the cracks. Thus, it can be said that, the formation of small size of BUE at high cutting speed reduce the amount of defects on the machine surface. In contrast to the base alloy, adding 0.1%wt

Bi improves workpiece surface roughness by decreasing adhesion on the cutting tools. However, it is evident that Sr and Sb increases surface roughness by adding amount of BUE on the rake face of the tools during machining process, respectively (Figure 4.37f).

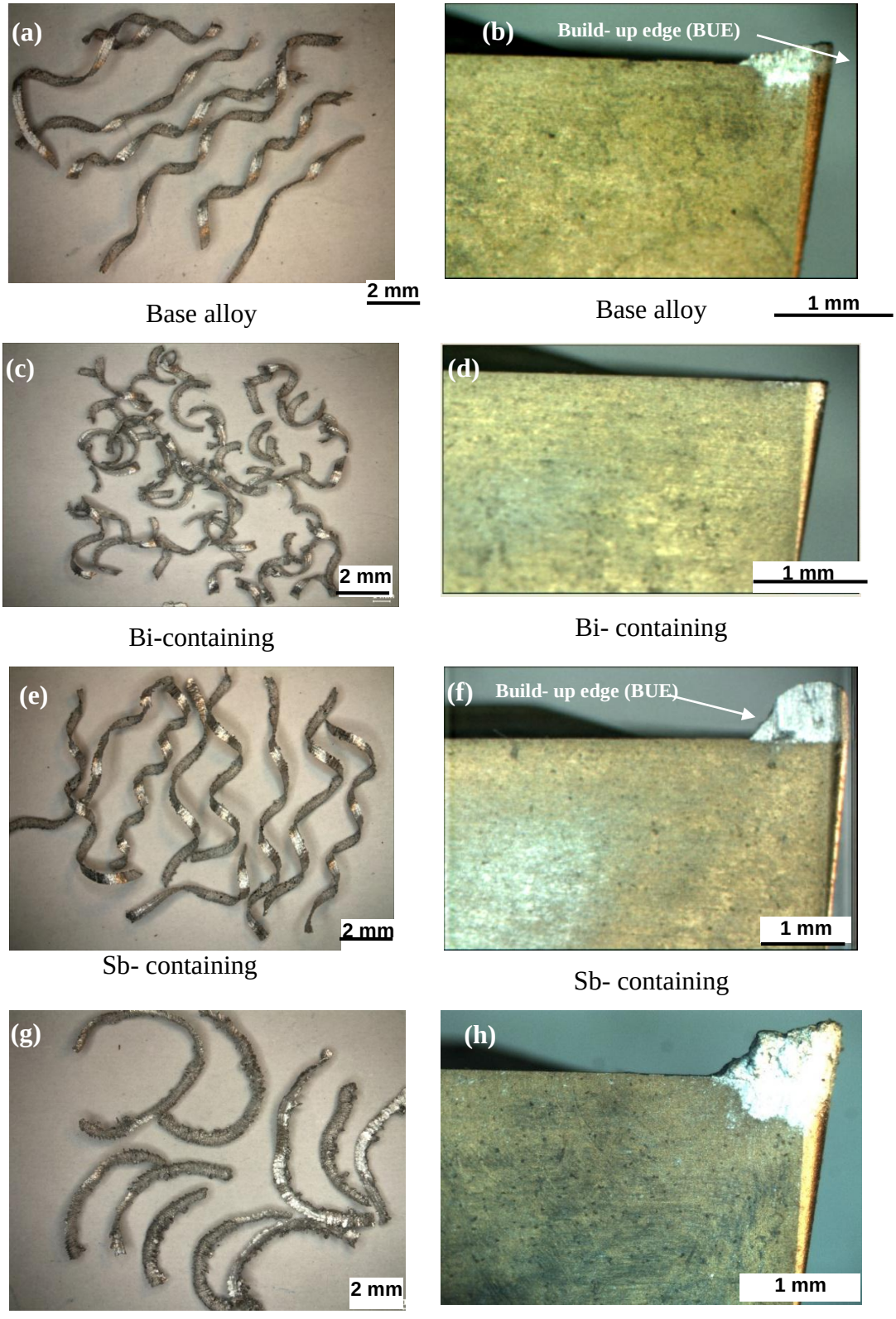

Figure 4.37: Chip shapes and optical images of cutting tools at speed of 250 m/min and feed rate of 0.15 mm/rev and depth of cut 0.5 mm: (a and b) base alloy, (c and d) Bi- and (e and f) Sb-containing alloys, (g and h) Sr-containing alloy

Chapter 5: CONCLUSION AND FUTURE WORKS

The present study concentrated on a new experimental alloy belonging to the Al-Si near-eutectic cast alloy group, and containing about 11% Si. In addition some additives such as Sr, Sb and Bi were also investigated for comparison purposes. The study was carried out with the aim of providing a better understanding of the effects that silicon morphology, microstructure and free-machining elements would have on the machinability characteristics of this alloy. Turning operations were carried out under different machining conditions as applied to the examination of the alloys under discussion.

5.1 Conclusion

From the analysis and discussion of the results obtained, the following conclusions may be formulated:

1) Bi, Sb, and Sr when added into the Al-Si alloy melt refine the eutectic silicon structure. Based on microstructure observations, the optimal concentrations of Bi, Sb and Sr to refine the eutectic Si were 1 wt.% , 0.5 wt.% and 0.04 wt%, respectively. The tensile and impact test were shown that mechanical properties of base alloy improved by addition of elements.
2) The highest yield strength was obtained in the untreated base alloy compared with the untreated alloys with Sr, Bi and Sb. This can be associated with the fact that the yield strength is strongly dependent on aluminum dendrite size rather than silicon morphology. Plus, with the addition of Bi, Sb and especially Sr the ductility and values of elongation have increased by two-fold. The increase in

elongation is likely related to the Si structure and morphology which changes from flake-like to fibrous or lamellar structure with element additions.

3) Surface roughness increased when feed rates increased from 0.05 mm/rev to 0.15 mm/rev, and surface roughness improved when cutting speed increased from 70 m/min to 250 m/min for all workpieces. This is due to the domination of feed mark and increase of distance from peak to valley of the machined surface. In terms of additives, the best surface roughness was obtained for Bi-containing alloys possibly because the formation of pure Bi behaves as lubricant during turning.
4) Bi acts as an internal lubricant by forming a viscous layer, and also as a diffusion barrier between the tool and the chip, thereby prolonging tool life and improving productivity. Their globules do not adversely affect the strength or the hardness of the casting but enable surfaces of the casting to be machined without the use of a coolant or a lubricating machining fluid.
5) Bi-containing alloy shows the lowest cutting force in comparison with Base alloy, Sr and Sb-containing alloys. It may be caused by decreasing friction between tool and workpiece and decreased built-up edge during turning process. Sr-containing alloy shows highest cutting force. It may be attributed to the formation of massive BUE on the rake face of insert, together with the formation of large size of chip during machining process.
6) In the turning tests, Sr-containing alloy showed the maximum wear (just above 0.2 mm). The main wear mechanism observed was adhesion, and some abrasion occurred for Sr and Sb-containing alloys, respectively. Bi-containing alloy showed the lowest wear value (around 1 mm) compared with other workpieces. It was related to wettability of Bi and segmented chips during machining process.

7) The base alloy which is composed of the brittle flake silicon showed lower cutting force compared to Sr and Sb-containing alloys at the different cutting conditions. This result can be related to the change of silicon shape, where fibrous silicon had the highest cutting force value. Moreover, antimony addition, which induced lamellar silicon, increased the ductility compared to the base alloy, and therefore increased the force as well. In fact, the change in silicon morphology increased the ductility of the Al-Si phase which changed the tool geometry, resulting in a plastic deformation of the soft phase of the workpiece material and causing an increase in the cutting force.

8) Sr and Sb- containing alloys had a detrimental effect on tool life. The reduction of tool life may be attributed to the highest ductility of these alloys which leads to provide massive BUE together with formation of spiral chip shape with less breakability and free from the formation of cracks during machining operation. On the other hand, Bi-containing alloy showed segmentation chips (C-type) in comparison with other alloys. It leads to improved surface roughness of machined workpieces and improved machinability.

9) Bismuth addition was found to produce the best surface finish during turning and improves machinability of Al–12Si– 2Cu cast alloy. This addition is suitable alloying element to add into the aluminum alloys in order to fabricate casting components with good mechanical properties and machinability which are usually used in automotive industry.

5.2 Recommendations for Future Work

As mentioned in chapter 1, there is a need for an in-depth understanding of the role of elements with low melting point and its effect on microstructure and machinability of Al-Si-Cu alloys containing bismuth, antimony and strontium throughout. Therefore, having an understanding of these alloys' machinability is imperative when it is necessary to fabricate some industrial products which are produced by casting process. To complete the study, it is suggested that investigations be extended to cover the following aspects:

1. Investigating the high temperature performance of Al-11%Si type alloys with respect to the role of additives in preserving the mechanical properties under elevated temperature conditions.

2. Investigating the use of insert materials other than the cemented carbide tools used in the present study, from the point of view of reducing the machining costs and thereby, the overall production costs.

3. Investigating the addition of low melting-point elements such as tin which, with its tendency to melt during dry machining at high speeds of-12,000 rpm, would serve as a lubricant during the machining process, thus eliminating the need for external lubricants.

References

Abdollahi, A. (1998). *Effect of Ca as a Modifier in Hypoeutectic AI-Si alloys*. *Department of Mining and Metallurgical Engineering*. McGili University, Montreal.

Akdemir, A., Yazman, S., Saglam, H., & Uyaner, M. (2012). The Effects of Cutting Speed and Depth of Cut on Machinability Characteristics of Austempered Ductile Iron. *Journal of Manufacturing Science and Engineering*, *134*(2), 021013. doi:10.1115/1.4005805

Andrewes, C. J. ., Feng, H.-Y., & Lau, W. . (2000). Machining of an aluminum/SiC composite using diamond inserts. *Journal of Materials Processing Technology*, *102*(1-3), 25–29. doi:10.1016/S0924-0136(00)00425-8

Ang, C., Dasch, J., Cheng, Y., Rezhets, V., Powell, B., & Paluch, R. (2006). Dry machining of aluminum castings. us: *Google Patents*.

Arumugam, P. U., Malshe, A. P., & Batzer, S. A. (2006). Dry machining of aluminum–silicon alloy using polished CVD diamond-coated cutting tools inserts. *Surface and Coatings Technology*, *200*(11), 3399–3403. doi:10.1016/j.surfcoat.2005.08.127

Axinte, D. A., Belluco, W., & De Chiffre, L. (2001). Reliable tool life measurements in turning — an application to cutting fluid efficiency evaluation. *International Journal of Machine Tools and Manufacture*, *41*(7), 1003–1014. doi:10.1016/S0890-6955(00)00110-3

Backerud, L., Chai, G., & Tamminen, J. (1990). *Solidification Characteristics of Aluminum Alloys. Vol. 2. Foundry Alloys*. *American Foundrymen's Society, Inc., 1990* (p. 266). American Foundry Society.

Bardetsky, A., Attia, H., & Elbestawi, M. (2005). Evaluation of Tool Wear Suppressive Ability of Lubricants Usein in Minimum Quantity Lubrication Application in High Speed Machining of Cast Aluminum Alloys. In *Manufacturing Engineering and Materials Handling, Parts A and B* (Vol. 2005, pp. 23–29). ASME. doi:10.1115/IMECE2005-80597

Barzani, M. M. (2012). MOHSEN MARANI BARZANI Master of Mechanical Engineering (Advanced Manufacturing). doi:10.4028/www.scientific.net/AMR.566.443.

Barzani, M. M., Farahany, S., Yusof, N. M., & Ourdjini, A. (2013). The Influence of Bismuth, Antimony, and Strontium on Microstructure, Thermal, and Machinability of Aluminum-Silicon Alloy. *Materials and Manufacturing Processes*, *28*(11), 1184–1190. doi:10.1080/10426914.2013.792425

Barzani, M. M., Sarhan, A. a. D., Farahani, S., & Singh, R. (2015). Investigation into Effect of Cutting Conditions on Surface Roughness while Dry Machining Al-11%Si and Al-11%Si-1% Bi Die Casting Alloy. *Advanced Materials Research*, *1119*, 617–621. doi:10.4028/www.scientific.net/AMR.1119.617

Barzani, M. M., Sarhan, A. A. D., Farahany, S., Ramesh, S., & Maher, I. (2015). Investigating the Machinability of Al–Si–Cu cast alloy containing bismuth and antimony using coated carbide insert. *Measurement*, *62*, 170–178. doi:10.1016/j.measurement.2014.10.030

Barzani, M. M., Zalnezhad, E., Sarhan, A. A. D., Farahany, S., & Ramesh, S. (2015). Fuzzy logic based model for predicting surface roughness of machined Al–Si–Cu–Fe die casting alloy using different additives-turning. *Measurement*, *61*, 150–161.

Basavakumar, K. G., Mukunda, P. G. ., & Chakraborty, M. (2007). Influence of melt treatments and turning inserts on cutting force and surface integrity in turning of Al–12Si and Al–12Si–3Cu cast alloys. *Surface and Coatings Technology*, *201*(8), 4757–4766. doi:10.1016/j.surfcoat.2006.10.015

Benga, G. C., & Abrao, A. M. (2003). Turning of hardened 100Cr6 bearing steel with ceramic and PCBN cutting tools. *Journal of Materials Processing Technology*, *143–144*(0), 237–241. Retrieved from http://www.sciencedirect.com/science/article/pii/S0924013603003467

Bhowmick, S., & Alpas, A. T. (2008). The performance of hydrogenated and non-hydrogenated diamond-like carbon tool coatings during the dry drilling of 319 Al. *International Journal of Machine Tools and Manufacture*, *48*(7-8), 802–814. doi:10.1016/j.ijmachtools.2007.12.006

Bian, X. F., Zhang, Z. H., & Liu, X. F. (2000). Effect of Strontium Modification on Hydrogen Content and Porosity Shape of Al-Si Alloys. *Materials Science Forum*, *331-337*, 361–366. doi:10.4028/www.scientific.net/MSF.331-337.361

Campbell, J. (2006). An overview of the effects of bifilms on the structure and properties of cast alloys. *Metallurgical and Materials Transactions B*, *37*(6), 857–863. doi:10.1007/bf02735006

Ciftci, I., Turker, M., & Seker, U. (2004a). CBN cutting tool wear during machining of particulate reinforced MMCs, *257*, 1041–1046. doi:10.1016/j.wear.2004.07.005

Ciftci, I., Turker, M., & Seker, U. (2004b). CBN cutting tool wear during machining of particulate reinforced MMCs. *Wear*, *257*(9-10), 1041–1046. doi:10.1016/j.wear.2004.07.005

Ciftci, I., Turker, M., & Seker, U. (2004c). Evaluation of tool wear when machining SiCp-reinforced Al-2014 alloy matrix composites. *Materials & Design*, *25*(3), 251–255. doi:10.1016/j.matdes.2003.09.019

Dabade, U. A., & Joshi, S. S. (2009a). Analysis of chip formation mechanism in machining of Al/SiCp metal matrix composites. *Journal of Materials Processing Technology*, *209*(10), 4704–4710. doi:10.1016/j.jmatprotec.2008.10.057

Dabade, U. A., & Joshi, S. S. (2009b). Analysis of chip formation mechanism in machining of Al/SiCp metal matrix composites. *Journal of Materials Processing Technology*, *209*(10), 4704–4710. doi:10.1016/j.jmatprotec.2008.10.057

Dandekar, C. R., & Shin, Y. C. (2012). Modeling of machining of composite materials: A review. *International Journal of Machine Tools and Manufacture*, *57*, 102–121. doi:10.1016/j.ijmachtools.2012.01.006

Dasch, J. M., Ang, C. C., Wong, C. A., Waldo, R. A., Chester, D., Cheng, Y. T., … Konca, E. (2009). The effect of free-machining elements on dry machining of B319 aluminum alloy. *Journal of Materials Processing Technology*, *209*(10), 4638–4644. doi:10.1016/j.jmatprotec.2008.11.041

Davim, J. P. (2010). *Surface Integrity in Machining*. (J. P. Davim, Ed.). London: Springer London. doi:10.1007/978-1-84882-874-2

Davoodi, B., & Eskandari, B. (2015). Tool wear mechanisms and multi-response optimization of tool life and volume of material removed in turning of N-155 iron–nickel-base superalloy using RSM. *Measurement*, *68*, 286–294. doi:10.1016/j.measurement.2015.03.006

Debnath, S., Reddy, M. M., & Yi, Q. S. (2014). Environmental friendly cutting fluids and cooling techniques in machining: a review. *Journal of Cleaner Production*, *83*, 33–47. doi:10.1016/j.jclepro.2014.07.071

DeGarmo, E. P., Black, J. T., & Kohser, R. A. (2011). *Degarmo's Materials and Processes in Manufacturing*. John Wiley & Sons. Retrieved from http://books.google.com.my/books?id=8roLjMs08zoC

Drouzy, M., Jacob, S., & Richard, M. (1980). INTERPRETATION OF TENSILE RESULTS BY MEANS OF QUALITY INDEX AND PROBABLE YIELD STRENGTH-APPLICATION TO AL-SI7 MG FOUNDRY ALLOYS-FRANCE. *International Cast Metals Journal*, *5*(2), 43–50.

Dursun Sedat Kilic, S. R. (2008). Observations of the tool–chip boundary conditions in turning of aluminum alloys. *Wear*, *262 (2007)*.

El-Gallab, M. S., & Sklad, M. P. (2004). Machining of aluminum/silicon carbide particulate metal matrix composites. *Journal of Materials Processing Technology*, *152*(1), 23–34. doi:10.1016/j.jmatprotec.2004.01.061

Elgallad, E. M., Samuel, F. H., Samuel, A. M., & Doty, H. W. (2010). Machinability aspects of new Al–Cu alloys intended for automotive castings. *Journal of Materials Processing Technology*, *210*(13), 1754–1766.

Fang, F. Z., & Liu, Y. C. (2004). On minimum exit-burr in micro cutting. *Journal of Micromechanics and Microengineering*, *14*(7), 984.

Farahany, S., Ourdjini, A., & Idris, M. H. (2011). The usage of computer-aided cooling curve thermal analysis to optimise eutectic refiner and modifier in Al–Si alloys. *Journal of Thermal Analysis and Calorimetry*, *109*(1), 105–111. doi:10.1007/s10973-011-1708-1

Farahany, S., Ourdjini, A., Idris, M. H., Takaloo, A. V, & Thai, L. T. (2013). Combined effect of bismuth content and cooling rate on microstructure and mechanical

properties of Al–8·5Si–0·4Mg–0·3Fe alloy. *Canadian Metallurgical Quarterly*, *52*(2), 208–216. doi:10.1179/1879139512Y.0000000045

FARAHANY, S., OURDJINI, A., IDRIS, M. H., & THAI, L. T. (2011a). Effect of bismuth on microstructure of unmodified and Sr-modified Al-7Si-0.4Mg alloys. *Transactions of Nonferrous Metals Society of China*, *21*(7), 1455–1464. doi:10.1016/S1003-6326(11)60881-9

FARAHANY, S., OURDJINI, A., IDRIS, M. H., & THAI, L. T. (2011b). Poisoning effect of bismuth on modification behaviour of strontium in LM25 alloy. *Bulletin of Materials Science*, *34*(6), 1223–1231. doi:10.1007/s12034-011-0239-5

Flood, S. C., & Hunt, J. D. (1981). Modification of Al-Si eutectic alloys with Na. *Metal Science*, *15*(7), 287–294. doi:http://dx.doi.org/10.1179/030634581790426813

Galoppi, G. de S., Filho, M. S., & Batalha, G. F. (2006). Hard turning of tempered DIN 100Cr6 steel with coated and no coated CBN inserts. *Journal of Materials Processing Technology*, *179*(1-3), 146–153. doi:10.1016/j.jmatprotec.2006.03.067

Godowsky, T. (2007). casting since about 4000BC. (12th, Ed.). Retrieved from http://web.mit.edu/lienhard/www/ahtt.html

Govender, G., & Ivanchev, L. H. (2005). Near net shape forming unsing semi-solid metal forming.

Grum, J., & Kisin, M. (2003). Influence of microstructure on surface integrity in turning—part I: the influence of the size of the soft phase in a microstructure on surface-roughness formation. *International Journal of Machine Tools and Manufacture*, *43*(15), 1535–1543. doi:10.1016/S0890-6955(03)00199-8

Grum, J., & Kisin, M. (2006). The influence of the microstructure of three Al–Si alloys on the cutting-force amplitude during fine turning. *International Journal of Machine Tools and Manufacture*, *46*(7-8), 769–781. doi:10.1016/j.ijmachtools.2005.07.032

Grzesik, W. (2008). *Advanced machining processes of metallic materials: theory, modelling and applications*. Elsevier.

Hegde, S., & Prabhu, K. N. (2008). Modification of eutectic silicon in Al–Si alloys. *Journal of Materials Science*, *43*(9), 3009–3027. doi:10.1007/s10853-008-2505-5

Hua, J., Shivpuri, R., Cheng, X., Bedekar, V., Matsumoto, Y., Hashimoto, F., & Watkins, T. R. (2005). Effect of feed rate, workpiece hardness and cutting edge on subsurface residual stress in the hard turning of bearing steel using chamfer+hone cutting edge geometry. *Materials Science and Engineering: A*, *394*(1-2), 238–248. doi:10.1016/j.msea.2004.11.011

Iuliano, L., Settineri, L., & Gatto, A. (1998). High-speed turning experiments on metal matrix composites. *Composites Part A: Applied Science and Manufacturing*, *29*(12), 1501–1509.

J.Zhang Y.Q.Wang, and B.L.Zhou, Z. F. (2000). microstracture and mechanical properties of in situ AL-MG2Si composite. *Material Science and Technology*, *1693*.

Jiang, W., More, A. S., Brown, W. D., & Malshe, A. P. (2006). A cBN-TiN composite coating for carbide inserts: Coating characterization and its applications for finish hard turning. *Surface and Coatings Technology*, *201*(6), 2443–2449. doi:10.1016/j.surfcoat.2006.04.026

K.G. Basava Kumar, P. G. M. (2007). Influence of melt treatments and polished CVD diamond-coated insert on cutting force and surface integrity in turning of Al-12Si and Al-12Si-3Cu cast alloys, *Surface and Coatings Technology 2*, 117–137.

Kalpakjian, S., & Schmid, S. R. (2009). *Manufacturing Engineering and Technology*. Pearson Education Canada. Retrieved from http://books.google.com.my/books

KAMIYA, M., YAKOU, T., SASAKI, T., & NAGATSUMA, Y. (2007). Effect of Si content on turning machinability of Al-Si binary alloy castings. *Journal of Japan Institute of Light Metals*, *57*(5), 191–196. doi:10.2464/jilm.57.191

Kamiya, M., Yakou, T., Sasaki, T., & Nagatsuma, Y. (2008). Effect of Si Content on Turning Machinability of Al-Si Binary Alloy Castings. *MATERIALS TRANSACTIONS*, *49*(3), 587–592. doi:10.2320/matertrans.L-MRA2007886

Kannan, S., & Kishawy, H. a. (2006). Surface characteristics of machined aluminium metal matrix composites. *International Journal of Machine Tools and Manufacture*, *46*(15), 2017–2025. doi:10.1016/j.ijmachtools.2006.01.003

Kannan, S., & Kishawy, H. a. (2008). Tribological aspects of machining aluminium metal matrix composites. *Journal of Materials Processing Technology*, *198*(1-3), 399–406. doi:10.1016/j.jmatprotec.2007.07.021

Kerr, D., Pengilley, J., & Garwood, R. (2005). Assessment and visualisation of machine tool wear using computer vision. *The International Journal of Advanced Manufacturing Technology*, *28*(7-8), 781–791. doi:10.1007/s00170-004-2420-0

Kılıçkap, E., Çakır, O., Aksoy, M., & İnan, A. (2005). Study of tool wear and surface roughness in machining of homogenised SiC-p reinforced aluminium metal matrix composite. *Journal of Materials Processing Technology*, *164-165*, 862–867. doi:10.1016/j.jmatprotec.2005.02.109

Koch, S., & Antrekowitsch, H. (2008). Free-Cutting Aluminium Alloys with Tin as Substitution for Lead. *BHM Berg- Und Hüttenmännische Monatshefte*, *153*(7), 278–281. doi:10.1007/s00501-008-0390-5

Kouam, J., Djebara, A., & Songmene, V. (2014). Experimental Investigation on the Effect of Pre-holes on Drilling Process Performance of Aluminum Alloys: Forces, Surface Finish and Dust Emission. *Advances in Materials Science and Applications*, *3*(1), 13–23. doi:10.5963/AMSA0301003

Kouam, J., Songmene, V., Zedan, Y., Djebara, A., & Khettabi, R. (2013). on Chip Formation During Drilling of Cast Aluminum Alloys. *Machining Science and Technology*, *17*(2), 228–245. doi:10.1080/10910344.2013.780546

Liao, H., Sun, Y., & Sun, G. (2002). Effect of Al-5Ti-1B on the microstructure of near-eutectic Al-13.0% Si alloys modified with Sr. *Journal of Materials Science*, *37*(16), 3489–3495. doi:10.1023/A:1016519307997

machovec cj ZINDEL JW, G. (2000). Effect of Bi-Sr intractions on Si morphology in a 319-type aluminum alloy, *Journal of Materials Science,108:439-44*, 439–444.

Manna, A., & Bhattacharyya, B. (2002). A study on different tooling systems during machining of Al/SiC-MMC. *Journal of Materials Processing Technology*, *123*(3), 476–482. doi:10.1016/S0924-0136(02)00127-9

Mohamed, A. M. A., Samuel, F. H., Samuel, A. M., & Doty, H. W. (2008). Effects of Individual and Combined Additions of Pb, Bi, and Sn on the Microstructure and Mechanical Properties of Al-10.8Si-2.25Cu-0.3Mg Alloy. *Metallurgical and Materials Transactions A*, *40*(1), 240–254. doi:10.1007/s11661-008-9692-1

Moustafa, M. A., Samuel, F. H., & Doty, H. W. (2003). Effect of solution heat treatment and additives on the hardness, tensile properties and fracture behaviour of Al-Si (A413. 1) automotive alloys. *Journal of Materials Science*, *38*(22), 4523–4534. doi:10.1023/A:1027385619114

Moustafa, M. A., Samuel, F. H., Doty, H. W., & Valtierra, S. (2002). Effect of Mg and Cu additions on the microstructural characteristics and tensile properties of Sr-modified Al-Si eutectic alloys. *International Journal of Cast Metals Research*, *14*(4), 235–253.

Muthukrishnan, N., Murugan, M., & Prahlada Rao, K. (2008). *Machinability issues in turning of Al-SiC (10p) metal matrix composites*. *The International Journal of Advanced Manufacturing Technology* (Vol. 39, pp. 211–218). Springer London. doi:10.1007/s00170-007-1220-8

Nishido, S., Kaneso, M., Kobayashi, T., & Toda, H. (2004). Role of Si particle damage on fatigue characteristics of cast Al–Si alloys. *International Journal of Cast Metals Research*, *17*(6), 345–350. doi:http://dx.doi.org/10.1179/136404604225022702

Noordin, M. Y., Venkatesh, V. C., Chan, C. L., & Abdullah, A. (2001). Performance evaluation of cemented carbide tools in turning AISI 1010 steel. *Journal of Materials Processing Technology*, *116*(1), 16–21. doi:10.1016/S0924-0136(01)00838-X

Nouri, M., Fussell, B. K., Ziniti, B. L., & Linder, E. (2015). Real-time tool wear monitoring in milling using a cutting condition independent method. *International Journal of Machine Tools and Manufacture*, *89*, 1–13. doi:10.1016/j.ijmachtools.2014.10.011

Ozben, T., Kilickap, E., & Çakır, O. (2008). Investigation of mechanical and machinability properties of SiC particle reinforced Al-MMC. *Journal of Materials Processing Technology*, *198*(1-3), 220–225. doi:10.1016/j.jmatprotec.2007.06.082

Ozcatalbas, Y. (2003). Chip and built-up edge formation in the machining of in situ Al4C3–Al composite. *Materials & Design*, *24*(3), 215–221. doi:10.1016/S0261-3069(02)00146-2

Palanikumar, K., & Karthikeyan, R. (2007). Assessment of factors influencing surface roughness on the machining of Al/SiC particulate composites. *Materials & Design*, *28*(5), 1584–1591. doi:10.1016/j.matdes.2006.02.010

Patel, K. M., & Joshi, S. S. (2006). Mechanics of machining of face-milling operation performed using a self-propelled round insert milling cutter, *171*, 68–76. doi:10.1016/j.jmatprotec.2005.06.046

Pedersen, W., & Ramulu, M. (2006). Facing SiCp/Mg metal matrix composites with carbide tools. *Journal of Materials Processing Technology*, *172*(3), 417–423. doi:10.1016/j.jmatprotec.2005.07.016

Pérez-Prado, M. (2001). Microstructural evolution in adiabatic shear bands in Ta and Ta–W alloys. *Acta Materialia*, *49*(15), 2905–2917. doi:10.1016/S1359-6454(01)00215-4

Polmear, I. J. (2006). *Light alloys: from traditional alloys to nanocrystals*. Elsevier/Butterworth-Heinemann. Retrieved from http://books.google.com.my/books?id=td0jD4it63cC

Pramanik, A., Zhang, L. C., & Arsecularatne, J. A. (2007). An FEM investigation into the behavior of metal matrix composites: Tool–particle interaction during orthogonal cutting. *International Journal of Machine Tools and Manufacture*, *47*(10), 1497–1506. doi:10.1016/j.ijmachtools.2006.12.004

Pratibha, S. (2010). Deformation State of Aluminum-6% Silicon Alloy (319 Al) Subjected to Orthogonal Cutting at Different Speeds and Feed Rates.

Qin, Q. D., Zhao, Y. G., & Zhou, W. (2008). Dry sliding wear behavior of Mg2Si/Al composites against automobile friction material. *Wear*, *264*(7-8), 654–661. doi:10.1016/j.wear.2007.05.008

Ren, B., Liu, Z., Zhao, R., Zhang, T., Liu, Z., Wang, M., & Weng, Y. (2010). Effect of Sb on microstructure and mechanical properties of Mg2Si/Al-Si composites. *Transactions of Nonferrous Metals Society of China*, *20*(8), 1367–1373. doi:10.1016/S1003-6326(09)60306-X

Roy, P., Sarangi, S. K., Ghosh, A., & Chattopadhyay, A. K. (2009). Machinability study of pure aluminium and Al–12% Si alloys against uncoated and coated carbide inserts. *International Journal of Refractory Metals and Hard Materials*, *27*(3), 535–544. doi:10.1016/j.ijrmhm.2008.04.008

Sahin, Y. (2003). Preparation and some properties of SiC particle reinforced aluminium alloy composites. *Materials & Design*, *24*(8), 671–679. doi:10.1016/S0261-3069(03)00156-0

Samuel, F. H., Samuel, A. M., Ouellet, P., & Doty, H. W. (1998). Effect of Mg and Sr additions on the formation of intermetallics in Al-6 wt pct Si-3.5 wt pct Cu-(0.45) to (0.8) wt pct Fe 319-type alloys. *Metallurgical and Materials Transactions A*, *29*(12), 2871–2884.

Seeman, M., Ganesan, G., Karthikeyan, R., & Velayudham, A. (2009). Study on tool wear and surface roughness in machining of particulate aluminum metal matrix composite-response surface methodology approach. *The International Journal of Advanced Manufacturing Technology*, *48*(5-8), 613–624. doi:10.1007/s00170-009-2297-z

Senthil Kumar, A., Raja Durai, A., & Sornakumar, T. (2003). Machinability of hardened steel using alumina based ceramic cutting tools. *International Journal of Refractory Metals and Hard Materials*, *21*(3-4), 109–117. doi:10.1016/S0263-4368(03)00004-0

Shaw, M. C. (2005). *Metal cutting principles* (Vol. 2). Oxford university press New York.

Sjölander, E., & Seifeddine, S. (2010). The heat treatment of Al–Si–Cu–Mg casting alloys. *Journal of Materials Processing Technology*, *210*(10), 1249–1259. doi:10.1016/j.jmatprotec.2010.03.020

Songmene, V., Kouam, J., Zaghbani, I., Parson, N., & Maltais, A. (2013). Global Machinability of Al-Mg-Si Extrusions.

Stephenson, D. A., & Agapiou, J. S. (2005). *Metal cutting theory and practice* (Vol. 68). CRC press.

Swamy, N. H. S., Joseph, M. A., Nagarajan, N. M., & Sudarsan, N. (2011). Effects of rapid heating on microstructure and mechanical properties of modified vibrated Al–Si–Mg alloys using a fluidized bed. *Materials and Manufacturing Processes*, *26*(2), 210–217. doi:http://dx.doi.org/10.1080/10426914.2010.505621

Tan, Y.-H., Lee, S.-L., & Lin, Y.-L. (1995). Effects of Be and Fe additions on the microstructure and mechanical properties of A357.0 alloys. *Metallurgical and Materials Transactions A*, *26*(5), 1195–1205. doi:10.1007/BF02670615

Tash, M., Samuel, F. H., Mucciardi, F., & Doty, H. W. (2007). Effect of metallurgical parameters on the hardness and microstructural characterization of as-cast and heat-treated 356 and 319 aluminum alloys. *Materials Science and Engineering: A*, *443*(1-2), 185–201. doi:10.1016/j.msea.2006.08.054

Taylor, J. A., Schaffer, G. B., & StJohn, D. H. (1999). The role of iron in the formation of porosity in Al-Si-Cu-based casting alloys: Part III. A microstructural model. *Metallurgical and Materials Transactions A*, *30*(6), 1657–1662. doi:10.1007/s11661-999-0103-z

Tenekedjiev, N., & Gruzleski, J. E. (1990). Hypereutectic Aluminum-Silicon Casting Alloys—A Review. *Cast Met*, *3*(2), 96–105. doi:org/10.1179/174313309X380422

Teti, R. (2002). Machining of Composite Materials. *CIRP Annals - Manufacturing Technology*, *51*(2), 611–634. doi:10.1016/S0007-8506(07)61703-X

Thai, L. T. (2006). *The Effects of Bismuth, Strontium and Antimony Additions on the= Microstructure and Mechanical Properties of A356 Aluminium Casting Alloy*. M. Sc. Thesis, Technological University of Malaysia.

Totten, G. E., & MacKenzie, D. S. (2003). *Handbook of Aluminum: Vol. 1: Physical Metallurgy and Processes* (Vol. 1). CRC Press. doi:10.1023/A:1016519307997

Uthayakumar, M., Prabhakaran, G., Aravindan, S., & Sivaprasad, J. V. (2012). Influence of Cutting Force on Bimetallic Piston Machining by a Cubic Boron Nitride (CBN) Tool. *Materials and Manufacturing Processes*, *27*(10), 1078–1083. doi:10.1080/10426914.2012.677913

Vernaza-Peña, K. M., Mason, J. J., & Li, M. (2002). Experimental study of the temperature field generated during orthogonal machining of an aluminum alloy. *Experimental Mechanics*, *42*(2), 221–229. doi:10.1007/BF02410886

Walker TJ, S. M. C. (1969). Failure of metals in machining. Oxford, UK. doi:org/10.1179/174313309X380422

Wang, R., Lu, W., & Hogan, L. . (2003). Self-modification in direct electrolytic Al–Si alloys (DEASA) and its structural inheritance. *Materials Science and Engineering: A*, *348*(1-2), 289–298. doi:10.1016/S0921-5093(02)00732-3

Wright, E. M. T. and P. K. (2000). *mettal cutting*. Elsevier.

Xiufang, B., Weimin, W., & Jingyu, Q. (2001). Liquid structure of Al–12.5% Si alloy modified by antimony. *Materials Characterization*, *46*(1), 25–29. doi:10.1016/S1044-5803(00)00089-9

Zedan, Y., Samuel, F. H., Samuel, a. M., & Doty, H. W. (2010). Effects of Fe intermetallics on the machinability of heat-treated Al–(7–11)% Si alloys. *Journal of Materials Processing Technology*, *210*(2), 245–257. doi:10.1016/j.jmatprotec.2009.09.007

Zhang, J., Fan, Z., Wang, Y. Q., & Zhou, B. L. (2000). Microstructural development of Al – 15wt .% Mg 2 Si in situ composite with mischmetal addition, *281*, 104–112. doi:S0921-5093(99)00732-7

Zhang, X. H., Su, G. C., Ju, C. W., Wang, W. C., & Yan, W. L. (2010). Effect of modification treatment on the microstructure and mechanical properties of Al–0.35%Mg–7.0%Si cast alloy. *Materials & Design*, *31*(9), 4408–4413. doi:10.1016/j.matdes.2010.04.032

List of Publications and Paper Presented

Mohsen Marani Barzani, Ahmed A.D. Sarhan, Saaed Farahan, Ramesh Sing "*Machinability of Al-Si-Cu cast alloy containing bismuth and antimony when dry turning using coated carbide insert*". Published in: Measurement 61 (2015) 150–161.

Mohsen Marani Barzani*, "ErfanZalnezhad, Saeed Farahany, Ahmed A.D. Sarhan, Singh Ramesh, *Fuzzy Logic Based Model for Predicting Surface Roughness of Machined Al-Si-Cu Cast Alloy Using Different Additives-Turning*". Publish in: Measurement 62 (2015) 170–178.

Mohsen Marani Barzani, Ahmed Sarhan, Saeed Farahany and Ramesh Singh "*Investigation into effect of cutting conditions on surface roughness while dry machining Al%11Si and Al%11 Si %1 Bi die casting alloys"* published in: Advanced Materials Research Vol. 1119 (2015) pp 617-621 doi:10.4028/www.scientific.net/AMR.1119.617 (2015)

Mohsen Marani.**Barzani**, Ahmed. A.D. Sarhan, Ramesh Singh, Saeed Farahany " *Investigation into effect of silicon morphology on surface roughness while machining Al-Si-Cu-Mg alloy*" Malaysian International Tribology Conference 2015- Penang, Malaysia, Malaysian Tribology Society.

APPENDIX

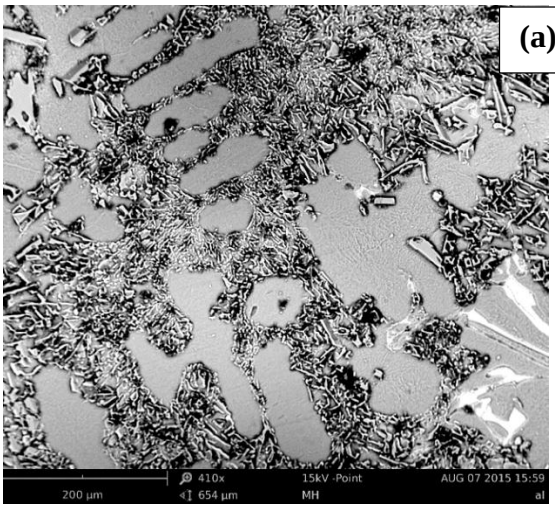

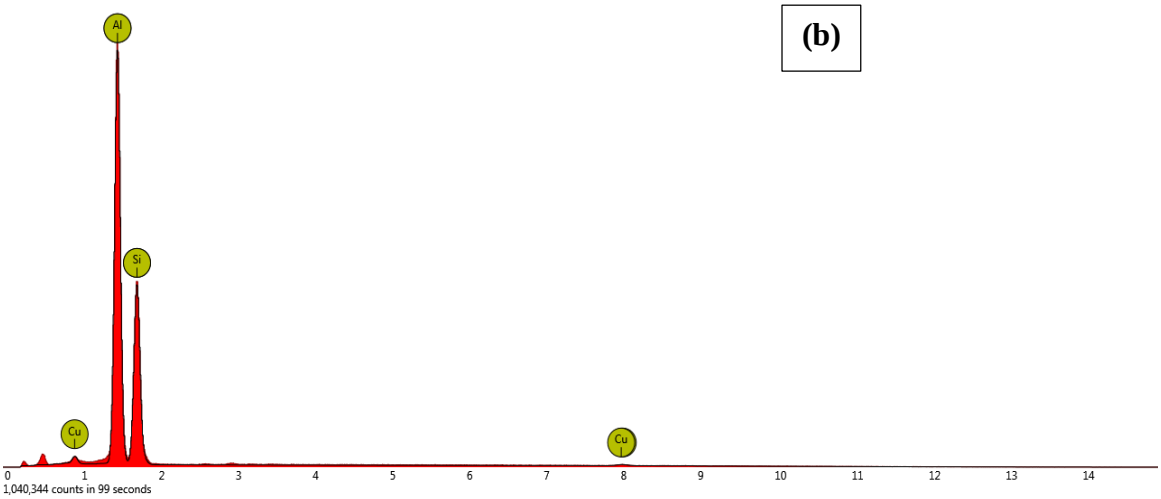

(a) SEM and (b) EDX of base alloy (Ai-11Si-2Cu)

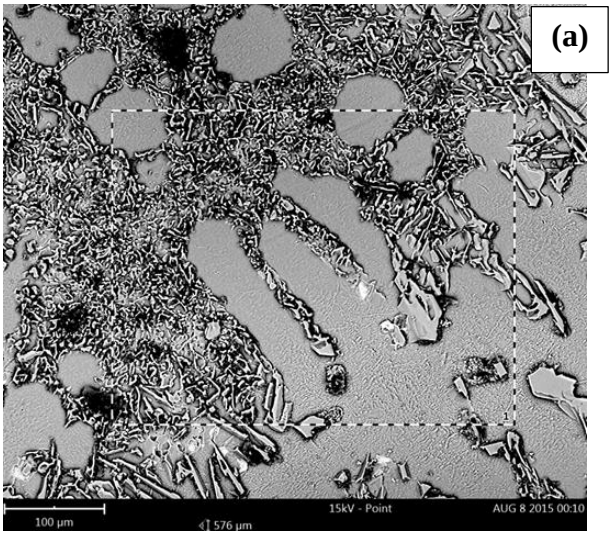

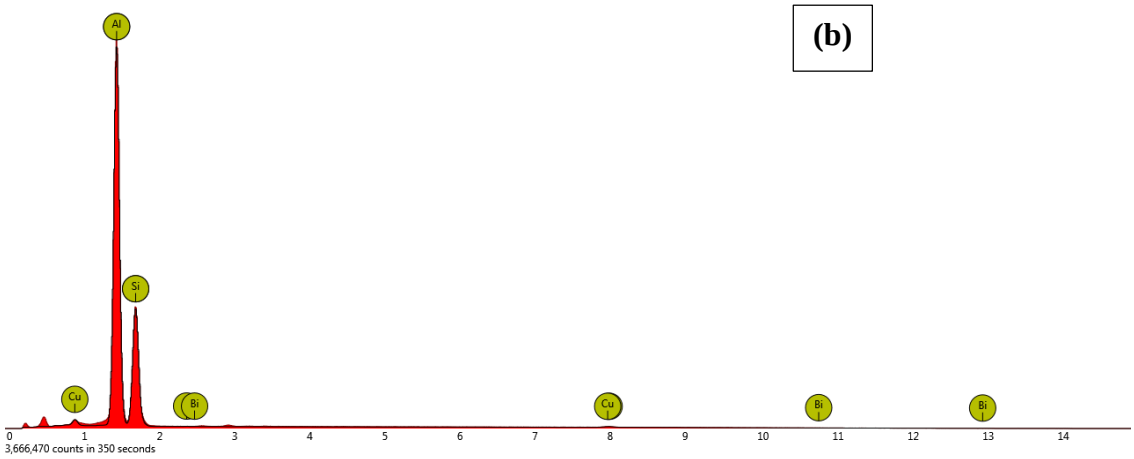

(a) SEM and (b) EDX of Bi-containing alloy (Ai-11Si-2Cu-0.1bi)

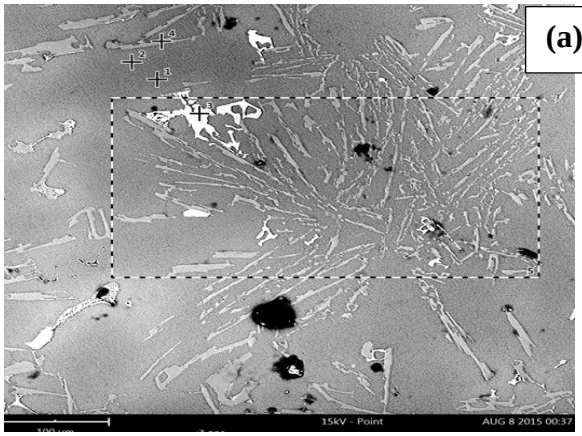

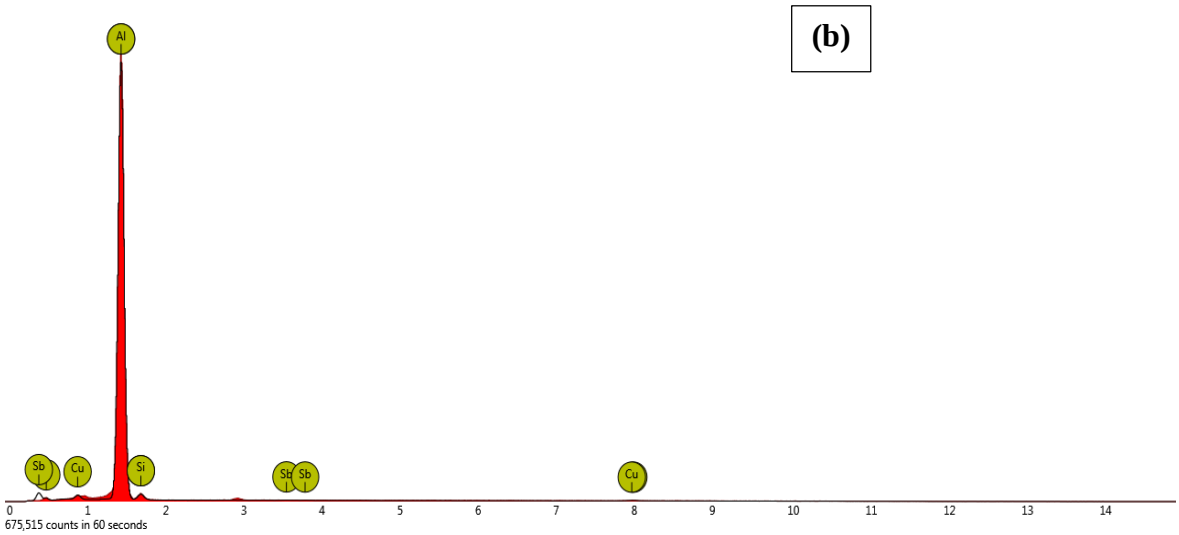

(a) SEM and (b) EDX of Sb-containing alloy (Ai-11Si-2Cu-0.5Sb)

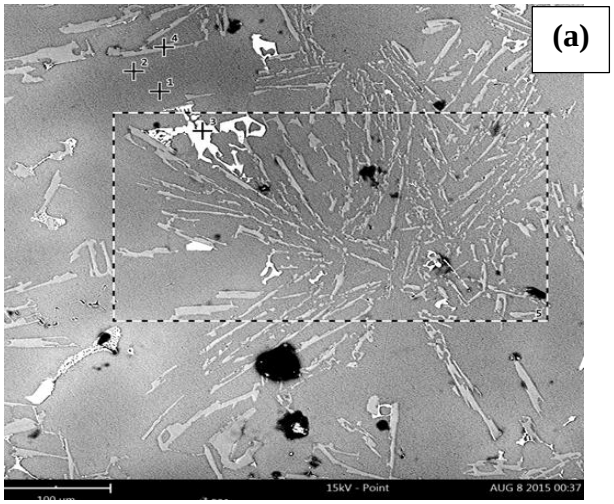

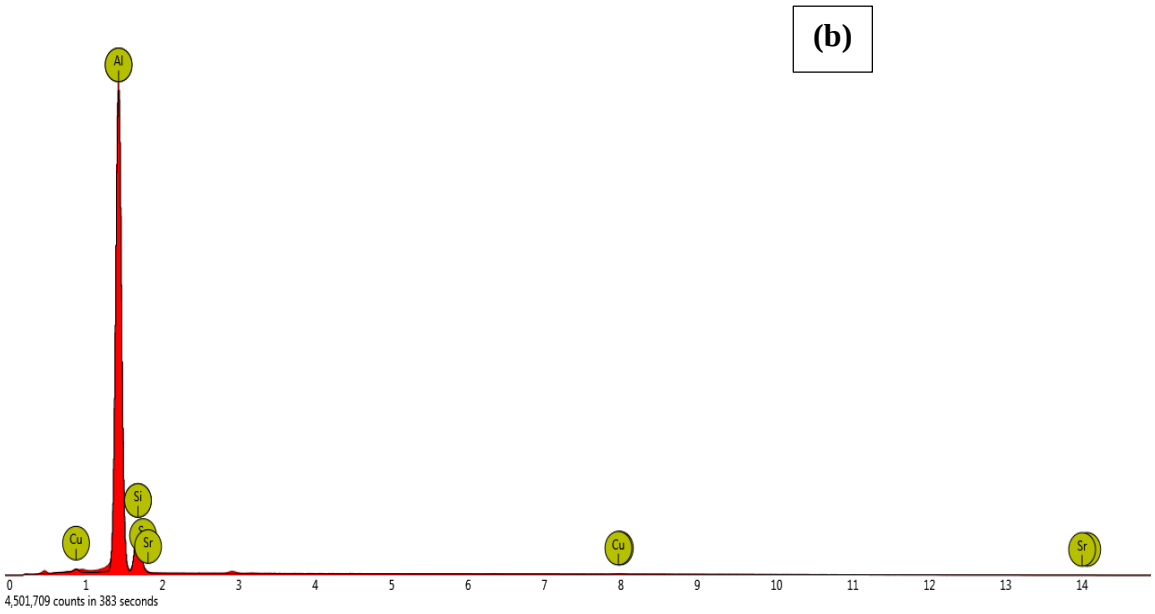

(a) SEM and (b) EDX of Sr-containing alloy (Ai-11Si-2Cu-0.04Sr)